Polymeric micelles as drug delivery system and MRI contrast agent

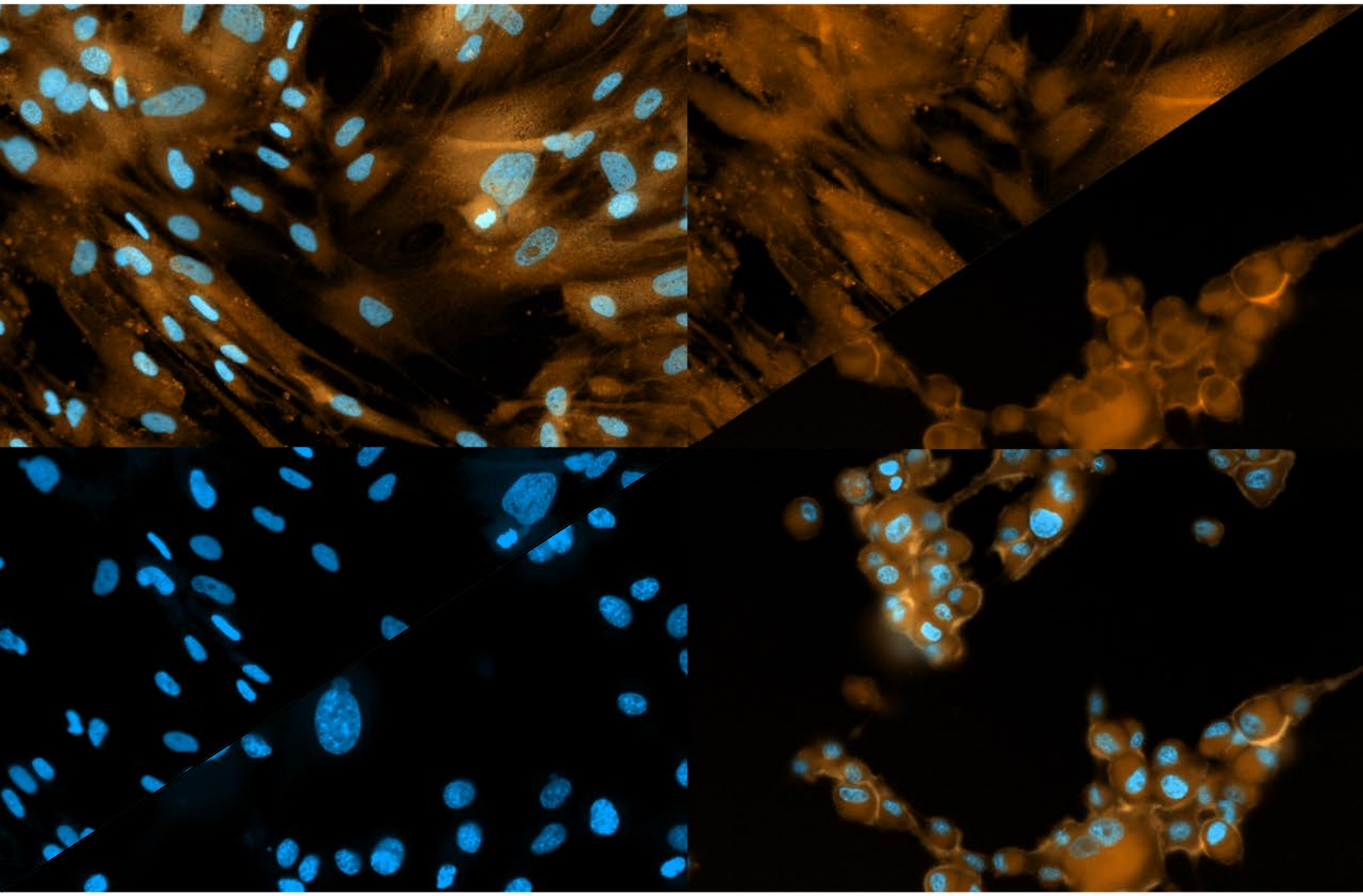

Aalborg University

Institute of Physics and Nanotechnology
Supervised by
Leonid Gurevich and Peter Fojan

Master Thesis by
Sven Buskov Romme

AALBORG UNIVERSITY
STUDENT REPORT

Nanotechnology
Institute of Physics and Nanotechnology
Skjernvej 4A, 9220 Aalborg Oest
Phone 99 40 92 15, Fax 99 40 92 35
www.nano.aau.dk

Title:

Polymeric micelles
as drug delivery system
and MRI contrast agent

Project Period:

Master, 9th and 10th semester, 2014-2015

Author:

Sven Buskov Romme

Supervisors:

Peter Fojan
Leonid Gurevich

Amount Published: 5

Number of Pages: 91

Published: 15-9-2015

Synopsis:

The thesis explored the potential application of amphiphilic PVP micelles as drug delivery system and gadolinium MRI contrast agent. PVP micelles were produced in 30 to 100 nm size range, and their drug delivery ability was investigated. Glioblastoma and fibroblast cells were exposed to curcumin loaded PVP micelles in the presence of endocytic inhibitors, dynasore and wortmannin, and drug uptake was observed within 5 minutes of exposure across all experimental lines.
The curcumin loaded PVP micelles were functionalised by gadolinium to serve as a contrast agent for *in vivo* MRI scan of nude mice. An intravascular T1 weighted signal was observed, of about half the magnitude compared to commercial agent Dotarem as reference.
The enhanced permeability and retention time (EPR) effect was observed in the tumour of the mouse subject to sample of strongest signal intensity, by the accumulated signal after 24 hours.

AALBORG UNIVERSITY
STUDENT REPORT

Nanoteknologi
Institut for Fysik og Nanoteknologi
Skjernvej 4A, 9220 Aalborg Oest
Telefon nummer +45 99 40 92 15, Fax +45 99 40 92 35
www.nano.aau.dk

Titel:

Polymeriske miceller
som drug delivery system
og MRI contrast stof

Projekt Periode:
Master, 9. og 10. semester 2014 - 2015

Forfatter:
Sven Buskov Romme

Vejledere:
Peter Fojan
Leonid Gurevich

Antal Printet: 5

Antal Sider: 91

Afleverings Dato: 15-9-2015

Synopsis:

Afhandlingen udforskede den potentielle anvendelse af amphifile PVP miceller som laegemiddeladministrationssystem og gadolinium MRI-kontrastmiddel. PVP miceller blev fremstillet i 30 til 100 nm stoerrelsesorden, og deres evne til laegemiddelafgivelse blev undersoegt. Glioblastoma og fibroblastceller blev udsat for curcumin fyldte PVP miceller under tilstedevaerelse af endocytiske inhibitorer, dynasore og wortmannin, og optagelse af laegemiddel blev observeret efter mindre end 5 minutters eksponering pÃ¥Ã¥ tvaers af alle eksperimentelle linjer.
Curcumin fyldte PVP miceller blev funktionaliseret med gadolinium for at fungere som kontrastmiddel til *in vivo* MR-scanning af noegne mus. Et intravaskulaer T1 vaegtet signal blev observeret, som var omkring halv saa stort som en kommerciel standard Dotarem som reference.
"Enhanced permeability and retention time" (EPR) effekten blev observeret i tumoren i musen underlagt proeven af staerkeste signal intensitet, i form af akkumuleret signal efter 24 timer.

Preface

The thesis was produced by master student Sven Buskov Romme at Aalborg University, in the period of 1st of September 2014 to the 15th of September 2015

Reading Guide
Throughout the report, there will be references to various sources. These will be found on the form [#] where the number in the angular brackets refers to a specific source in the bibliography at the end of the report. In the bibliography the sources will be listed with its title, author, and other relevant information depending on whether the source is a book, article, or web page. The bibliographic references will be listed after the specific section in which they are used; this indicates that the reference applies to all of the above if nothing else is stated.

Tables and figures are listed after the number of the chapter in which they are displayed. Hence the first figure in chapter 4 would be named 'figure 4.1' whereas the second one would be 'figure 4.2' et cetera. Since tables are numbered according to the same system both 'table 4.1' and 'figure 4.1' are possible in the same chapter. To each figure/table a short descriptive caption will be made together with a bibliographic reference where necessary. All figures can be found on the attached DVD.

The author would like to express extraordinary thanks and appreciation of the help and guidance provided by the staff of Laboratory for Stem Cell Research Aalborg University and staff at the Radiology and the Oncology departments of Aalborg University Hospital.

Aalborg University, 15/09-2015

Sven Buskov Romme

List of abbreviations used through out the report:

AEGLAFK	:	Ala-Glu-Gly-Leu-Ala-Phe-Lys
AFM	:	Atomic Force Microscopy
DCM	:	Dichloromethane
DIPEA	:	N,N-Diisopropylethylamine
DMEM	:	Dulbecco's Modified Eagle Medium
DMF	:	Dimethylformamide
DMSO	:	Dimethylsulfoxide
DTPA	:	Diethylenetriamine Pentaacetic Acid
EDC	:	N-(3-Dimethylaminopropyl)-N-ethylcarbodiimide hydrochloride
EDTA	:	(Ethane-1,2-diyldinitrilo)tetraacetic acid
EN	:	Ethylenediamine
ETA	:	Ethanolamine
FA	:	Fluorescamine
HPLC	:	High Performance Liquid Chromatography
IPA	:	Isopropanol
MES	:	2-(N-morpholino)ethanesulfonic acid
MRI	:	Magnetic Resonance Imaging
NHS	:	N-hydroxysuccinimide
NTA	:	Nanoparticle Tracking Analysis
PBS	:	Phosphate-Buffered Saline
PVP	:	C18H37-polyvinylpyrrolidone
PVP-COOH	:	C18H37-poly(carboxy vinylpyrrolidone)
PVGP	:	C18H37-poly(vinyl 2-glycidylamido pyrrolidone)
TFA	:	Trifluoroacetic acid
TIS	:	Triisopropylsilane
T/E	:	Trypsin/EDTA

Contents

Introduction 1

1.1 Drug delivery

Drug delivery is the transport of a therapeutic agent to areas of disease. The means of transport may include targeted delivery and controlled release. By controlling the rate, time, and place of release of drugs in the body it is possible to achieve higher efficacy of a therapeutic effect.

It relies on these three core concepts. First there is the therapeutic agent, the drug. A therapeutic effect is "the treatment of disease or disorders by remedial methods". An agent is "something that produces an effect". The various types of therapies are about as numerous as the amount of diseases, but major categories exist such as cancer, cardiovascular disease, genetic disease, and infectious diseases. The therapies overlap these categories, but any therapy involving ingestion or injection of an agent is relevant to drug delivery as a science.

By definition, the treatment is not exclusive to the disease. The aim of the effect is treating an illness, and healthy cells may become collateral damage. A strong example is chemotherapy, to which hair loss is an obvious side effect caused by the treatment. It is by no means the only one, and the list includes (in addition to hair loss):

- Fatigue
- Pain (Headaches, muscle pain, stomach pain, pain from nerve damage)
- Mouth and throat sores
- Diarrhea
- Nausea and vomiting
- Constipation
- Blood disorders
- Nervous system effects
- Changes in thinking and memory

- Sexual and reproductive issues
- Appetite loss
- Long-term side effects

[1]

1.1.1 Targeted delivery

Upon injection or ingestion of a drug by a patient, it is distributed in the body proportional to the regional circulation, but with no further direction. The goal for the drug is systemic circulation, and unless the drug is administered intravenously it will have to pass through several semipermeable membranes to reach that point. In addition, it will pass other organs and intracellular compartments where it can be degraded or inactivated by lymphatic enzymes in a process called first-pass metabolism. This means, to achieve the required therapeutic effect, a much larger quantity has to be administered. A significant part is lost in normal tissue, where it may induce the unwanted side effects. [2]

As chemotherapy aims to damage proliferating cells, the non-specificity is a large drawback as the side effects increase and become more harmful to the patient [3]. The effect is best decribed by the therapeutic index, TI:

$$TI = \frac{TD_{50}}{ED_{50}} \tag{1.1}$$

where TD_{50} is the toxicity dose, meaning the dose that produces toxicity in 50% of the population. ED_{50} is the minimum effective dose for 50% of the population. This leads to the second concept of drug delivery, targeted delivery. A defition may be presented as "achieving the maximal potential intrinsic activity of drugs by optimising their exclusive availability to their pharmacological receptors in a manner that affords protection both to the drug and to the body alike".

It is an attempt to isolate to or enhance the therapeutic effect in the areas of interest. By doing this, the ideal scenario allows for a lower systemic concentration of the therapeutic agent, while still producing the required effect. Or it may allow increased dosage as the side effects at a higher concentration are more tolerable. Targeting ideally works by a simultaneous increase of TD_{50} and lessening ED_{50}. [4]

The advantages of targeted drug delivery are:

- Simpler administration
- effective dose is lowered
- administered dose in non-intravenous routes and thereby cost efficiency increased
- reduction of side effects with an increase in therapeutic effect

The principle is illustrated on figure 1.1, again using chemotherapy as an example. The dose-response curve is sigmoid in shape [5], applying to most drugs and tumours, and the doses used in clinical practise

lie on the linear part of the curve.. The introduction of targeted delivery chemotherapy pushes the curve for normal cells to the right towards a lower response per unit dose. But multidrug resistance (MDR), which is a widespread issue most often occurring in infectious diseases, also plays a role in chemotherapy and pushes the curve for cancers closer to the curve for normal cells, hindering effective treatment. [6][7]

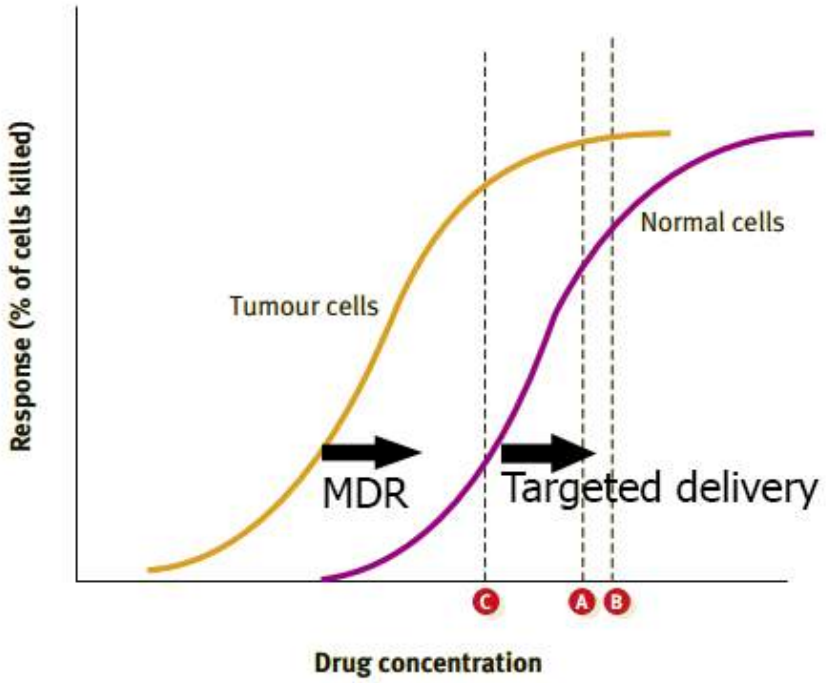

Figure 1.1: *The effect of chemotherapy on cancer cells, normals cells, and normal cells using targeted delivery as a function of dosage. [3]*

The level of targeting can be carried out an organ level, cellular level, or molecular level. Directly injecting the drug into diseased areas have been attempted, but the administration can be technically quite difficult in many cases. In addition to the fact that many diseases are spread over a variety of cells this severely limits the applicability of the approach. Attempts have been made at using temperature- or pH sensitive carriers to react and deliver to the microenvironment of specific tumour or inflammatory tissue [8], or using external forces such as ultrasound or magnetic fields to active release [9]. Lastly, the use of specific delivery peptides with high affinity towards the target area can target drugs towards almost anywhere in the body. [2]

1.1.1.1 Passive targeting

An effect that often comes into play for many tumours and inflamed tissue is the enhanced permeability and retention effect (EPR). The effect is illustrated on figure 1.2. As tumours grow and deplete local supplies of oxygen and nutrients necessary to continuously proliferate, they release signaling molecules that recruit new blood vessels to the tumour in a process called angiogenesis. The blood vessels of this process, called angiogenic, have large interstitial gaps ranging upwards 600-800 nm. This space allows carrier molecules (containing drugs) to leak from within veins to the tumour interstitial space. Due to

impaired lymphatic drainage, the carrier molecules will accumulate and have a higher concentration in this area. Using this effect for targeted delivery is called passive targeting, and upwards 10-fold increases of drug concentration in the tumour can be observed when comparing to free drug concentrations [10]. The method requires the drug delivery system to be long-circulating, staying in the blood for temporally extended periods.

Recent advances in passive targeting have been made in the field of hyperthermia responsive delivery systems [11] and in using so-called phosphatiosomes as drug delivery vesicles [12]

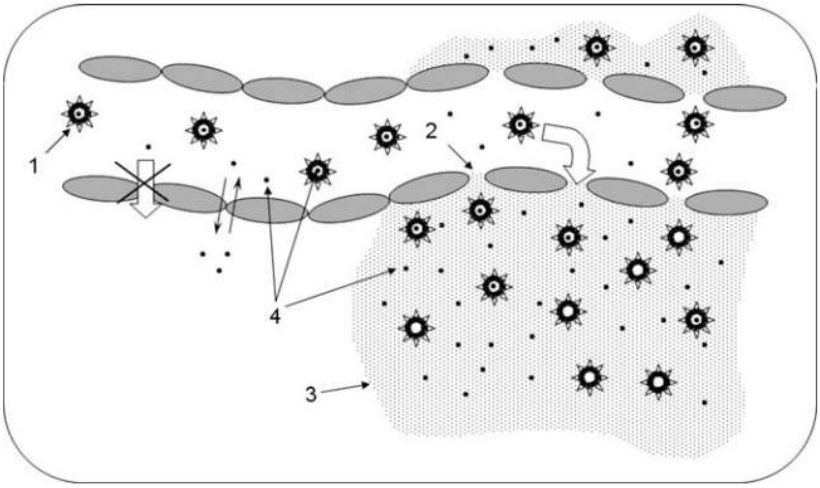

Figure 1.2: *As tumours grow and deplete local supplies of oxygen and nutrients necessary to continue proliferation, they recruit new blood vessels to the tumour in a process called angiogenesis. The blood vessels of this process, called angiogenic, have large interstitial gaps ranging upwards 600-800 nm (2). This space allows carrier molecules containing drugs (1) to leak from within intravenous space to the tumour interstitial space (3). Due to impaired lymphatic drainage, the carrier molecules will accumulate and have a higher concentration in this area. (4) are free drug molecules, shown to be able to penetrate normal interstitial gaps. [2]*

The EPR effect has seen a progressive increase in related citations in recent years, as evidenced by figure 1.3

It has become a central part of anticancer drug design and anticancer strategies using gene delivery, molecular imaging, antibody therapy, micelles, liposomes, and protein-polymer conjugates.

1.1.1.2 Active targeting

Passive targeting is useful and effective when it is applicable, but that is not always the case. The diseased area can be too similar to healthy tissue in terms of temperature, pH, and vascular permeability that it is not a feasible strategy to rely on passive targeting.

Instead, a more universal approach is active targeting, to which there is an illustration on figure 1.4. It refers to binding another molecule to the drug, which is capable of specific recognition and binding to a targeted site of disease. Substances exhibiting this quality include: Antibodies, lectins, proteins,

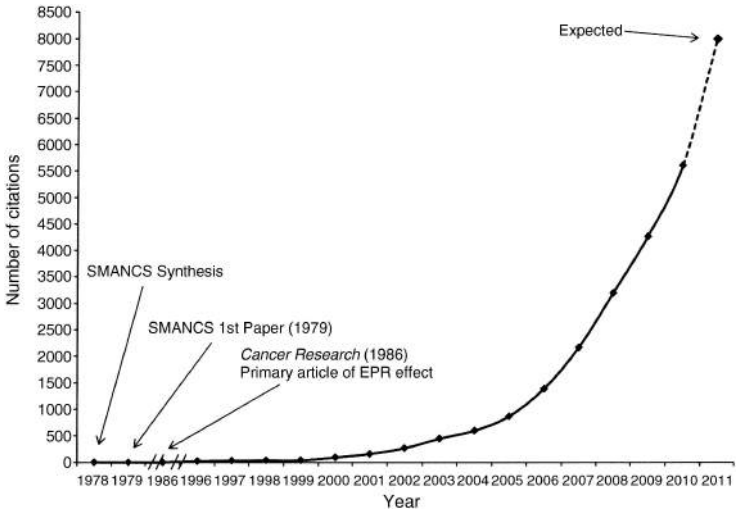

Figure 1.3: *A graph of the increased number of citations related to the Enhanced Permeability and Retention effect in recent years, and projected development of the tendency. [13]*

hormones, charged molecules, mono-, oligo-, and polysaccharides, and low-molecular weight ligands. Monoclonal antibodies are most frequently used.

Efficacy determining factors in targeted delivery are: Size of the target, circulation through the target, number of binding sites for the targeted drug or drug carrier within the target, and number and affinity of targeting moieties on the drug carrier. [2]

Active targeting is a broad field of science. A very literal form of targeting is by the use of photothermal treatment. As in the case of [14], using micelle-like (Gold nanoparticles coated with amphiphilic block copolymers) plasmonic nanoparticles with strong near-infrared absorption facilitating bioimaging and the aforementioned phototermal treatment.

1.1.2 Drug delivery routes

The availability of a drug to their pharmacological receptors is also known as bioavailability. The major deciding factor is first-pass metabolism and it becomes evident that bioavailability relies heavily on the route of administration.

1.1.2.1 Parenteral drug delivery

Parenteral drug delivery is the injection of substances by subcutaneous, intramuscular, intravenous, and intra-arterial routes. It is the most commonly used invasive method of drug delivery. The advantages of parenteral drug delivery include rapid onset of action, it is predictable and features almost complete bioavailability, avoids first-pass metabolism, and it is applicable to patients who are unable to ingest drugs orally (for instance comatose). As for disadvantages, it is foremost painful, and self-administration becomes an issue so it requires trained personnel.

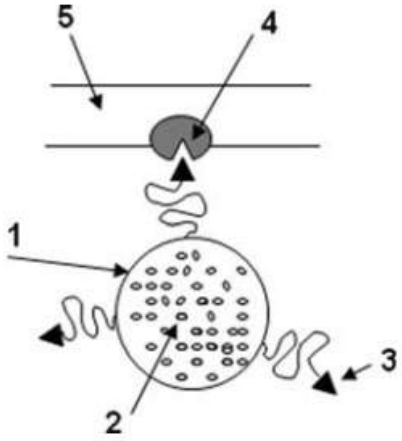

Figure 1.4: *Illustration drug carrier (1) loaded with drug (2) and bound to a ligand molecule (3). The ligand binds to a receptor (4) which is situated on a cell surface (5). It results in the carrier molecule being attached to the cell and eventually releasing its drug or being internalised by the cell. [2]*

1.1.2.2 Oral drug delivery

Oral drug delivery has historically been the most used route of administration, as it is very easy and patient compliance is generally not an issue. But a major disadvantage is the first-pass metabolism, and absorption of the drug through to systemic circulation. Drugs on this route are subject to a variation of conditions that degrade a percentage of the dose along the way, lowering the bioavailability in the end. This means oral drug delivery is less predictable, and it is a strong subject to controlled release systems, explained in the following.

1.1.2.3 Other drug delivery routes

Other routes of drug delivery include:

- Transdermal drug delivery
- Transmucosal and nasal drug delivery
- Colorectal drug delivery
- Pulmonary drug delivery
- Intra-osseus Infusion
- Cardiovascular drug delivery
- Central nervous system drug delivery

Deciding whether to use either of these delivery routes is on a case-to-case basis. [15]

1.1.3 Controlled release

Free drugs administered to the body face a number of potential problems such as poor solubility, tissue damage on extravasation, rapid breakdown of the drug *in vivo*, unfavourable pharmacokinetics, poor bioavailability, and lack of selectivity for target tissue [10].

But controlling the release rate of the drug by various means offers a number of potential advantages and solutions such as:

- Improved efficacy by increasing therapeutic activity
- Reduced toxicity by keeping concentration within an appropriate threshold
- Improved patient compliance due to simpler and/or less administration

Controlled release aims to deliver the drug over an extended time period or at a specific time during treatment. A schematic of an ideal outcome of a controlled release rate is shown on figure 1.5. The aim is to keep the drug concentration within the therapeutic window while keeping fluctuation to a minimum to avoid peaking into toxic levels or dropping down to ineffective levels.

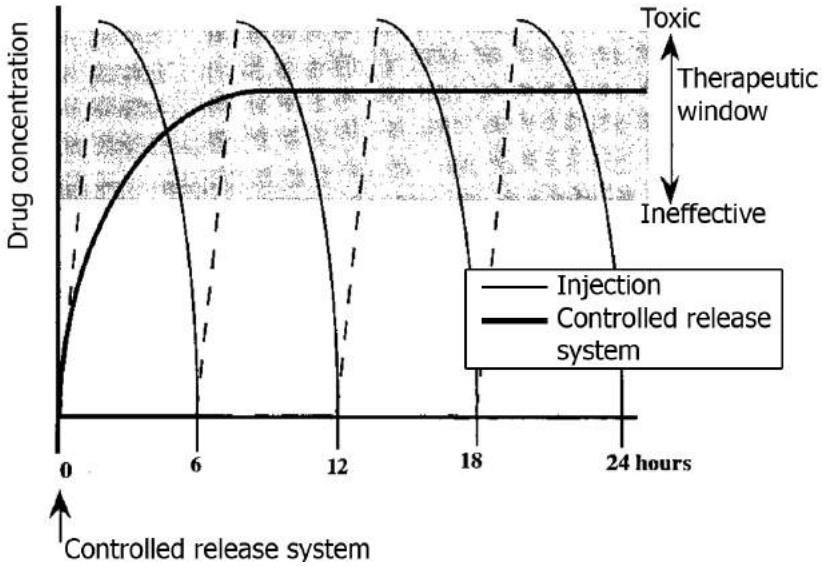

Figure 1.5: *Illustration drug carrier (1) loaded with drug (2) and bound to a ligand molecule (3). The ligand binds to a receptor (4) which is situated on a cell surface (5). It results in the carrier molecule being attached to the cell and eventually releasing its drug or being internalised by the cell. [2]*

1.1.4 Ideal drug delivery systems

To sum it up, an ideal drug delivery system should exhibit the following qualities:

- Relevant bioavailability of drug

- Controlled release of drug
- Targeted transport of drug to diseased site
- Stable system
- Wide compatibility
- Easy administration
- Safe and reliable
- Cost-effective

Each point provides a set of challenges. One the one hand, passive targeted delivery is easily applicable in tumours where the EPR effect is protruding but this is by far not always the case. On the other hand, active targeted delivery has broad applicability regardless of tumour types, but faces challenges of degradation along the way to diseased sites, additional fabrication steps, and identification of proper binding sites to target. [16]

1.2 Polymeric drug delivery systems

Polymeric drug delivery can potentially tackle some of the challenges discussed in the previous section. A contributor to poor bioavailability is the solubility of many drugs being low in the aqueous environment of the body. Micelles can solubilise drugs of this category and in effect increase not only their availability, but also the time that the drugs stay in circulation.

This is of particular importance when considering the fact that micelles can be fabricated in sizes that enable utilisation of the EPR effect to great extent. Additionally, drugs are usually kept from degradation and inactivation while solubilised by micelles.

Polymeric drug delivery systems include soluble polymers, microparticles of polymers, microcapsules, lipoproteins, liposomes, and micelles. Whichever system is used, they all share the same clearance pathways, as they are long-circulating drugs. The most important of these - extravasation, renal clearance and uptake by cells - are independent processes. But, extravasation is of particular relevance as it is an important factor in the bioavailability of the drug.

As mentioned earlier the process occurs to an increased extent under the EPR effect, but it has been shown to also be of significance for all particulates below a certain size threshold. That threshold has been shown to be 5-10 nm, and as a result it has been seen fit to divide all long circulating drug carriers into two groups above and below this threshold. The non-extravasating group (above 5-10 nm) includes cells, cell ghosts, particles, and large liposomes. The extravasating group includes small liposomes, proteins and their derivatives, and polymers of more than 40 kDa.

Micelles fit in both these categories, as their size distribution, depending on means of fabrication, ranges from below 10 nm to often being 400-500 nm in diameter. According to the literature they are categorised as extravasating. [17]

The inclusion of polyethylene glycol (PEG) in drug delivery systems can help improve circulation time, as it inhibits opsonisation of the particulate drug delivery system. More specifically, PEG blocks adhesion of opsonins. [18]

1.2.1 Micelles

Micelles belong to a large family of dispersed systems, which in technical terms consists of a dispersed phase within a dispersion medium. In this family, micelles are classified as association or amphiphillic colloids or in broader terms a colloidal dispersion.

They are formed by self-assembly under certain conditions. Amphiphillic molecules, or surfactants, consist of two distinct regions with opposite or in some cases just differential affinity towards a solvent. At low concentration the surfactants are evenly dispersed in the solvent, possibly with a preference towards an interface. Increasing the concentration does little, until a critical micelle concentration (CMC) is reached. At this point, aggregration occurs and the surfactant molecules form micelles. As they are amphiphillic, they will be arranged in a manner that maximises contact of the region, with higher affinity towards the solvent, to its surroundings. The micelles formed at CMC contain a number of surfactant molecules. That number is called the aggregation number.

In an aqueous environment a potentially hydrophilic region will be facing outwards, forming the corona. A hydrophobic or less hydrophilic region will be packed inside as the core. Schematically, the structure can be seen on figure 1.6. It shows a method of determining the CMC by using a fluorescent dye. The dye has limited solubility in water, so as micelles form the dye is solubilised in the core, increasing the concentration and thus the fluorescence intensity. [17]

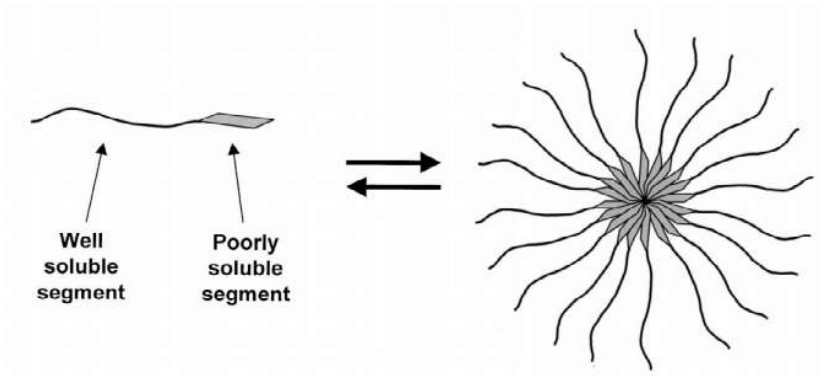

Figure 1.6: *Aa method of determining the CMC by using a fluorescent dye. The dye has limited solubility in water, so as micelles form the dye is solubilised, concentration increases and the fluorescence intensity follows. [17]*

Micelles can be composed of several different surfactants, and in that case the term mixed micelles applies. In the ideal scenario, the CMC of a mixed micellar system can be calculated from CMCs and molar fractions (M) of individual species:

$$\frac{1}{CMC} = \frac{M_1}{CMC_1} + \frac{M_2}{CMC_2} \tag{1.2}$$

Analogous to the CMC, critical micelle temperature exists and follows to a large extent the same principles as CMC. [17]

1.2.1.1 Micelle synthesis

The major driving force behind micelle formation is the decrease of free energy, due to core formation which allows packing hydrophobic blocks away from aqueous environments. At and just above CMC the micelles are loose and packing a small percentage of water in the core. As the concentration of surfactant increases the equilibrium shifts further towards micelle formation. The micelles pack tighter becoming more stable, reducing size and the residual water is pushed out. In this sense, the size and stability efficiency per mole surfactant increases as the CMC decreases.

This fact is important for micelles intended for pharmacological use, since upon delivery and entering any biological system, the micelles are diluted by biological fluids. Only micelles with a low CMC are stable in those circumstances. [17]

1.2.1.2 Solubilisation by micelles

As mentioned in the former, an attractive quality of micelles is the ability to increase the solubility of hydrophobic drugs. Micelles of nonionic surfactants are known to have anisotropic water distribution in their structure, where it decreases from the corona and inwards. This results in a polarity gradient, which means that the spatial position of drugs solubilised by micelles with follow this gradient depending on their polarity. The drug loading capacity of micelles depends on the chemical structure of both drug and surfactant molecules of the micelles, polarity of the drug, temperature and pH, whereof the latter two contribute to controlled release and targeting properties as mentioned in previous sections. In effect, in an aqueous environment, the hydrophobic region of the surfactant molecule facilitates the solubilisation of drugs. In general having a larger region means higher loading capacity. Thermodynamically, solubilisation can be considered as the drug being in one of two phases. It is either in a micellar phase or an aqueous phase, and by that the standard free energy of solubilisation ($\Delta G^\circ{}_s$) can be expressed by the partition coefficient:

$$\Delta G^\circ{}_s = -RTlnK \tag{1.3}$$

So a decrease of free energy occurs as the drug enters micellar phase if the drug is hydrophobic.

Mathematical simulation of the solubilisation process shows that it starts by displacing solvent molecules from the micelle core. The drug or substance being loaded by the micelle then accumulates in the center, and starts pushing out on the hydrophobic ends. This consideration means extensive solubilisation, if allowed by the micelle, may result in larger micellar diameter. [19]

The compatibility between hydrophobic region and drug determines the loading efficacy of the micelles. It is based on polarity, hydrophobicity, and charge. Proper preparation or selection of the hydrophobic region allows compatibility with almost any drug of poor solubility. The compatibility can be considered by a Flory-Huggins interaction parameter, χ_{sp}, expressed as:

$$\chi_{sp} = (\delta_s - \delta_p)^2 \frac{V_s}{RT} \tag{1.4}$$

Index 's' denotes solubilised drug and 'p' is for polymer, in this case concerning the hydrophobic region (or more generally the core forming region in the event on a non-aqueous environment). δ is a Scatchard-Hildebrand solubility parameter, and V_s is the molar volume of the drug. δ is also known in connection with the phrase "like-dissolves-like", and like-ness refers to similar δ values. In short, lower values of χ_{sp} means better compatibility as this implies the δ are more similar in magnitude.

The balance and individual sizes of hydrophilic and hydrophobic region also play a role in the drug loading efficacy of micelles. A larger hydrophobic block means a larger core and thus better loading capacity. But, a larger hydrophilic block results, in general, in a higher CMC value and a smaller amount of surfactant molecules, at a given concentration, will contribute to the micellar phase and thereby not contribute to drug loading.

It was said that the balance between these two regions factors in. It does so, by influencing the release rate of a hydrophobic drug. The balance decides where in the core this particular drug is situated, and this results in the drug being trapped to a higher or lower degree depending on its properties in terms of polarity and hydrophobicity. Molecules trapped close to the corona will be responsible for a 'fast release' profile, whereas the drug molecules closer to the core center will be slow in their release profile. [20]

On the one hand, loading therapeutic agents into micelles provides stability, long circulation and, given proper loading conditions, better bioavailability. But, in continuation of the hydrophobic/hydrophilic balance contributing to slow or fast release, this balance can also be excessive in terms of entrapment and keeping drugs in the micelle. The drugs can become too stable in the micellar phase, because their partition coefficent 'K' is too high, recalling equation 1.3. [17]

The real challenge in the use of polymeric micelle drug delivery systems is finding a proper balance between micelle stability, their drug loading capacity, and ability to dissociate drugs again. [21]

1.2.1.3 Polymeric micelles in medical diagnostic imaging

Another use of polymeric micelles is in the area of medical diagnostic imagine. Methods of imaging include: Gamma-scintigraphy, magnetic resonance, computed tomography, ultra-sonography. Each method provides its own set of advantages and disadvantages in terms of sensitivity, resolution, need for contrast agents, cost, and safety. Regardless of method, medical diagnostic imaging requires sufficient separation of signal from are of interest and surrounding tissue. This means achieving the highest possible target-to-nontarget ratio is the primary focus of diagnostics. This is in opposition to therapeutics where it is key to achieve maximum target accumulation with less regard for the ratio.

Magnetic resonance imaging (MRI) is of particular interest here. Chelated paramagnetic metal moieties represent major interest areas when designing MR positive (T1) contrast agents. Figure 1.7 schematically depicts different strategies of incorporating contrast agents into micelles. They can be chemically attached to the surfactant molecule, added as monomers (requires the contrast molecule is connected to a hydrophobic region compatible with the surfactant core blocks), or chelated by the surfactant molecule by for instance the corona forming blocks.

It is important that the contrast molecules are able to interact with water molecules, as the contrast agent properties rely on changing the T1 relaxation time of the water in the sample. [22]

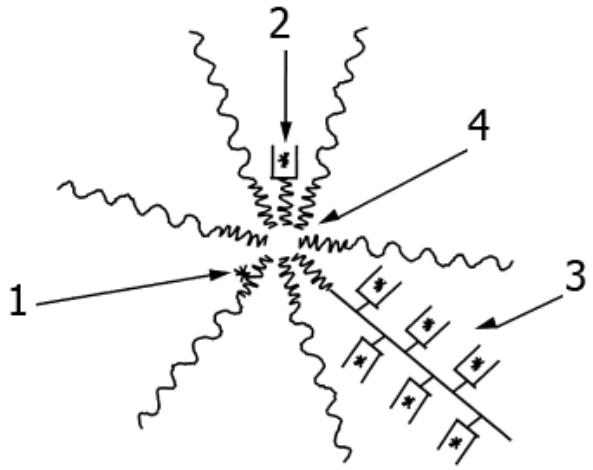

Figure 1.7: *It shows a method of determining the CMC by using a fluorescent dye. The dye has limited solubility in water, so as micelles form the dye fluoresces more intensely due to being solubilised in the core.[17]*

The latter mentioned method of incorporating contrast agent molecules relies on using a sort of polymers called polychelating amphiphilic polymers (PAP). Using PAPs allows an increase in the amount of contrast molecules per micelles, as it becomes a multiple of the aggregation number.

[17] reports developing a ca. 40% (w/w) Gd micellar system, corresponding to 8-10 metal atoms per polymer molecule. The method of fabrication reacts DTPA cyclic anhydride with primary amines on poly-L-lysine (PLL), creating numerous sites for chelation. The polychelating PLLs are then combined with a hydrophobic region to form PAPs and micellised.

1.2.1.4 Hydrogels for controlled release drug delivery

Hydrogels are homo- or copolymer gel networks with high water content, sometimes as high as 90% w/w. They have unique swelling abilities and 3D structural properties. As they are often comprised of hydrophilic polymers, the swelling ability allows uptake of large volumes of aqueous solutions containing for instance drugs as part of a drug delivery system. These qualities combined with their high degree of biocompatilibity and tissue-likeness means they are topics of extensive research and has been for decades. They are useful in a variety of scientific topics, including, as the section title suggests, drug delivery systems and biomedicine in general.

The tissue resemblance is attributed to the high water content, soft rubbery consistency and a low interfacial tension with water or biological fluids. Crosslinking between the network forming polymers means the gel does not dissolve when exposed to aqueous environments. The crosslinks are formed by covalent bonds, hydrogen bonds, van der Waals interactions, or physical entanglements.

Hydrogels are most often prepared from hydrophilic polymer matrices, and the subsequent crosslinking can be either chemical or physical. They are classifiable by different parameters such as polymer structure, method of preparation, or their thermo- and pH-sensitivity to name a few. The latter category is of greater interest with respect to drug delivery systems, as it allows degrees of targeting. Controlled release rate of

the drug loaded by the hydrogel can be diffusion-, swelling-, or chemically controlled. If for instance the swelling is controlling the release mechanism by physical entanglement, tuning the swell responsiveness to be thermo- or pH-sensitive allows simultaneous controlled release and targeted delivery by the same parameter.

An overview of various categories of hydrogels can be seen on figure 1.8

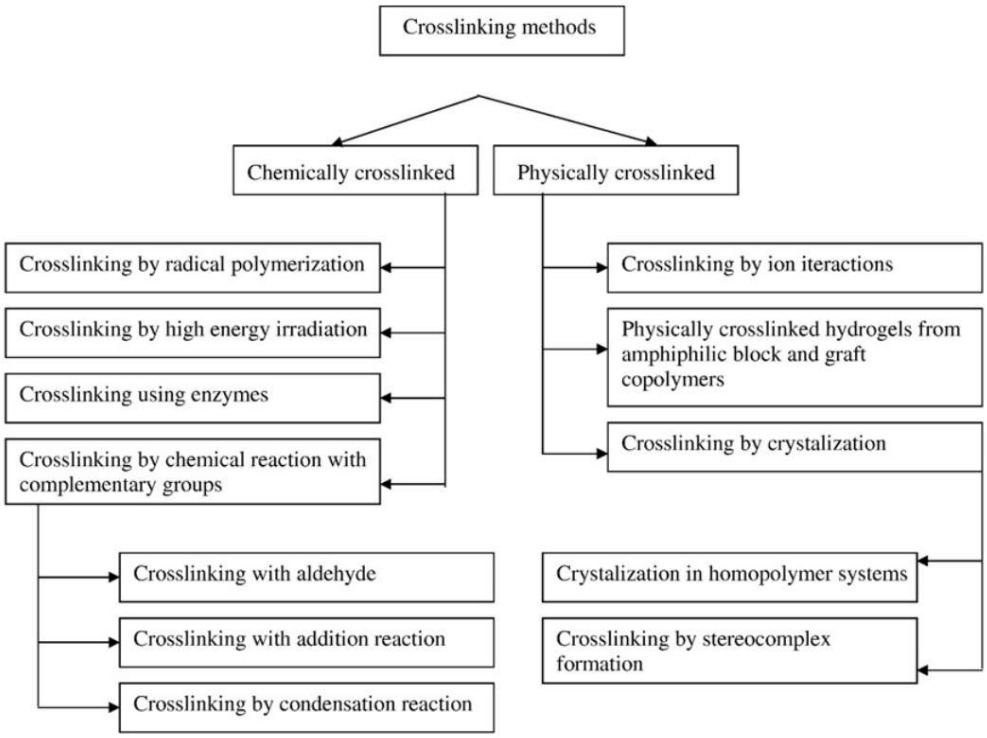

Figure 1.8: *Schematic of various crosslinking methods used for the synthesis of hydrogels.*

1.3 Copolymers

In a simple concept, the combination of two or more monomers forming one polymer molecule makes up a copolymer. Copolymers can be built following various patterns, where figure 1.9 shows a few of them.

As copolymers are built of different units, their properties can be tuned across the length of the molecule. In a block copolymer, the units chained in blocks. If A and B refer to two different units, A can be a hydrophilic unit and B can be hydrophobic. By building a block copolymer of A and B, called a di-block copolymer as it features two units, the result is an amphiphilic molecule. Expanding further, adding either A or B to the B or A terminal will create a tri-block copolymer and so forth.

A graft polymer (not shown on figure 1.9) looks similar to a block copolymer, except it has branched blocks. An amphiphile can be crafted in this case as well, by making the branched blocks hydrophobic or hydrophilic depending on main chain.

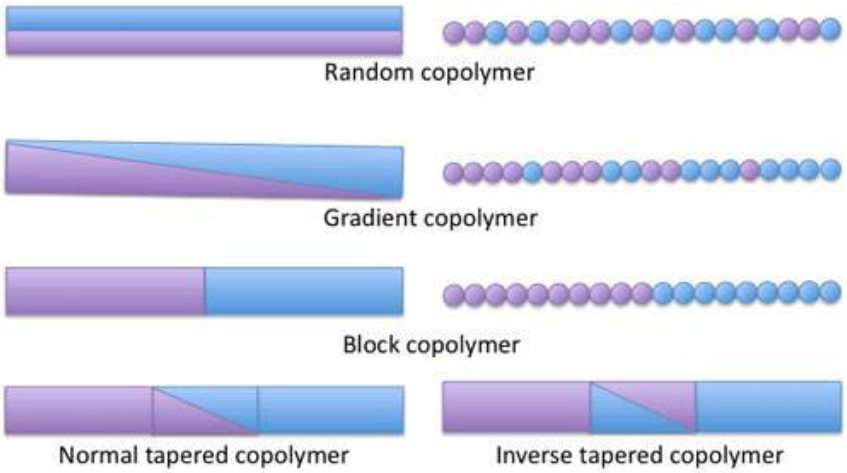

Figure 1.9: *Schematic of various types of copolymers. [23]*

A few examples of di-block, tri-block and graft copolymers are given on figure 1.10

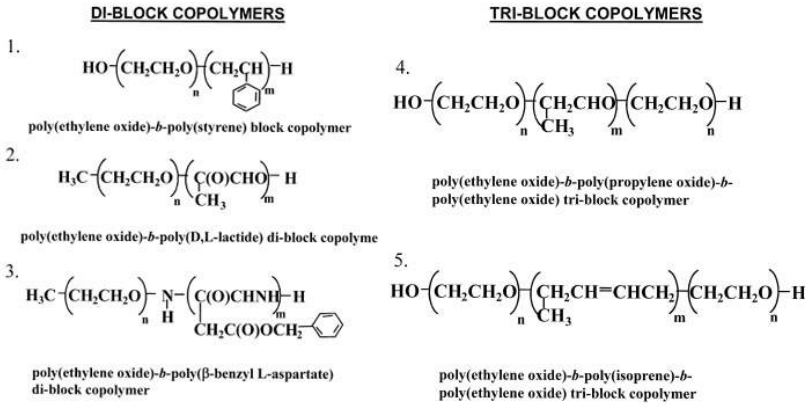

Figure 1.10: *Examples of various amphiphilic di- and tri-block copolymers. [17]*

Block copolymers are synthesised by anionic polymerisation, ring-opening polymerisation, or by polymerisation with the use of poly(ethylene glycol)-based initiators. These methods allow synthesis of amphiphilic copolymers of 1 to 10 kDa. [17][24]

1.4 Mechanisms of Endocytosis

Exposing cells, proteins, membranes, DNA, and organelles to nanoparticles causes a series of interactions to occur. These interactions depend on colloidal forces and biophysicochemical dynamics of the biological species at the 'nano-bio' interface. It is impossible to understand all the biochemical activity at play at this interface, but with pocket knowledge it is possible to create a conceptual framework to describe some of the interactions.

1.4.1 Boundaries of the nano-bio interface

Upon formation of the nano-bio interface, three dynicamilly interacting components can be classified: The nanoparticle surface, the solid-liquid interface to medium, and solid-liquid to the membrane of the biological substrate.

The nanoparticle surface is determined by its physicochemical composition, and the most important properties of this include: Chemical composition, surface functionalisation, shape, heterogeneity, hydrophobicity and -philicity.

Factors such as zeta potential, particle aggregation, state of dispersion, stability, dissolution characteristics, hydration and valence of surface layer are determined by the suspending medium: ionic strength, pH, temperature and presence of large organic molecules.

These properties determine the forces operating at the solid-liquid interface with the medium, whether they are dominated by van der Waals forces, electrostatic interactions, or short range interactions such as charge, steric, solvation, and solvent interactions.

A solid-liquid interface is often considered steady-state when handling bulk properties, but that is not the case for the nano-bio interface. The dynamic biological environment contributes to an inhomogenous distribution of proteins and lipis and other structures on both the particle-medium interface and the particle-bioconstituent interface. As a result, the nano-bio interface becomes less predictable and involves large numbers of forces and molecular interactions. [25]

1.4.2 Forces at the nanobio interface

Although the forces at play seem similar to those between colloidal particles, they require special consideration for the interactions at the nano-bio interface.

First of all, in biological fluids the ionic strength, often being about 150 mM, screens the electrostatic forces to within a few nanometres of the surface, and obscures zero frequency van der Waals forces.

The solvation effect is also important to consider, as it helps stabilise lyophilic nanoparticles.

Cell surfaces are readily deforming as a result of the fluidity and thermodynamics of the membrane. This in combination with issue of the cell surface being non-uniform in its charge distribution means interacting particles may experience different forces. This is dependent on the interacting particle as well, as the cells have heterogeneity of these sorts in the range of 10-50 nm, meaning a microparticle experiences little to no difference. But, a particle of 30 nanometers might not experience any charge or interaction at all, depending to a large degree on its specific location.

Figure 1.11 shows a table of the main forces interacting at the nano-bio interface. [25]

1.4.3 Protein corona

In biological fluids, nanoparticles are automatically coated with proteins. This coating is an important factor in deciding the surface properties, charge, resistance to aggregation, and hydrodynamic radius of the nanoparticles in situ.

Force	Origin and nature	Range (nm)	Possible impact on the interface
Hydrodynamic interactions	Convective drag, shear, lift and Brownian diffusion are often hindered or enhanced at nanoscale separations between interacting interfaces	10^2 to 10^6	Increase the frequency of collisions between nanoparticles and other surfaces responsible for transport
Electrodynamic interactions	VDW interactions arising from each of the interacting materials and the intervening media	1 to 100	Universally attractive in aqueous media; substantially smaller for biological media and cells owing to high water content
Electrostatic interactions	Charged interfaces attract counter-ions and repel co-ions through Coulombic forces, giving rise to the formation of an electrostatic double layer	1 to 100	Overlapping double layers are generally repulsive as most materials acquire negative charge in aqueous media, but can be attractive for oppositely charged materials
Solvent interactions	Lyophilic materials interact favourably with solvent molecules Lyophobic materials interact unfavourably with solvent molecules	1 to 10	Lyophilic materials are thermodynamically stable in the solvent and do not aggregate Lyophobic materials are spontaneously expelled from the bulk of the solvent and forced to aggregate or accumulate at an interface
Steric interactions	Polymeric species adsorbed to inorganic particles or biopolymers expressed at the surfaces of cells give rise to spring-like repulsive interactions with other interfaces	1 to 100[a]	Generally increase stability of individual particles but can interfere in cellular uptake, especially when surface polymers are highly water-soluble
Polymer bridging interactions	Polymeric species adsorbed to inorganic particles or biopolymers expressed at the surfaces of cells containing charged functional groups can be attracted by oppositely charged moieties on a substrate surface	1 to 100	Generally promote aggregation or deposition, particularly when charge functionality is carboxylic acid and dispersed in aqueous media containing calcium ions

[a]Depending on the length of adsorbed or expressed polymeric species

Figure 1.11: *Main forces of interaction and the nano-bio interface. [25]*

The proteins making up the corona is controlled by the particle surface composition, as this decides what proteins can interact. Carbon nanotubes, iron oxide particles, liposomes, and polymeric nanoparticles are most often coated by albumin, immunoglobulins, complement, fibrinogen, and apolipoproteins. In continuation, immunoglobulins and complement promotes receptor-mediated phagocytosis, and opsonisation to name an example. This has its uses in immunology for instance, but can also be an issue in cases where long circulation times are required.

Endocytic activity can be increased by deliberate attachment of protein ligands in the would-be corona space, or by using the spontaneously formed corona. It is not very well understood however. [25]

1.4.4 Membrane particle wrapping

Particle adhesion and wrapping by the membrane require specific and nonspecific binding interactions to be greater than the forces resisting particle uptake. The membrane receptors must be present at the site by diffusion to perform a series of critical operations.

Cellular uptake is determined by a number of factors such as size, shape, and curvature. In terms of size, optimal conditions exist, above and below which uptake is reduced. A value of 30 nm has been deduced as optimal for spherical particles. Coating of particle surfaces, be that the protein corona or deliberate coating, will affect this wrapping efficiency based on size, coating density, receptor diffusion, and free energy changes.

When wrapping around an exterior particulate system it is important entirety of said particle can be taken up by the cell. In the case of multi-walled carbon nano tubes (MWCNTs), which are able to form fibrous structures, problems arise when their aspect ratio is too great for the cell. One dimension of the tubes facilitate efficient uptake initially, but the fibrous tubes are too long ($>20\mu$) and protrude the cell wall, causing a phenomenon called 'frustrated phagocytosis' to occur. In an attempt to remedy the situation, a

large number of harmful oxygen radicals and hydrolytic enzymes are called to the site, leading to chronic inflammation. [25]

Materials and methods 2

2.1 Materials

Material	Manufacturer	Description
Acetic acid	Sigma-Aldrich	⩾99%
Acetone	Sigma-Aldrich	⩾99.5%
Acetonitrile	Th.Geyer	
Amino acids (Fmoc-AA)	Advanced Chemtech	Stored at 5°C
Arsenazo	Sigma-Aldrich	
Chloroacetamide	Sigma-Aldrich	
Chloroform	Sigma-Aldrich	
Curcumin	Sigma-Aldrich	Stored at 5°C
DCM	Iris Biotech Gmbh	
Diethylether	Iris Biotech Gmbh	Stored at -20°C
DIPEA	Sigma-Aldrich	
Dialysis tubing	Spectrum Labs	Standard grade, 3,000 MWCO
DiI	Life technologies	Molecular Probes, protect from light
DMEM 1X	Gibco, Thermo Fisher Scientific	Glutamax
DMEM F12	Gibco, Thermo Fisher Scientific	
DMF	Iris Biotech Gmbh	
DMSO	Th.Geyer	
DTPA	Fluka	
DTPA dianhydride	Sigma-Aldrich	Stored at -20°C
EDC	Fluka	Stored at -20°C
EDTA	Sigma-Aldrich	Anhydrous crystalline
Ethylenediamine	Fluka	⩾99.5%
Fibroblast cells	LSR stock	CRL 2429, *Homo sapiens*, from skin tissue
Fluorescamine	Sigma-Aldrich	
Continued		

Table 2.1: *List of materials used throughout the project.*

Material	Manufacturer	Description
Formaldehyde	Sigma-Aldrich	Formalin solution, 10% neutral buffered
$GdCl_3$	Strem Chemicals	
Glioblastoma cells	LSR stock	U87 2429, *Homo sapiens*, from brain tissue
HBTU	Iris Biotech Gmbh	
HCl	Sigma-Aldrich	⩾37%
Heparin	-	Supplied by Aalborg University Hospital
Imidazole	Sigma-Aldrich	
Isoproanol	Sigma-Aldrich	
KCl	Fluka	
K_2HPO_4	Sigma-Aldrich	
KOH	AppliChem	
MES	Fluka	
NaCl	-	Aalborg University
Na_2HPO_4	Merck	
$NaHCO_3$	Fluka	
NaOH	Bie & Berntsen	Old at the time of use
NHS	Sigma-Aldrich	
Nude mice	-	Supplied and handled by Aalborg University Hospital
OxymaPure	Merck Millipore	
PBS 10X	Thermo Fisher Scientific	Without calcium and magnesium
Piperidine	Iris Biotech Gmbh	
Polymers	-	Supplied by Aalborg University
Resin	Advanced Chemtech	Stored at 5°C
Sodium Ethoxide	Sigma-Aldrich	
TFA	Iris Biotech Gmbh	
TIS	Iris Biotech Gmbh	
Trypsin	Thermo Fisher Scientific	2.5% without phenol red
Ultrafiltration tubes	EMD MilliPore	Amicon, 3,000 MWCO
4 well falcon culture slides	Thermo Fisher Scientific	Borosilicate
12-well cell culture plates	Greiner Bio-One, Thermo Fisher Scientific	Polystyrene
Equipment	**Manufacturer**	**Description**
Activo-P11 Automated Peptide Synthesizer	Activotec	With UV monitoring
Activo-P12 Cleavage Device	Activotec	
Axio Observer.Z1	Carl Zeiss	Inverted microscope
AxioCam MRm	Carl Zeiss	Digital Camera
NanoSight LM10	Malvern	
UltiMate 3000 Standard LC Systems	Dionex	With peak collector

Table 2.2: *List of materials and equipment used throughout the project.*

2.2 Methods

Chemical structure of polymer PVP and the two variants used in this project are shown on figure 2.1.

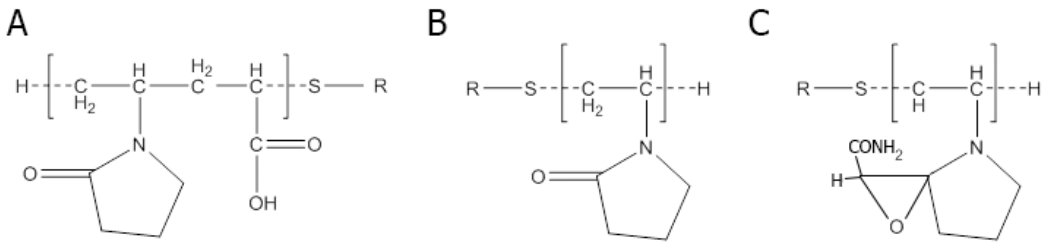

Figure 2.1: *Chemical structure of the polymers used throughout the project. R = $C_{18}H_{37}$, octadecyl.* ***A:*** *PVP-COOH,* ***B:*** *PVP, and* ***C:*** *PVGP.*

2.2.1 Synthesis of DiI loaded micelles

2.2.1.1 DiI loaded PVP_{1000} micelles

1. (1): Dissolve 50 mg PVP_{1000} in 8 mL MilliQ
2. (2): Dissolve 5 mg DiI in 1 mL Chloroform
3. (3): Mix (1) and (2)
4. Sonicate (3) by probe 10 minutes, 50%, 1s on 2s off
5. Vacuum rotary evaporate (3) until dry
6. Freeze (3) in liquid nitrogen and lyophilise

2.2.1.2 DiI loaded PVP_{12000} micelles

1. (1): Dissolve 50 mg PVP_{12000} in 8 mL MilliQ
2. (2): Dissolve 5 mg DiI in 1 mL Chloroform
3. (3): Mix (1) and (2)
4. Sonicate (3) by probe 10 minutes, 50%, 1s on 2s off
5. Vacuum rotary evaporate (3) until dry
6. Freeze (3) in liquid nitrogen and lyophilise

2.2.2 Synthesis of curcumin loaded PVP_{1000} micelles

2.2.2.1 Protocol A

1. (1): Dissolve 50 mg PVP_{1000} in 8 mL MilliQ
2. (2): Dissolve 5 mg curcumin in 1 mL acetone
3. (3): Mix (1) and (2)
4. Sonicate (3) by probe 10 minutes, 50%, 1s on 2s off
5. Vacuum rotary evaporate (3) until dry
6. Freeze (3) in liquid nitrogen and lyophilise

2.2.2.2 Protocol B

1. (1): Dissolve 50 mg PVP_{1000} in 8 mL MilliQ
2. (2): Dissolve 5 mg curcumin in 1 mL acetone
3. (3): Mix (1) and (2)
4. Sonicate (3) by probe 10 minutes, 50%, 1s on 2s off
5. Freeze (3) in liquid nitrogen and lyophilise

2.2.2.3 Protocol C

1. (1): Dissolve 50 mg PVP_{1000} in 8 mL MilliQ
2. (2): Dissolve 5 mg curcumin in 1 mL dichloromethane
3. (3): Mix (1) and (2)
4. Sonicate (3) by probe 10 minutes, 50%, 1s on 2s off
5. Freeze (3) in liquid nitrogen and lyophilise

2.2.3 Nanoparticle tracking analysis for size distribution

2.2.3.1 Protocol A - no preparation steps

1. (1): After drying, weigh out 5-10 mg lyophilisate and dissolve in 1 ml
2. Using 1 mL Luer syringe, transfer (1) to Nanosight prism cell
3. With softwate NTA 2.1 locate thumbprint, move slightly right and adjust focus to particles
4. Record at least 120 seconds of acculumated footage
5. Adjust settings until all particles are marked by a cross, and only one cross each
6. Process recording

2.2.3.2 Protocol B - preparation included

1. (1): After drying, weigh out 5-10 mg lyophilisate and dissolve in 1 ml
2. Sonicate (1) in ultrasound bath for 60 minutes, optionally agitate (shaking) after 30 minutes
3. Centrifugate (1) at 10,000g 10 minutes
4. Using 1 mL Luer syringe, transfer (1) to Nanosight prism cell
5. With softwate NTA 2.1 locate thumbprint, move slightly right and adjust focus to particles
6. Record at least 120 seconds of acculumated footage
7. Adjust settings until all particles are marked by a cross, and only one cross each
8. Process recording

2.2.4 Standard epoxidation protocol

1. (1): Dissolve PVP and chloroacetamide in dry isopropanol in a container with a lid
2. Add sodium ethoxide dropwise to (1)
3. Stir (1) 5 hours at room temperature
4. Centrifugate (1) at 7,000 rcf 10 minutes 4 °C
5. Discard supernatant as waste
6. Freeze and lyophilise the pellet
7. Pellet should be stored in airtight containter

Molar ratios of 'functional groups of PVP':chloroacetamide:Sodium(Sodium ethoxide) should be 1:0.75:1, and the volume of isopropanol should be roughly 1 ml per 100 mg PVP.

2.2.4.1 Epoxy titration

1. Dissolve 100 mg standard epoxidised PVP in 10 ml 0.1 M HCl
2. Titrate by adding volumes of 0.1 M NaOH until equivalence
3. The concentration can be calculated by the molar offset at the point of equivalence

2.2.5 Synthesis of PVP_{12000}-DTPA-GD

2.2.5.1 Protocol A

1. (1): Dissolve 0.75 g PVP_{12000} and 0.54 g chloroacetamide in 10 ml dry isopropanol
2. Add sodium ethoxide dropwise to (1)
3. Stir (1) 5 hours at room temperature
4. Centrifugate (1) at 7,000 rcf 10 minutes 4 °C
5. Discard supernatant as waste
6. Resuspend pellet in isopropanol and dissolve, may need bath ultrasound to dissolve
7. Repeat steps 4-6 at least 2 times
8. (2): Split the volume of (1) in two and store one half in the fridge (dissolved in isopropanol). The other half is (2)
9. Centrifugate (2) at 10,000 rcf 4 °C and discard supernatant
10. (3): Dissolve 100 mg DTPA and 80 mg imidazole in 15 ml DMSO
11. Add (3) to the pellet of (2) and dissolve
12. Stir (3) and leave reaction running 72 hours
13. Centrifugate (3) at 7,000 rcf 10 minutes at 4 °C
14. (4): Transfer supernatant to 50 ml Greiner centrifuge tube
15. Add 10 ml MilliQ to pellet of (3), but do not dissolve
16. Centrifugate (3) and add supernatant to (4) (exoterm reaction will be observed combining DMSO and MilliQ)
17. Dissolve pellet of (3) in 10 ml MilliQ
18. Dialyse (3) and (4) against MilliQ 48 hours
19. Freeze (3) and (4) in liquid nitrogen and lyophilise (splitting the samples is convenient before lyophilysis due to volume increase following dialysis)
20. Dissolve 600 mg $GdCl_3$ in 10 ml MilliQ and add 5 ml to (3) and (4)
21. Incubate 24 hours room temperature
22. Freeze in liquid nitrogen and lyophilise
23. Reconstitute in 0.5 ml MilliQ and apply ultrafiltration

2.2.5.2 Protocol B

1. (1): Dissolve 0.75 g PVP_{12000} and 0.54 g chloroacetamide in 10 ml dry isopropanol
2. Add sodium ethoxide dropwise to (1)
3. Stir (1) 5 hours at room temperature
4. Centrifugate (1) at 7,000 rcf 10 minutes 4 °C
5. Discard supernatant as waste
6. Resuspend pellet in isopropanol and dissolve, may need bath ultrasound to dissolve
7. Repeat steps 4-6 at least 2 times
8. (2): Split the volume of (1) in two and store one half in the fridge (dissolved in isopropanol). The other half is (2)
9. Centrifugate (2) at 10,000 rcf 4 °C and discard supernatant
10. (3): Dissolve 100 mg DTPA and 80 mg imidazole in 15 ml DMSO
11. Add (3) to the pellet of (2) and dissolve
12. Heat to 65°C and stir 24 hours
13. Dialyse (3) against MilliQ 48 hours
14. Freeze (3) in liquid nitrogen and lyophilise
15. Dissolve 30 mg $GdCl_3$ in 0.5 ml MilliQ and add to (3)
16. Wait 15 minutes while mildly agitating sample
17. Apply ultrafiltration

2.2.5.3 Protocol C

1. (1): Dissolve 100 mg DTPA and 80 mg imidazole in 20 ml DMSO
2. Dissolve 200 mg standard epoxidised PVP_{12000} in (1)
3. Stir 24 hours at 65°C
4. Dialyse (1) 48 h against MilliQ
5. Freeze (1) in liquid nitrogen and lyophilise
6. Reconstitute (1) in 0.5 ml 60 mg/ml aqueous $GdCl_3$
7. Wait 15 minutes while mildly agitating sample
8. Apply ultrafiltration

2.2.5.4 Protocol D

1. (1): Dissolve 100 mg DTPA and 80 mg imidazole in 20 ml DMSO
2. Dissolve 200 mg standard epoxidised PVP_{12000} in (1)
3. Stir 24 hours at room temperature
4. Dialyse (1) 48 h against MilliQ
5. Freeze (1) in liquid nitrogen and lyophilise
6. Reconstitute (1) in 0.5 ml 60 mg/ml aqueous $GdCl_3$
7. Wait 15 minutes while mildly agitating sample
8. Apply ultrafiltration

2.2.5.5 Protocol E

1. (1): Dissolve 800 mg DTPA and 400 mg imidazole in 100 ml DMSO and split in four flasks
2. Dissolve 30, 60, 120 and 200 mg standard epoxidised PVP_{12000} in (1) respectively (resulting in four different ratios of polymer:DTPA)
3. Stir 24 hours at room temperature
4. Dialyse (1) 48 h against MilliQ
5. Freeze (1) in liquid nitrogen and lyophilise
6. Reconstitute (1) in 0.5 ml 60 mg/ml aqueous $GdCl_3$
7. Wait 15 minutes while mildly agitating sample
8. Apply ultrafiltration

2.2.6 Synthesis of PVP_{12000}-EN-DTPA-Gd

2.2.6.1 Protocol A

1. (1): Dissolve and dilute 50 mg standard epoxidised PVP_{12000} and 10 μl EN in 1 ml MilliQ
2. Stir (1) for 2 hours at room temperature
3. Apply ultrafiltration to remove excess EN
4. (2): Dissolve 100 mg DTPA in 10 ml MilliQ by heating to 40 °C and stirring
5. Dissolve 120 mg NHS in (1)
6. Dissolve 100 mg EDC in (1)
7. (3): Add (1) to (2)

2.2.6.2 Protocol B

1. (1): Dissolve and dilute 50 mg standard epoxidised PVP_{12000} and 10 μl EN in 1 ml MilliQ
2. Stir (1) for 2 hours at room temperature
3. Apply ultrafiltration to remove excess EN
4. Dissolve 100 mg DTPA dianhydride in (1)
5. Stir (1) 2 hours at room temperature
6. Dissolve 150 mg $GdCl_3$ in (1) and wait 15 minutes
7. Apply ultrafiltration
8. Freeze in liquid nitrogen and lyophilise

2.2.6.3 Protocol C

1. (1): Dissolve and dilute 200 mg standard epoxidised PVP_{12000} and 40 μl EN in 10 ml MilliQ
2. Stir (1) 2 hours at room temperature
3. Freeze (1) in liquid nitrogen and lyophilise 24 hours
4. Reconstitute (1) in 10 ml MilliQ and repeat previous lyophilisation step
5. Reconstitute (1) in 2 ml MilliQ
6. Dissolve 200 mg DTPA dianhydride in (1)
7. Dissolve 17 mg $NaHCO_3$ in (1) and add NaOH until pH is 8
8. Stir (1) 2 hours at room temperature
9. Dissolve 200 mg $GdCl_3$ in (1) and wait 15 minutes
10. Apply ultrafiltration to (1)

2.2.6.4 Protocol D

1. (1): Dissolve 25 mg KOH in 10 ml DMSO by heating to 60 °C
2. Dissolve and dilute 50 mg standard epoxidised PVP_{12000} and 10 μl ethylenediamine in (1)
3. Stir (1) 2 hours at room temperature
4. Add 2 ml 1 M HCl (1) (check pH, should be less than 12)
5. Dialyse (1) 24 hours against MilliQ
6. Freeze (1) in liquid nitrogen and lyophilise

7. Reconstitute (1) in 2 ml MilliQ
8. Dissolve 100 mg DTPA dianhydride in (1)
9. Dissolve 17 mg $NaHCO_3$ in (1) and add NaOH until pH is 8
10. Stir (1) 2 hours at room temperature
11. Dissolve 100 mg $GdCl_3$ in (1) and wait 15 minutes
12. Apply ultrafiltration to (1)

2.2.7 Ultrafiltration

2.2.7.1 0.5 ml maximum volume

1. Transfer sample to 0.5 ml ultrafiltration tube
2. Centrifugate at 14,000g for 30 minutes, or until volume reaches bottom of outlet canals corresponding to 50 μl
3. Add 450 μl solvent
4. Repeat steps 2 and 3 until desired upconcentration is reached. Each round upconcentrates x10.
5. Recover sample by pipettation, or turn ultrafiltration tube upside down into clean container of fitting size, and centrifugate at 1,000 rcf for 2 minutes.

2.2.7.2 5 ml maximum volume

1. Transfer sample to 5 ml ultrafiltration tube
2. Centrifugate at 7,500g for 30 minutes, or until volume reaches bottom of outlet canals corresponding to 50 μl
3. Fill ultrafiltration tube to '5 ml' indent
4. Repeat steps 2 and 3 until desired upconcentration is reached. Each round upconcentrates x100.
5. Recover sample by pipettation, or turn ultrafiltration tube upside down into clean container of fitting size, and centrifugate at 1,000 rcf for 2 minutes.

Note for 5 ml maximum volume: If the supplied collection tube does not fit the centrifugation "cup" (the cup that adapts the size to fit the rotary vessel), it is necessary place the ultrafiltration tube in a regular 15 ml Greiner centrifuge tube.

2.2.8 Synthesis of PVP-COOH$_{12000}$-EN-DTPA-Gd

1. Dissolve 200 mg MES and 260 mg NHS in 8 ml MilliQ (1)
2. Dissolve 288 mg EDC in (1)
3. Dissolve 100 mg 90% carboxylated PVP in (1) and wait 15 minutes
4. Dilute 200 μl EN to 2 ml in MilliQ (2)
5. Add (1) slowly to (2), while stirring if possible
6. Dialyse (2) against MilliQ for 24 h against 3x1 L (changing water per first two hours)
7. Freeze (2) in liquid nitrogen and lyophilise
8. Reconstitute lyophilisate in 10 ml MilliQ
9. Centrifugate 10 minutes at 10,000 g
10. Discard supernatant and repeat above centrifugation step 3-4 times

2.2.9 Mixed micelles

2.2.9.1 Protocol A

1. Dissolve 200 mg MES in 20 ml 1:1 V(DMSO):V(MilliQ) (1) (50 ml Greiner centrifuge tube)
2. Dissolve 260 mg NHS in (1)
3. Dissolve 288 mg EDC in (1)
4. Dissolve 50 mg PVP$_{6000}$ and 100 mg 90% carboxylated in (1)
5. Dilute 200 μl EN 1:10 in MilliQ (2)
6. Slowly add (1) to (2) and leave on shaker at 100-150 RPM for 1 h
7. Transfer (2) to evaporator flask
8. Evaporate by rotary vacuum evaporation until solution stops bubbling, ~30 min
9. Add 10 ml MilliQ to PVP-EN
10. Add carbonate buffer and NaOH to (2)
11. Add DTPA anhydride to (2)
12. Shake 2 h at 100-150 RPM
13. Dialyse against MilliQ, gets rid of non-carboxylated polymer, as well as reactants and changes solvent back to MilliQ. Remaining product should be PVP-EN-DTPA and residual reactants
14. Add $GdCl_3$ to (2)

15. Wait 1 hour
16. Add 50 mg PVP_{6000} to (2)
17. Dissolve 15 mg Curcumin in 3 ml acetone and add to (2)
18. Transfer (2) to 250 ml bluecap bottle, cover in ice and sonicate by probe 10 minutes, 1s on 2s off at 50% amp
19. Freeze in liquid nitrogen or freezer (note: time consuming and allows sedimentation) and lyophilise
20. Reconstitute (2) and add 1 mmole NaOH to dissolve material
21. Centrifugate at 5,000 g and store supernatant (wrap in alufoil)
22. Add 2 ml 5% v/v DMSO MilliQ to pellet of (2), and sonicate by probe 10 minutes, 1s on 2s off at 50% amp
23. Combine redissolved pellet and supernatant of (2), and apply ultrafiltration

2.2.9.2 Protocol B

1. (1): Dissolve 200 mg MES in 20 ml 1:1 V(DMSO):V(MilliQ) (50 ml Greiner centrifuge tube)
2. Dissolve 250 mg NHS in (1)
3. Dissolve 270 mg EDC in (1)
4. Dissolve 50 mg PVP_{1000} and 100 mg 90% carboxylated in (1)
5. (2): Dilute 200 μl EN 1:10 in MilliQ
6. Slowly add (1) to (2) and leave on shaker at 100-150 RPM for 1 h
7. Transfer (2) to evaporator flask
8. Evaporate by rotary vacuum evaporation until solution stops bubbling, ~30 min
9. Add 10 ml MilliQ to (2)
10. Add carbonate buffer and NaOH to (2)
11. Add DTPA anhydride to (2)
12. Shake 2 h at 100-150 RPM
13. Dialyse against MilliQ, gets rid of non-carboxylated polymer, as well as reactants and changes solvent back to MilliQ. Remaining product should be PVP-EN-DTPA and residual reactants
14. Add $GdCl_3$ to (2)
15. Wait 1 h
16. Add 1 ml 1M NaOH to (2)

17. Dissolve 15 mg Curcumin in 3 ml acetone and add to (2)
18. Transfer (2) to 250 ml bluecap bottle, cover in ice and sonicate by probe 10 minutes, 1s on 2s off at 50% amp
19. Freeze in liquid nitrogen or freezer (time consuming and allows sedimentation) and lyophilise
20. Reconstitute in 5 ml MilliQ
21. (3): Centrifugate at 5,000 g and store supernatant (wrap in alufoil)
22. (4): Add 2 ml 5% v/v DMSO MilliQ to pellet, and sonicate by probe 10 minutes, 1s on 2s off at 50% amp
23. Recombine (3) and (4), and apply ultrafiltration to upconcentrate.

2.2.9.3 Protocol C

1. (1): Dissolve 25 mg PVP-COOH 95% and 25 mg PVP_{6000} in 7 ml MilliQ and add 1 ml 1 M NaOH
2. (2): Dissolve 5 mg Curcumin in 1 ml acetone
3. (3): Mix (1) and (2)
4. Cover (3) in ice and sonicate by probe 10 minutes, 1s on 2s off at 50% amp
5. Add 100 mg $GdCl_3$ to (3) while stirring heavily (an addition of 1ml of 1 M NaOH may be necessary)
6. Freeze in liquid nitrogen or freezer and lyophilise
7. Reconstitute in 5 ml PBS and apply ultrafiltration to upconcentrate and filter out free Gd^{3+} ions
8. Readjust pH by adding 2 μl 3M HCl

2.2.9.4 Protocol D

1. (1): Dissolve 40 mg PVP-COOH 95% and 10 mg PVP_{6000} in 7 ml MilliQ and add 1 ml 1 M NaOH
2. (2): Dissolve 5 mg Curcumin in 1 ml acetone
3. (3): Mix (1) and (2)
4. Cover (3) in ice and sonicate by probe 10 minutes, 1s on 2s off at 50% amp
5. Add 100 mg $GdCl_3$ to (3) while stirring heavily
6. Freeze in liquid nitrogen or freezer and lyophilise
7. Reconstitute in 5 ml PBS and apply ultrafiltration to upconcentrate and filter out free Gd^{3+} ions

2.2.9.5 Protocol E

1. (1): Dissolve 30 mg PVP-COOH 95% and 20 mg PVP_{6000} in 7 ml MilliQ and add 1 ml 1 M NaOH
2. (2): Dissolve 5 mg Curcumin in 1 ml acetone
3. (3): Mix (1) and (2)
4. Cover (3) in ice and sonicate by probe 10 minutes, 1s on 2s off at 50% amp
5. Add 100 mg $GdCl_3$ to (3) while stirring heavily
6. Freeze in liquid nitrogen or freezer and lyophilise
7. Reconstitute in 5 ml PBS and apply ultrafiltration to upconcentrate and filter out free Gd^{3+} ions

2.2.9.6 Protocol F

1. (1): Dissolve 40 mg PVP-COOH 95% and 10 mg PVP_{12000} in 7 ml MilliQ and add 1 ml 1 M NaOH
2. (2): Dissolve 5 mg Curcumin in 1 ml acetone
3. (3): Mix (1) and (2)
4. Cover (3) in ice and sonicate by probe 10 minutes, 1s on 2s off at 50% amp
5. Add 100 mg $GdCl_3$ to (3) while stirring heavily
6. Freeze in liquid nitrogen or freezer and lyophilise
7. Reconstitute in 5 ml PBS and apply ultrafiltration to upconcentrate and filter out free Gd^{3+} ions

2.2.9.7 Protocol G

1. (1): Dissolve 30 mg PVP-COOH 95% and 20 mg PVP_{12000} in 7 ml MilliQ and add 1 ml 1 M NaOH
2. (2): Dissolve 5 mg Curcumin in 1 ml acetone
3. (3): Mix (1) and (2)
4. Cover (3) in ice and sonicate by probe 10 minutes, 1s on 2s off at 50% amp
5. Add 100 mg $GdCl_3$ to (3) while stirring heavily
6. Freeze in liquid nitrogen or freezer and lyophilise
7. Reconstitute in 5 ml PBS and apply ultrafiltration to upconcentrate and filter out free Gd^{3+} ions

2.2.9.8 Protocol H

1. (1): Dissolve 50 mg PVP-COOH 95% in 7 ml MilliQ and add 1 ml 1 M NaOH
2. (2): Dissolve 5 mg Curcumin in 1 ml acetone
3. (3): Mix (1) and (2)
4. Cover (3) in ice and sonicate by probe 10 minutes, 1s on 2s off at 50% amp
5. Add 100 mg $GdCl_3$ to (3) while stirring heavily (an addition of 1ml of 1 M NaOH may be necessary)
6. Freeze in liquid nitrogen or freezer and lyophilise
7. Reconstitute in 5 ml PBS and apply ultrafiltration to upconcentrate and filter out free Gd^{3+} ions
8. Readjust pH by adding 2 μl 3M HCl

2.2.10 Attaching FALGEA to carboxylated PVP

Attachment of AEGLAFK to PVP-COOH using EDC amine coupling:

1. (1): Dissolve 200 mg MES and 260 mg NHS in 20 ml MilliQ
2. Dissolve 290 mg EDC in (1)
3. Dissolve 50 mg carboxylated PVP and 50 mg PVP_{1000} and dissolve in (1)
4. Dissolve 20 mg non-purified FALGEA (1)
5. Shake at 100 RPM for 30 minutes
6. Dialyse against MilliQ 24 hours
7. Freeze in liquid nitrogen or freezer and lyphilise

2.2.11 Synthesis of PVP-GD-FALGEA micelles

1. (1): Dissolve 30 mg carboxylated PVP, 30 mg PVP-FALGEA (lyophilisate) 30 mg PVP_{6000} in 10 ml MilliQ and add 2 ml 1 M NaOH
2. (2): Dissolve curcumine in acetone 5 mg/ml
3. (3): Add 1.5 ml of (2) to (1)
4. Cover (3) in ice and sonicate by probe 10 minutes, 1s on 2s off at 50% amp
5. Add 2 ml 1 M NaOH
6. Add 150 mg $GdCl_3$ while stirring and continue stirring 15 minutes
7. Freeze in liquid nitrogen and lyophilise
8. Reconstitute in 5 ml PBS and apply ultrafiltration to upconcentrate and filter out free Gd^{3+} ions
9. Readjust pH by adding 3 μl 3M HCl

2.2.12 Growing glioblastoma and fibroblast cell lines

The protocols used for glioblastoma U87 and fibroblast CRL 2429 cells lines were identical, and they will be referred to as 'cells'.

2.2.12.1 Preparation of growth medium DMEM 10% FCS 1% P/S

1. (1): Add 1 ml P/S and 10 ml FCS to 500 ml DMEM 1X Glutamax or DMEM F12
2. Filter through .22 μm sterile filter by vacuum pump into a suitable autoclaved container
3. Store in the fridge

2.2.12.2 Starting cell culture

1. (1): Heat 30 ml growth medium to 37 °C by waterbath
2. (2): Thaw a 1 ml vial containing 1 million cells suspended in DMSO
3. (3): Mix (1) and (2) and transfer to T175 cell culture flask
4. Incubate (3) overnight at 37 °C and change medium
5. Change medium every two or three days until cells become confluent
6. Split cells by passage to a suitable degree (1/5 or more) depending on confluency and required amount of cells

2.2.12.3 Preparing PBS

1. Dilute PBS 10X 1:10 in .22 μm sterile filter cup and filter by vacuum pump into a suitable autoclaved container
2. Store at room temperature

2.2.12.4 Prepating T/E

1. (1): Dilute trypsin 1:10 into 10 ml PBS and filter through .22 μm by vacuum pump
2. (2): Dissolve EDTA to 0.02% and filter through .22 μm by vacuum pump
3. (3): Mix (1) and (2) 1:1 v/v (result is 0.125% / 0.01% T/E)

2.2.12.5 Passing cells

1. (1): Heat 50 ml growth medium to 37 °C by waterbath
2. Wash cells by filtered PBS twice and empty the flask
3. Trypsinate by adding T/E to cover bottom of culture flask (3 ml for T175)
4. Incubate at 37 °C 5-10 minutes (This step is toxic to the cells so it must not be overdone, cells need to jump off the bottom)
5. (2): Add 10 ml of (1) (or less depending on flask size) to culture flask, and transfer entire volume to 15 ml Purple Cap Greiner centrifuge tube
6. Centrifugate (2) at 300 RPM for 5 minutes
7. Take out desired amount (known either by confluency prior to splitting or by counting cells), and transfer to new culture flask or multiwells

2.2.12.6 Cell transfer to wells

1. Prepare cells for passage by protocol 2.2.12.5
2. Add 50% well volume (1 ml for 12 well PS plates, 0.9 ml for 4 well borosilicate wells) to each well and incubate at 37 °C 10 minutes
3. Dilute cell suspension from step 1 to suitable volume for required amount of wells, and 50% well volume μl growth medium containing cells to each well and incubate at room temperature (without moving wells plates) 20 minutes
4. Move to incubation at 37 °C and grow until confluence is suitable for experimentation

2.2.13 Microscopy of drug uptake *in vitro*

The protocol features three lines per cell type and optional duplicate line. One blank line, one inhibited by dynasore and one inhibited by wortmannin. The total number of wells is then $wells = 3SDC$, where S is steps in time, D is amount of duplicate wells (D = 1 for none), and C is amount of cell types. The amount of wells has a large influene on the required volumes throughout the protocol. Well volume is 1 ml for 12 well polystyrene plates, 0.9 ml for 4 well borosilicate chambered slides.

Solutions:

- Dynasore: 250 μl 1mg/ml per 20 ml growth medium
- Wortmannin: 5 *mu*l 0.2 mg/ml per 47 ml growth medium
- Hoechst: Dilute 1:1000 in growth medium

Adding hoechst dye to cells:

1. Empty all wells of medium
2. Add 100% well volume of Hoechst solution to all wells
3. Incubate 15 minutes at room temperature
4. Wash all wells 2 times with growth medium

Incubating cells with endocytosis inhibitors:

1. Add 50% well volume growth medium too all wells labeled blank
2. Add 50% well volume Dynasore solution to all wells labeled Dynasore
3. Add 50% well volume Wortmannin solution to all wells labeled Wortmannin
4. Incubate all wells at 37 °C 30 minutes

Exposing cells to micelles:

1. Add 50% well volume of micelles in growth medium to wells corresponding to last time step
2. Wait appropriate amount of time (time from last to second-to-last time step) and repeat until first time step is fulfilled
3. Wash all wells 2 times by medium (start with the most time sensitive ones)
4. If no preservation step is performed, add 100 % well volume growth medium to all wells. The wells are now ready for experimentation
5. If preservation is desired, add 100% well volume formalin instead of of growth medium and wait 15 minutes
6. Following preservation, wash and store all wells in PBS. The wells are now ready for experimentation

2.2.14 Synthesis and purification of AEGLAFK peptide

The specific worklist for the synthesis of AEGLAFK contains following relevant information:

- N-terminal deprotected, C-terminal acid
- PV not used
- Single coupling, Swell, Final deprotection, Final DCM wash
- UV monitoring used

Resin data:

- Substitution: 0.580 mmoles/gram, Quantity: 259 mg (weighed 262 mg), Preloaded with Lys, Deprotect before first coupling

Amino acid quantities:

- Fmoc-Phe-OH: 303 mg
- Fmoc-Ala-OH.H_2O: 243 mg
- Fmoc-Leu-OH: 269 mg
- Fmoc-Gly-OH: 223 mg
- Fmoc-Glu(OtBu)-OH: 321 mg
- Fmoc-Ala-OH.H_2=: 240 mg

Synthesis performed using Peptide Synthesiser

Cleavage of resin:

1. (1): Mix 95% TFA, 2.5% TIS and 2.5% to 3 ml in 15 ml Greiner centrifuge tube
2. Put reactor containing synthesised peptide on the shaker and (1) in the injection holder
3. Run software option Cleavage 1 (80 minutes, 60 RPM and 170°). Take out (1) which now contains peptide
4. (2): Prepare 3 ml TFA in a 15 ml Greiner centrifuge tube, and place in injection holder
5. Rerun program for 1 minute and combine the products of (1) and (2)
6. Add diethylether fresh cold from the freezer until entire volume is precipitated
7. Centrifugate at 5000 RPM for 10 minutes
8. Decant and repeat diethylether step until nothing more precipitates
9. Freeze pellets in liquid nitrogen and lyophilise

Purification was performed by high performace liquid chromatography in 0.1 % TFA running buffer and acetonitrile eluent gradient with a C18 silica collumn and by UV-VIS 220 nm absorption monitoring.

2.3 Pixel count analysis with MATLAB

The scribt written for the pixel count analysis can be seen in the appendix section A.1. The first script creates a color histogram of a specified image, and outputs a sum of all the bars above a certain color threshold (to filter out black/background). The second script runs a loop of the first script of all files in a specified directory.

By analysing curcumin and hoechst dye images in separation, a graph of curcumin count normalised by hoechst count is created.

Results 3

3.1 Micelle size distribution

The following section provides size distributions of various micelle protocols. The data has been fit by a smooth function.

3.1.1 DiI loaded micelles

Size distribution of DiI loaded micelles. Graph 3.1*left* shows micelles produced by protocol 2.2.1.1 and analysed by NTA software using protocol 2.2.3.1 resulting in a size distribution peak at 250 nm. Graph 3.1*right* shows micelles produced by the same protocol, but analysed NTA software using protocol 2.2.3.2 resulting in a size distribution peak at 30 nm.

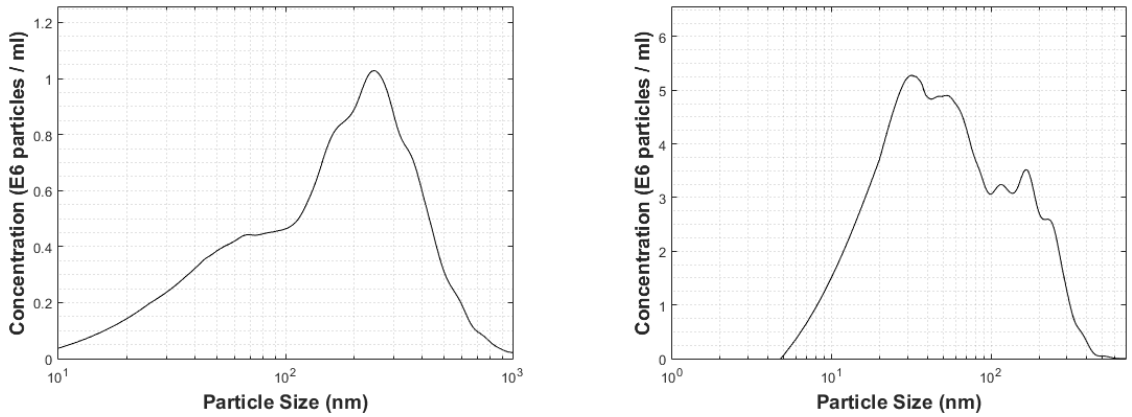

Figure 3.1: Left: *Micelles produced by protocol 2.2.1.1 and prepared for NTA analysis by protocol 2.2.3.1.* ***Right:*** *Micelles produced by protocol 2.2.1.1 and prepared for NTA analysis by protocol 2.2.3.2*

Graph 3.2*left* shows micelles produced by protocol 2.2.1.2 and analysed by NTA software using protocol 2.2.3.1 resulting in a size distribution peak at 50 to 200 nm. Graph 3.2*right* shows micelles produced by the same protocol, but analysed NTA software using protocol 2.2.3.2 resulting in a size distribution peak at 40 to 150 nm.

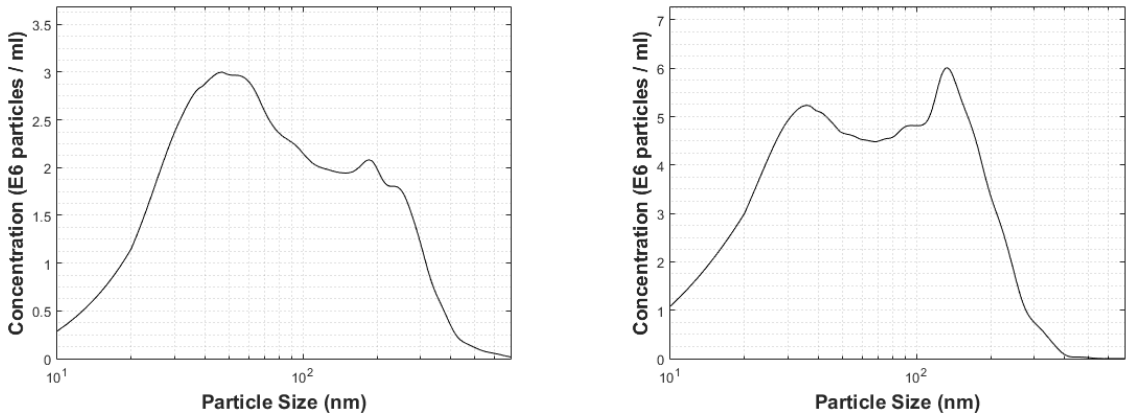

Figure 3.2: Left: *Micelles produced by protocol 2.2.1.2 and prepared for NTA analysis by protocol 2.2.3.1.* ***Right:*** *Micelles produced by protocol 2.2.1.2 and prepared for NTA analysis by protocol 2.2.3.2*

3.1.2 Curcumin loaded micelles

Size distribution of DiI loaded micelles. Graph 3.3*left* shows micelles produced by protocol 2.2.2.2 and analysed by NTA software using protocol 2.2.3.1 resulting in a size distribution peak at 40 nm. Graph 3.3*right* shows micelles produced by the same protocol, but analysed NTA software using protocol 2.2.3.2 resulting in a size distribution peak at 30 nm.

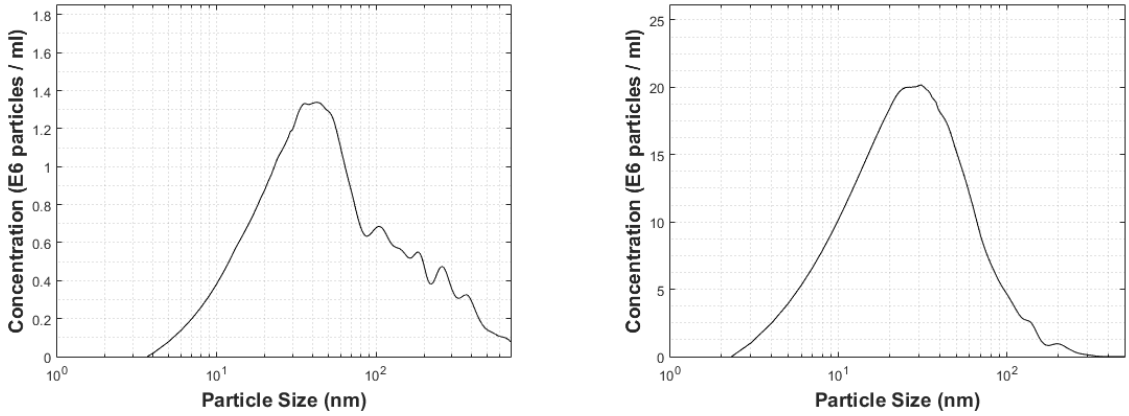

Figure 3.3: Left: *Micelles produced by protocol 2.2.2.2 and prepared for NTA analysis by protocol 2.2.3.1.* ***Right:*** *Micelles produced by protocol 2.2.2.2 and prepared for NTA analysis by protocol 2.2.3.2*

Size distribution of DiI loaded micelles. Graph 3.4*left* shows micelles produced by protocol 2.2.2.3 and analysed by NTA software using protocol 2.2.3.1 resulting in a size distribution peak at 90 to 300 nm. Graph 3.4*right* shows micelles produced by the same protocol, but analysed NTA software using protocol 2.2.3.2 resulting in a size distribution peak at 40 nm.

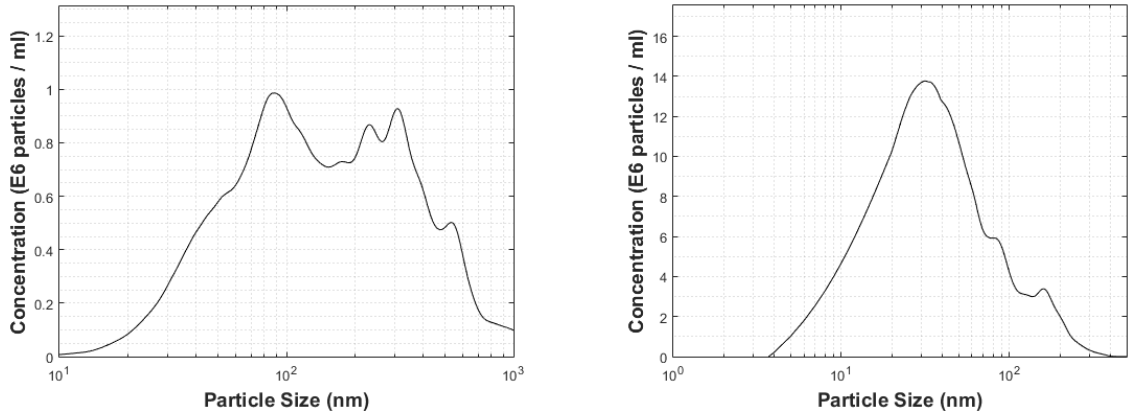

Figure 3.4: Left: *Micelles produced by protocol 2.2.2.3 and prepared for NTA analysis by protocol 2.2.3.1.* ***Right:*** *Micelles produced by protocol 2.2.2.3 and prepared for NTA analysis by protocol 2.2.3.2*

3.1.3 Curcumin loaded mixed micelles

Averaged size distribution of mixed micelles produced by protocols of section 2.2.9 as well as protocol 2.2.8 with various ratios of PVP-COOH:PVP are shown on graph 3.5*left*. The size distribution peaks at 120 nm. A graph comparing micelles produced by 2.2.9.1 and 2.2.11 for MRI in mice is shown on figure 3.5*right*. Protocol 2.2.9.1, using amine coupling by EDC, produced micelles with a base peak between 20-30 nm, and additional peaks at 80 and 150 nm. The micelles produced by protocol 2.2.11 feature one peak at 95 nm.

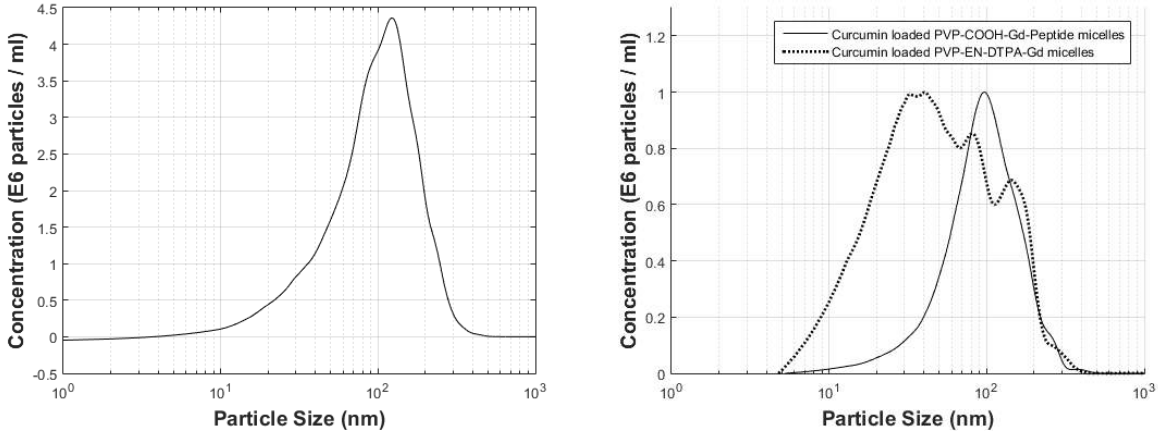

Figure 3.5: Left: *Average size distribution of all mixed PVP/PVP-COOH micelles produced by protocols of section 2.2.9 and protocol 2.2.8.* ***Right:*** *Size comparison of PVP_{6000}/PVP_{12000}-COOH-Gd-AEGLAFK micelles synthesised following protocol 2.2.11 and PVP-EN-DTPA-Gd micelles via protocol 2.2.9.1.*

3.1.4 Atomic force microscopy of micelles

Atomic force microscopy images and height analysis is provided. The micelles are adhered to mica substrate chips for subsequent analysis by AFM.

3.1.4.1 Curcumin loaded PVP micelles

Figure 3.6*left* shows AFM images of curcumin loaded micelles prepared by protocol 2.2.2.2. The cross-section profiles show structures of heights ranging from 1 - 3 nm , 20-40 nm across, as shown on figure 3.6*right* and accompanied by a bottom layer in the height range of 0.1 to 0.5 nm. The blue line on 3.6*left* represents the cross-section.

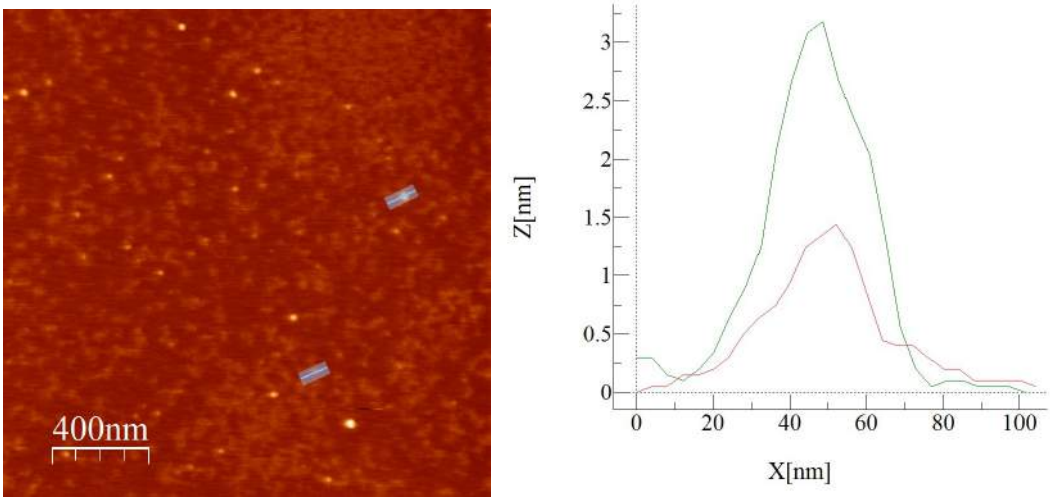

Figure 3.6: Left: *AFM of curcumin loaded PVP_{1000} micelles produced by protocol 2.2.2.2-A.* ***Right:*** *Cross-section profile of the blue line shown on the left figure.*

3.1.4.2 Curcumin loaded PVP:PVP-COOH-Gd-FALGEA mixed micelles

The AFM images of figure 3.7 show curcumin loaded micelles prepared by protocol 2.2.11, featuring 2:1 ratio of PVP:PVP-COOH. The cross-section height profile peak ranges from 5 to 15 nm, 30 to 60 nm across on a 1 to 2 nm bottom layer, as seen per figure 3.7e. The cross-section was made from the blue lines shown on figures 3.8c and 3.8d.

3.1.4.3 Curcumin loaded PVP-COOH-Gd micelles

Micelles prepared by protocol 2.2.9.8 are 95% PVP-COOH and imaged by AFM on figure 3.8. The cross-section height profile shows a peak at 2 nm on a 1 nm bottom layer, and the peak being 15 nm wide, as seen on figure 3.8*right*. The cross-section was made from the blue line shown on figure 3.8*middle*.

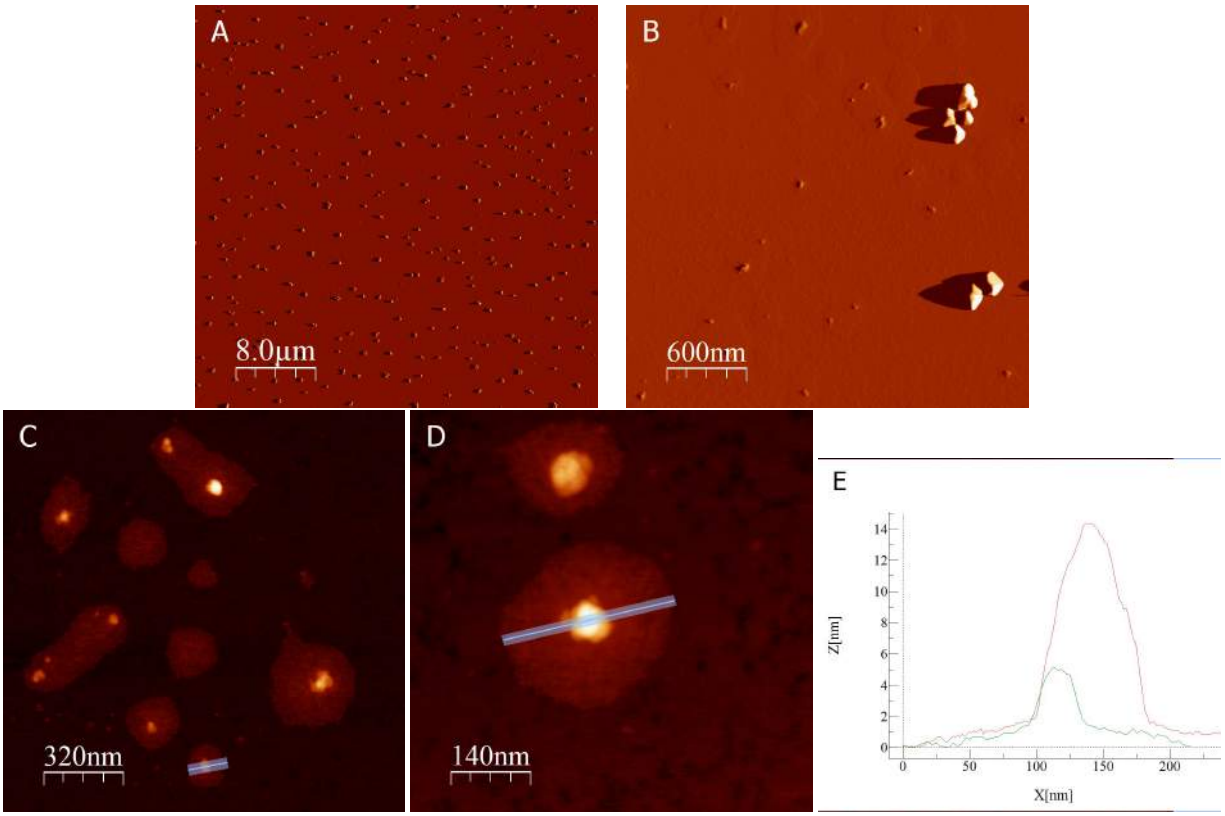

Figure 3.7: A, B, C, and D:*AFM images showing increasing degrees of magnification of curcumin loaded* PVP_{6000}*:*PVP_{12000}*-COOH-Gd-AEGLAFK mixed micelles, protocol 2.2.11.* ***E:*** *Cross-section profile of the blue lines seen on figures C (small peak) and D (large peak).*

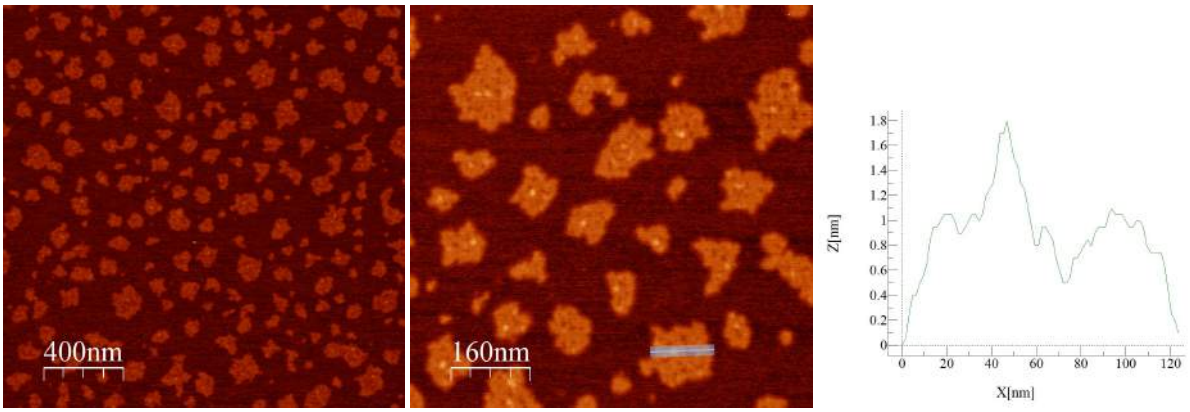

Figure 3.8: *Representative AFM images of curcumin loaded PVP-COOH-Gd mixed micelles produced by protocols of section 2.2.9. The graph to the right shows a cross-section profile at the blue line on the middle figure.*

3.2 Supporting data

3.2.1 Absorption spectroscopy

By absorption spectroscopy, PVP_{12000}-DTPA-Gd were shown to have the spectrum seen on figure 3.9*A*, which exhibits a peak at 274 nm, and an intensity of 2 mAU. A calibration curve of Gd/DTPA is provided for comparison.

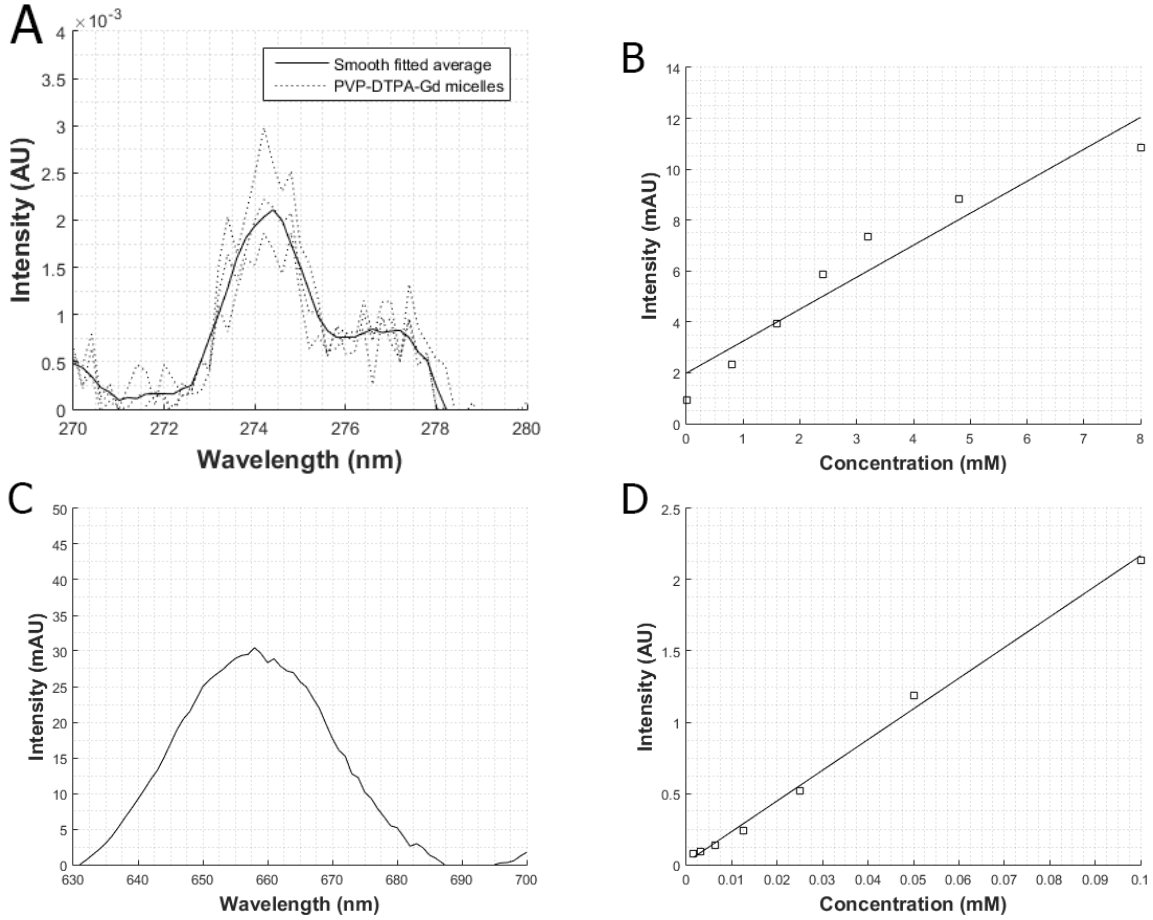

Figure 3.9: ***A:*** *Absorption spectrum of PVP-DTPA-Gd prepared following protocol 2.2.5.1 and ultrafiltration protocol 2.2.7.2.* ***B:*** *Calibration curve of Gd/DTPA in water. Concentrations ranging from 0.8 to 8 mM.* ***C:*** *PVP-DTPA-Gd of image A in 0.1 mM arsenazo aqueous solution.* ***D:*** *Arsenazo calibration curve against free gadolinium of halving concentrations from 0.1 mM, 0.05 mM etc. to 0.0016 mM.*

The same sample was examined by arsenazo assay, showing a peak at 650 nm of 30 mAU units, figure 3.9*C*. Free gadolinium in aqueous arsenazo is shown on a calibration curve on figure 3.9*D*, from 1.6 μM to 0.1 mM concentration.

3.2.2 Fluorescence spectroscopy

Following EN attachment to PVP-COOH, fluorescence spectroscopy of the product in the presence of FA is performed. Figure 3.10 shows the result of this step, with an ETA solution of 0.5 nM concentration as reference, and primary amines of EN contribute to a peak about 30% in magnitude compared to ETA. Further upconcentration of PVP-COOH-EN revealed no decline in signal.

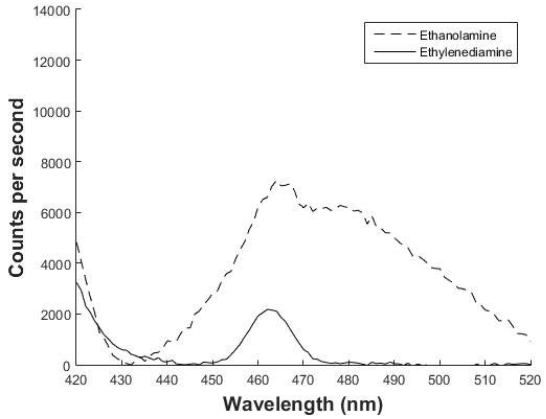

Figure 3.10: *Fluorescence sprectroscopy of PVP-COOH-EN and ETA in separate 0.5 nM FA solution. The molar concentration of ETA is 1:1 with FA. PVP-COOH-EN has been rinsed and upconcentrated by about a factor 100 since synthesis.*

Towards the end of protocol 2.2.9.1, a supernatant is formed from the micelle solution. Fluorescence spectroscopy was performed on this supernatant, as seen per figure 3.11, and a peak is seen at 309 nm following excitation at 280 nm. On the same graph, fluorescence spectroscopy of ultrafiltrate of said supernatant is seen too as a flat line in comparison.

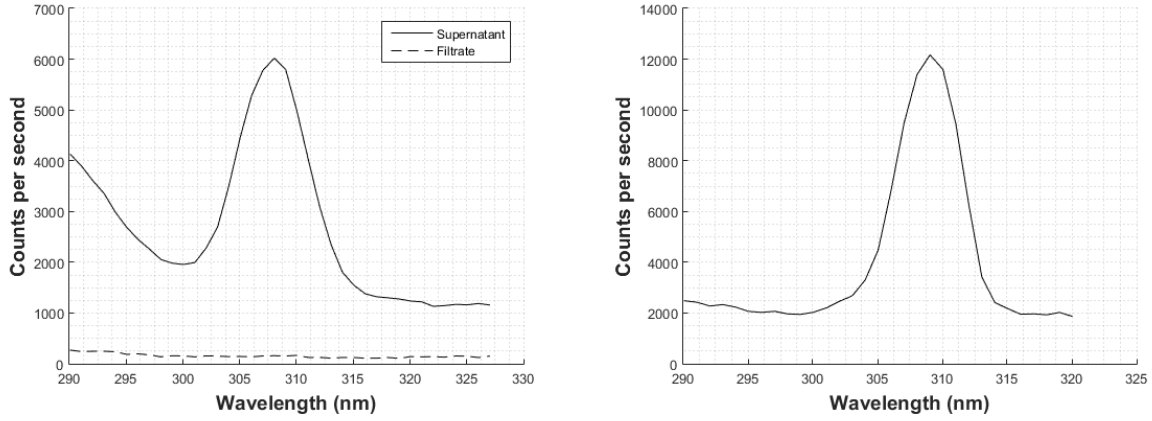

Figure 3.11: Left: *Supernatant of micelles prepared by protocol 2.2.9.1.* ***Right:*** *Ultrafiltrate of supernatant of micelles from the image to the left.*

3.2.3 Polymer epoxidation

The epoxidation yield was estimated to 4%, based on the titrations shown on graph 3.12. *Left* shows a titration of sodium hydroxide versus hydrochloric acid, the solutions used on the *right* side titration graph on epoxidised polymer.

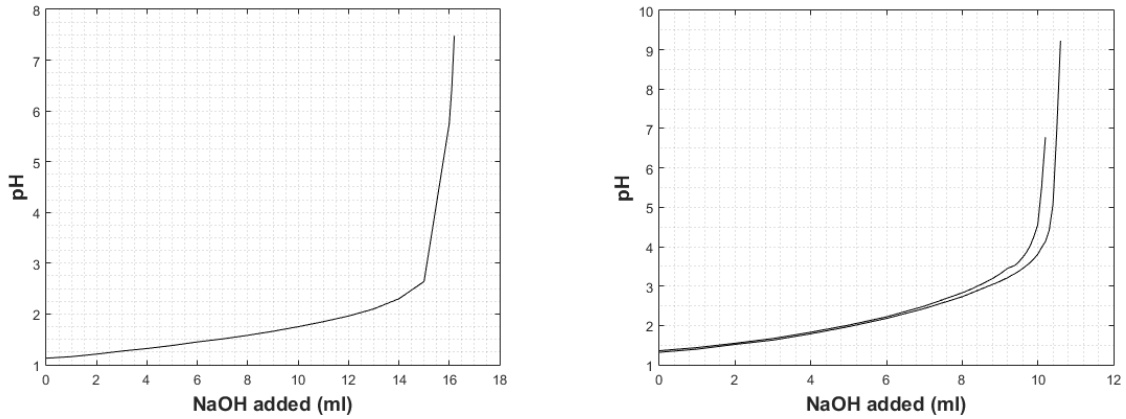

Figure 3.12: Left: *A titration of sodium hydroxide against 10 ml 0.1 M hydrochloric acid, equivalence occurs after adding 16 ml sodium hydroxide.* ***Right:*** *Titration of sodium hydroxide and 100 mg PVGP dissolved in 10 ml 0.1 M hydrochloric acid. Equivalence occurs after adding 10 ml sodium hydroxide. Both experiments use the same solution of sodium hydroxide.*

3.3 Peptide synthesis

By absorption spectroscopy, the concentration of an unknown mass of the synthesised peptide AEGLAFK was estimated at 0.4 mM in 1 ml using the intensity of the 220 nm peak on figure 3.13. Figure 3.14 shows an analytical run of purification by high performance liquid chromatography, and the peak of interest is identified (arrow) close to 16 min. The volume is $\sim$ 100 μl, corresponding to 40 nmole by the previous estimate.

An example of a preparative run with a resolved gradient and 2 ml column is shown on figure 3.15.

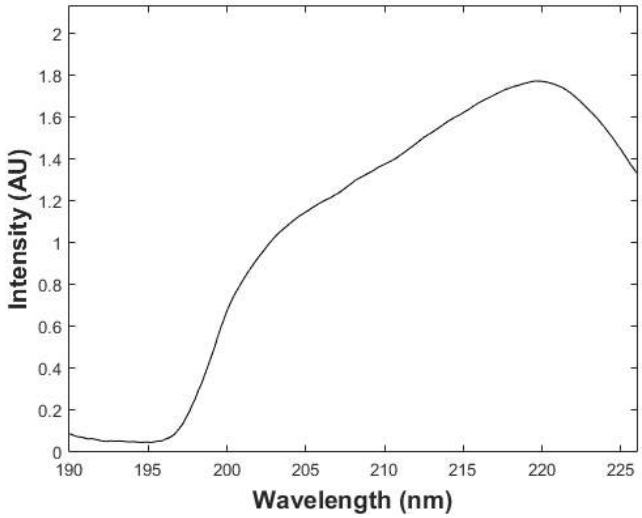

Figure 3.13: *Absorption spectroscopy of an unknown mass of synthesised AEGLAFK peptide following protocol 2.2.14. The absorption at 220 nm is 1.77 AU.*

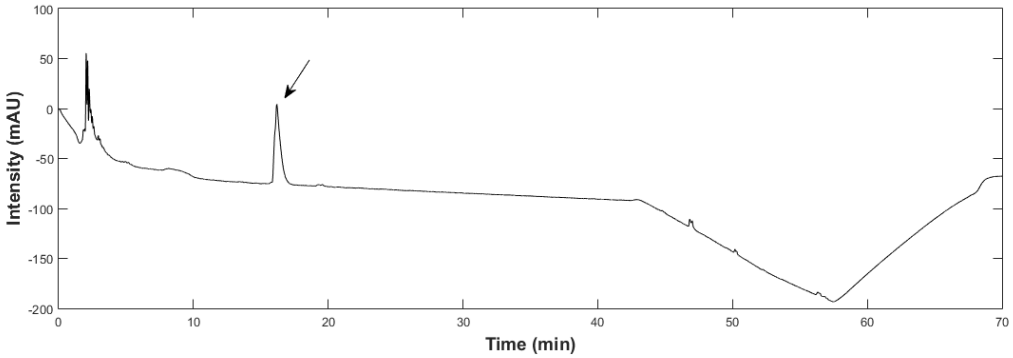

Figure 3.14: *HPLC-UV (220 nm) chromatograph of ~100 µl synthesised AEGLAFK peptide. The peak pointed out by the arrow is at 16 minutes and corresponds to the peptide.*

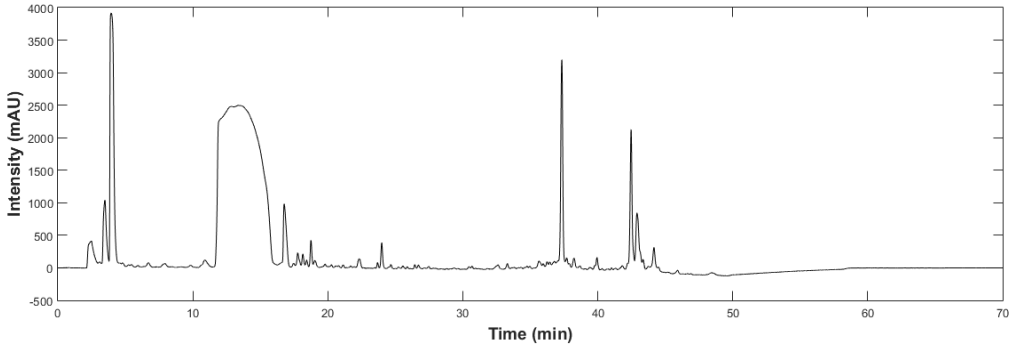

Figure 3.15: *HPLC-UV (220 nm) chromatograph of ~2 ml synthesised AEGLAFK peptide. Numerous peaks appear, and the large one at 12 minutes corresponds to the one identified in the analytical HPLC run.*

3.4 Magnetic resonance imaging of gadolinium chelating micelles *in vivo*

The injection of PVP-DTPA-Gd in Mouse One was not measurable by MRI. Preparation of sample followed protocol 2.2.6.2.

The sample injected in Mouse Two was measurable by MRI to a peak concentration at 0.07 mM, and the sample was prepared by protocol 2.2.9.1.

Mouse Three and Mouse Four were injected with the same sample as Mouse Two, but diluted 1:5 and 1:1 respectively with heparin. MRI was able to detect a weak signal.

Subsequent injection of micelles prepared by protocol 2.2.9.3 and diluted 1:1 with heparin in Mouse Three yielded the concentration profile seen on figure 3.16 when scanned with MRI. The concentration peak is 0.13 mM compared to that of Dotarem at 0.65 mM. The Dotarem concentration was 5 mM prior to injection.

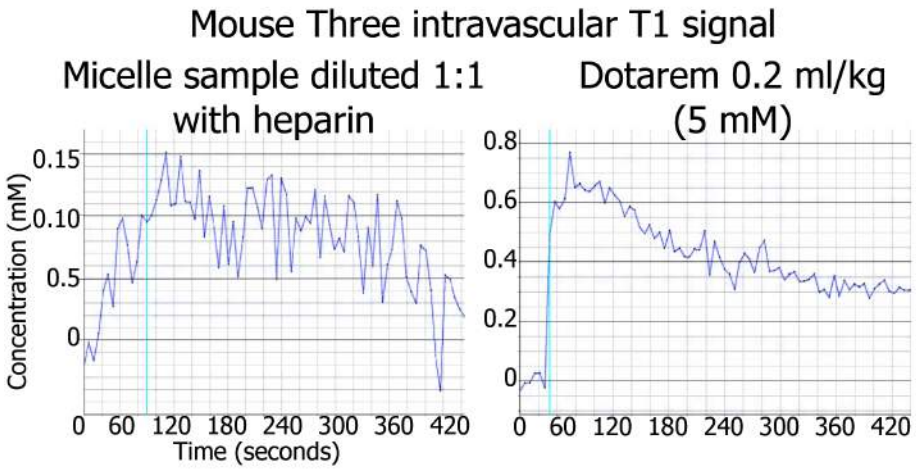

Figure 3.16: Left: *Mouse Three intravascular concentration of injected micelles prepared by protocol 2.2.9.3. The concentration peak is 0.13 mM.* ***Right:*** *Reference solution of Dotarem at a concentration of 5 mM prior to injection. Images produced with MRI by T1 relaxation.*

Mouse Four was injected a second time at a later date with micelles prepared by protocol 2.2.11 diluted 2:1 withe heparin, and the MRI profile can be seen on figure 3.17. The micelle injection peaks at 0.4 mM compared to 0.8 mM of Dotarem at the same initial concentration of 5 mM. The concentration of the micelle injection drops to 0.2 mM after 400s, while at this time Dotarem is at 0.35 mM.

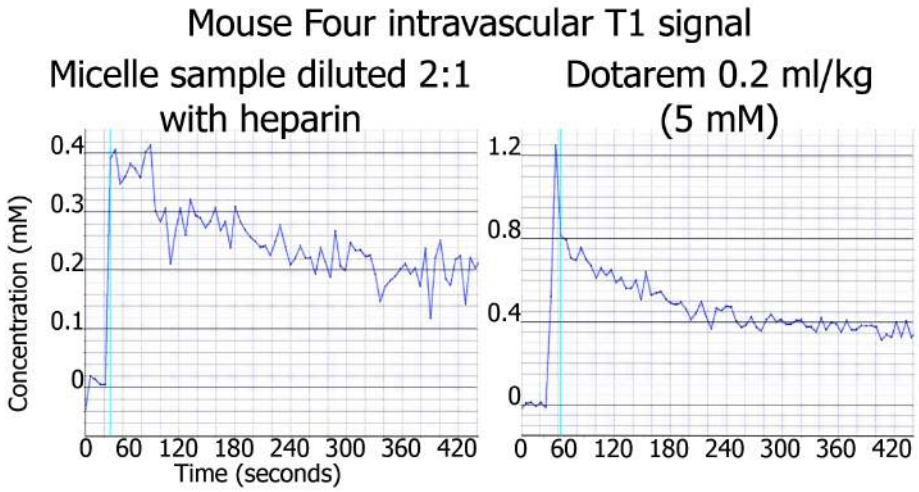

Figure 3.17: Left: *Mouse Four intravascular concentration of injected micelles prepared by protocol 2.2.11. The concentration peak is 0.13 mM.* ***Right:*** *Reference solution of Dotarem at a concentration of 5 mM prior to injection. Images produced with MRI by T1 relaxation.*

Figures 3.18 and 3.19 show double layered MR images of T2 weighted bottom and T1 weighted top. At t = 0 and t = 5 minutes the mice are in same position, but at t = 24 hours, they have been out of the scanner in the meantime so the position is different. The MRI scans slices along the axis of the mouse. Figure 3.18 show slice 5 and 6 (vertical) of Mouse Three at the aforementioned steps in time (horizontal) from the same injection shown on figure 3.16.

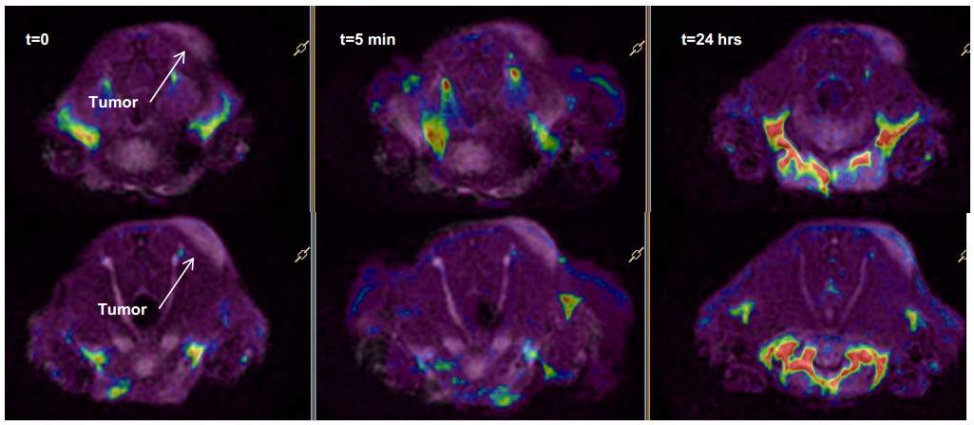

Figure 3.18: *Double layered MR images of Mouse Three injected with micelles of protocol 2.2.9.3. Underlayer is T2 relaxation signal, while overlayer is T1 relaxation. Each collumn is a step in time, of intervals 0, 5 minutes and 24 hours. Top row shows slice 5 and the bottom row shows slice 6.*

The same story follows figure 3.19, but for Mouse Four showing slices 5, 6 and 7.

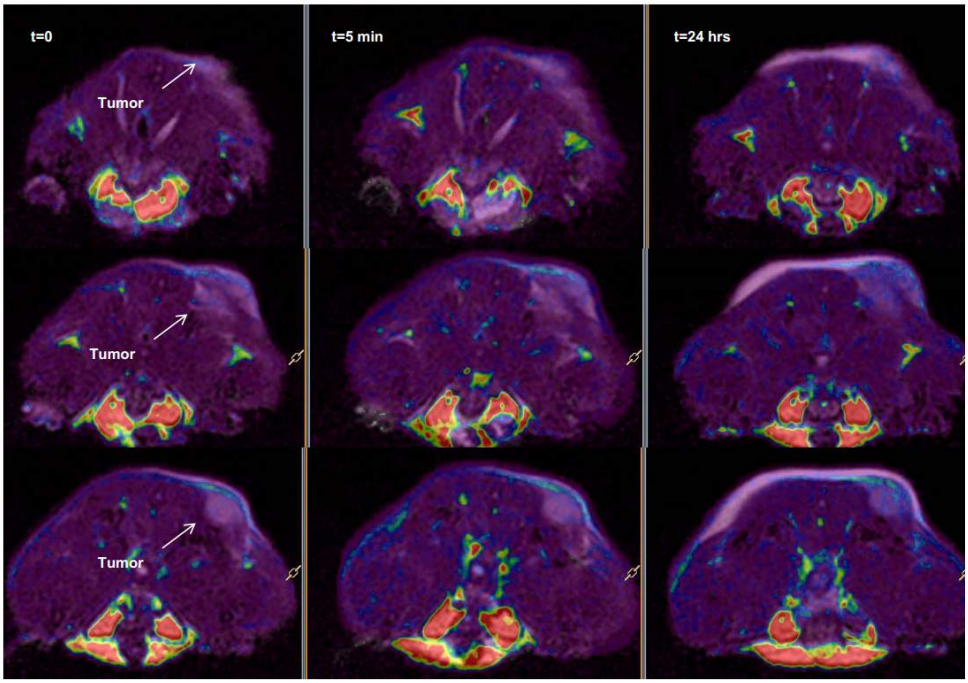

Figure 3.19: *Double layered MR images of Mouse Four injected with micelles of protocol 2.2.11. Underlayer is T2 relaxation signal, while overlayer is T1 relaxation. Each collumn is a step in time, of intervals 0, 5 minutes and 24 hours. Top row shows slice 5, middle row shows slice 6, and the bottom row shows slice 6.*

3.5 Optical fluorescence microscopy

Optical fluorescence microscopy was performed in polystyrene wells (experiment I) and borosilicate wells (experiment II and III). The 'hoechst' filter refers to fluorescence contrast method with excitation wavelength at 353 nm and emission wavelength 465 nm. The excitation wavelength is filtered through 335 to 383 and emission is filtered through 420 to 470. The exposure time through the hoechst filter is always 6 ms. For the 'curcumin' filter, the excitation occurs at wavelength 493 nm and emission at 517, while filtering through 450 to 490 for excitation, and 500 to 550 for emission. Exposure time through the curcumin filter is 600 ms for experiment I and 200 ms for experiment II and III. Unless otherwise shown, the scale bar represents 50 μm.

3.5.1 Experiment I

Figure 3.20 shows a representative image of optical fluorescence microscopy experiment I, with both filters on 3.20*A*, curcumin filter on 3.20*B*, and hoechst filter on 3.20C.

Figure 3.21 shows representative images of all three experimental lines from 10 minutes to 60 minutes exposure to blank (no endocytosis inhibitors), dynasore and wortmannin with respect to the order in which they appear. Top row is 10 minutes and bottom row is 60 minutes.

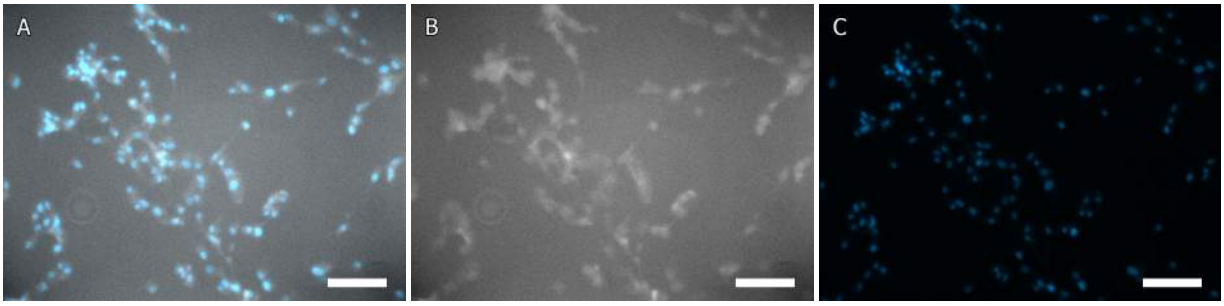

Figure 3.20: *A representative image of glioblastoma cells from experiement I.* ***A****: both filters shown,* ***B****: curcumin filter shwown, and* ***C****: hoechst filter shown.*

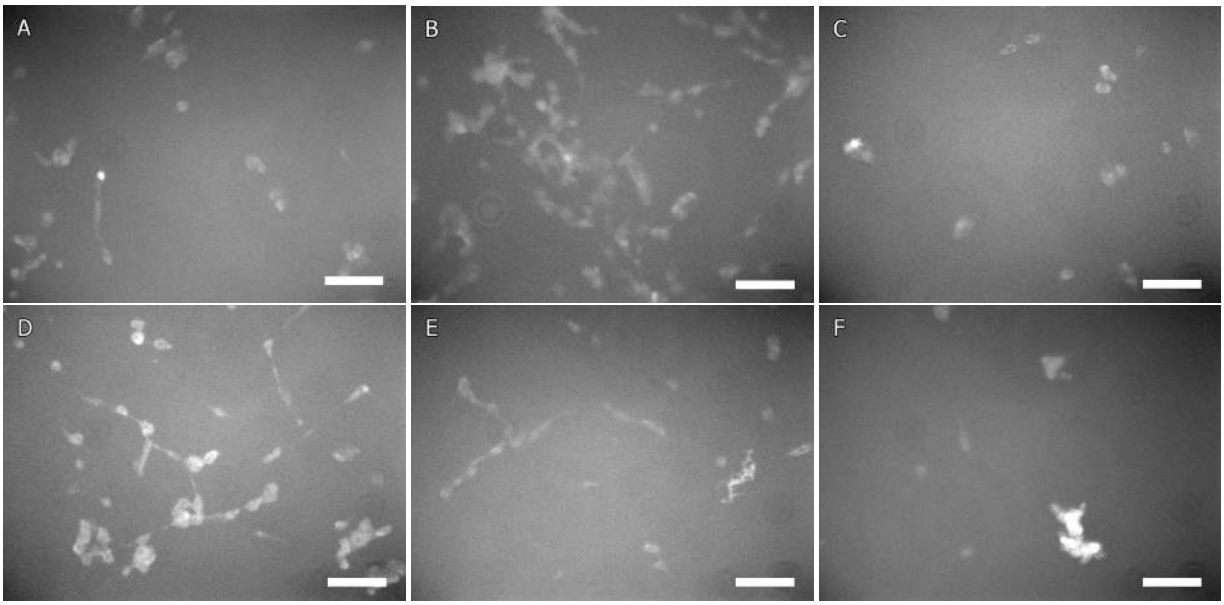

Figure 3.21: *Microscopy experiment I, all three experimental lines* ***(blank, dynasore, wortmannin respectively)*** *at* ***t = 10 minutes (top row)*** *to* ***t = 60 minutes (bottom row)*** *shown through the curcumin filter.*

3.5.2 Experiment II

A comparison of experiment I in polystyrene wells versus experiment II in borosilicate chambered slides. The bottom thickness of the polystyrene wells is 1.2 mm, versus 0.15 mm of borosilicate slides. Figure 3.22*A* and 3.22*B* show images of experiment I without background removal. 3.22*C* and 3.22*D* show the same images but with background removed, and 3.22*E*, 3.22*F* show to images of experiment II without background removed. The left row has both filters visible, while the right row is only the curcumin filter.

Figure 3.23 shows a comparison of resolution between the two experiments. 3.23*A* is experiment I and 3.23*B* is experiment II.

Figure 3.24 shows a representative image of experiment II, with both filters on 3.24*A*, curcumin filter on 3.24*B*, and hoechst filter on 3.24*C*.

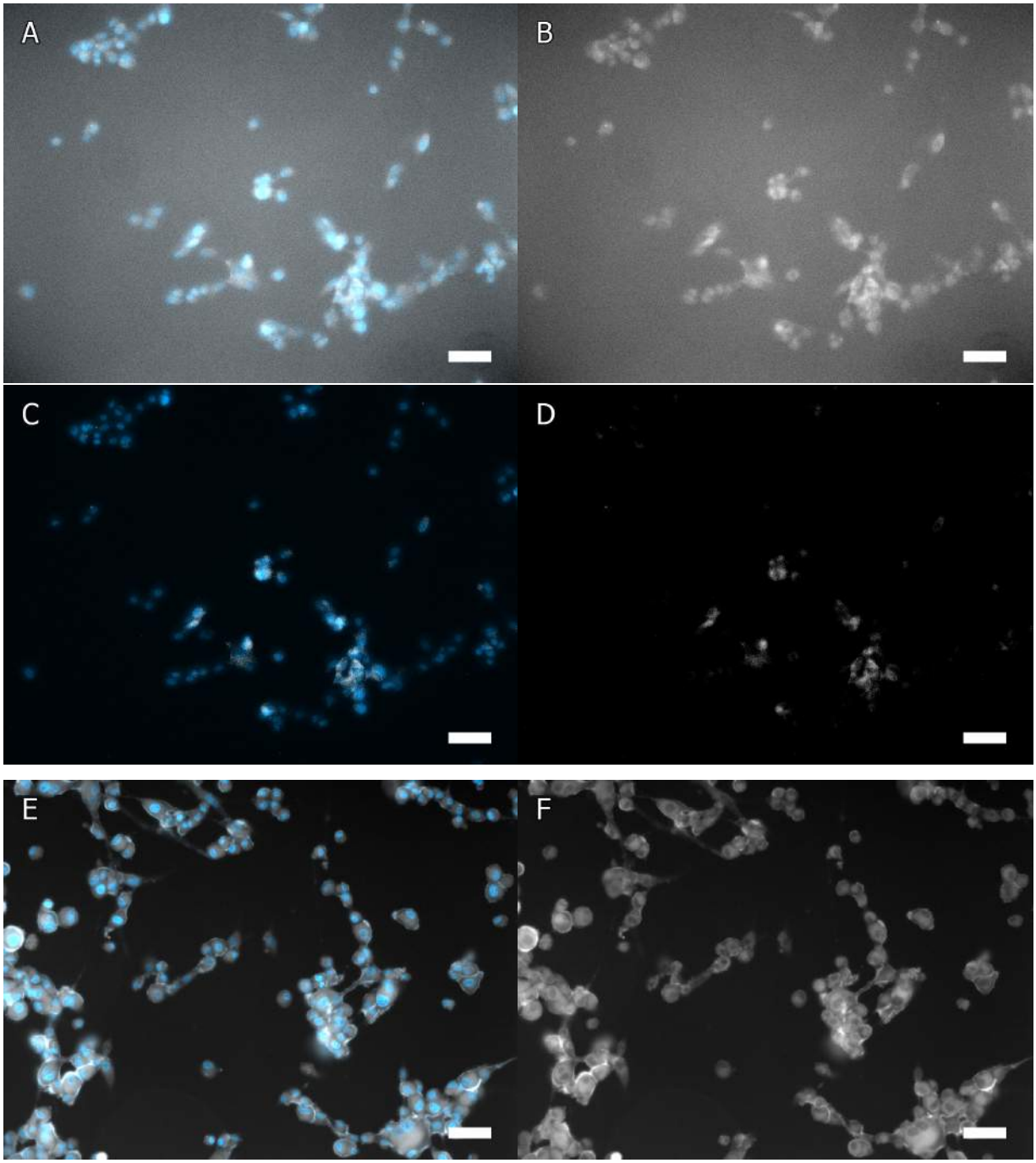

Figure 3.22: ***A*** *and* ***B*** *show images of experiment I without background removal.* ***C*** *and* ***D*** *show the same images but with background removed, and* ***E***, ***F*** *show to images of experiment II for comparison without background removed.*

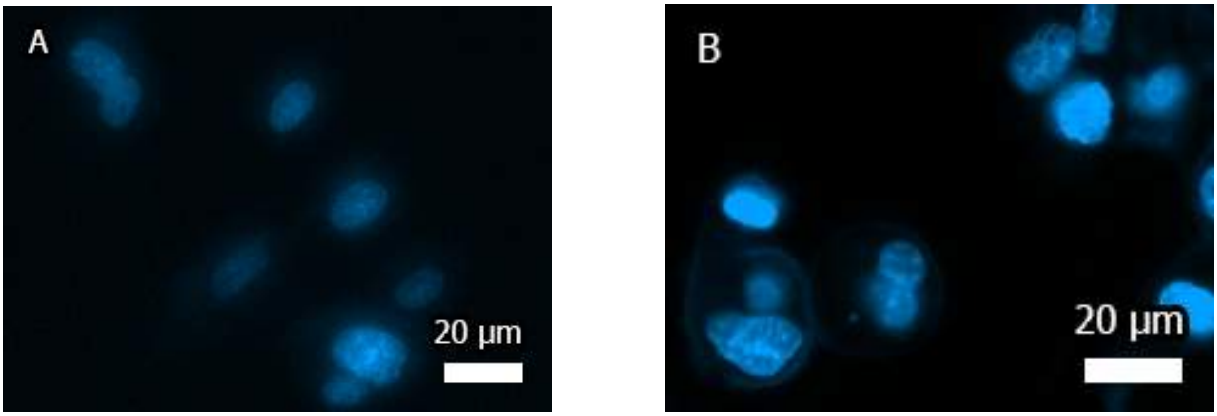

Figure 3.23: *A shows a close-up of a glioblastoma nucleus from experiment I, and* ***B*** *shows the same but from experiment II with a higher resolution.*

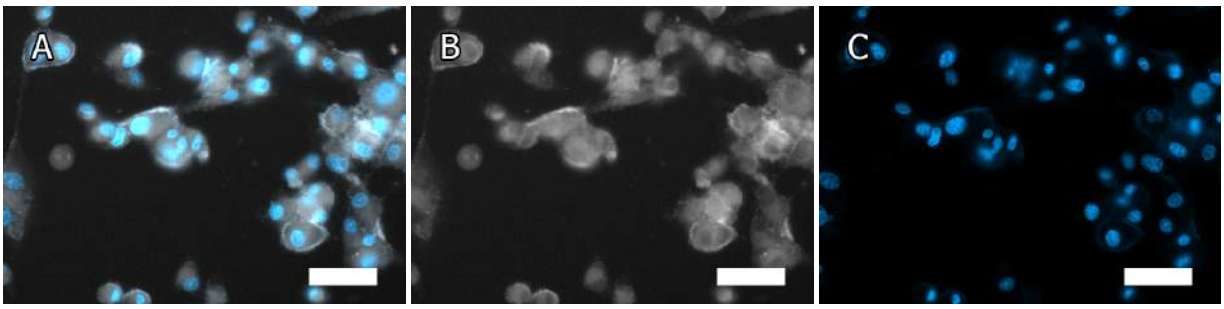

Figure 3.24: *A representative image glioblastoma cells from experiment II.* ***A****: both filters shown,* ***B****: curcumin filter shown, and* ***C****: hoechst filter shown.*

Figure 3.25 shows representative images of all three experimental lines from 20 minutes to 90 minutes exposure to blank (no endocytosis inhibitors), dynasore and wortmannin with respect to the order in which they appear. Top row is 20 minutes and bottom row is 90 minutes.

An area of glioblastoma cells on figure 3.26*A*, is shown zoomed-inthrough both filters on figure 3.26*C*. 3.26*B* is curcumin, and 3.26*D* is hoechst.

Figure 3.27 shows a comparison of glioblastoma cells of experiment II (3.27*left*) and experiment III (3.27*right*). The cells in experiment III are preserved in formalin post exposure. A clear difference in accumulated curcumin on the cell exterior is observed.

A graph is shown on figure 3.28 that quantitatively describes the curcumin uptake of the glioblastoma cells over the period of exposure during experiment II. The graph was produced by protocol 2.3, by comparing pixel count ratios of white and blue pixels in each respective layer of the image. Each data point is an average of a number of images. A varying number of images were recorded for each time step, but most often 4-5 images are analysed per data point. An artificial point at t = 0 has been added for clarity.

Two 3D images are shown in the following, to shed light on the spatial effects of the curcumin inhomogeneities. Figure 3.29 shows arrows pointing to an aggregate in the glioblastoma cell interior, and

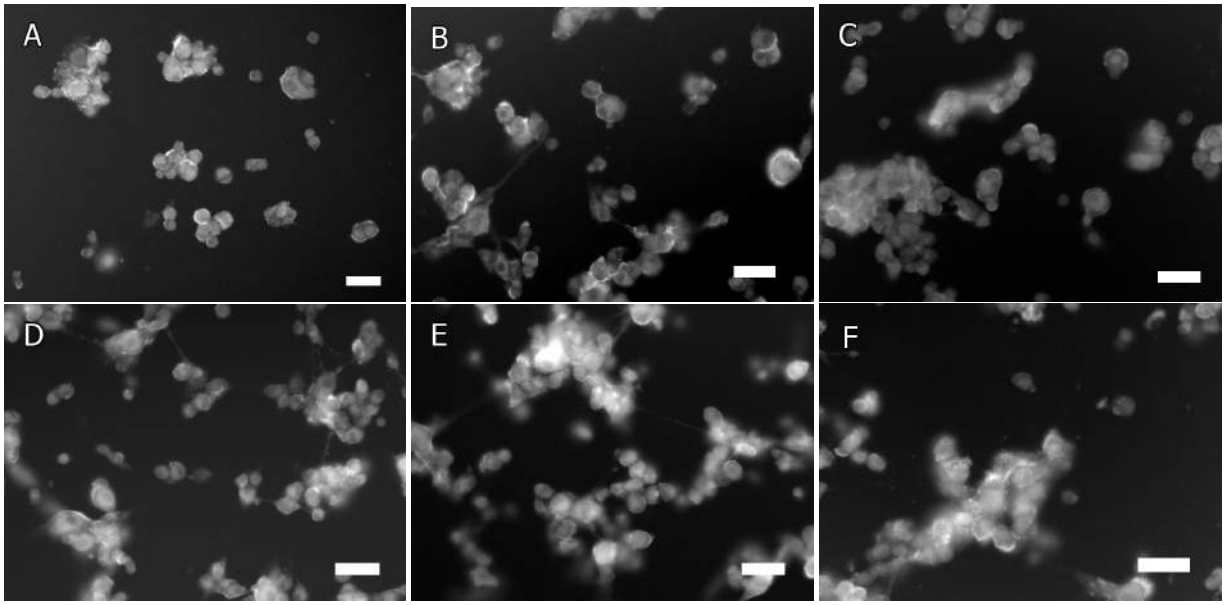

Figure 3.25: *Experiment II, all three experimental lines* ***(blank, dynasore, wortmannin respectively)*** *at* ***t = 20 minutes (top row)*** *to* ***t = 90 minutes (bottom row)*** *shown through the curcumin filter.*

figure 3.30 has arrows pointing to aggregations on glioblastoma cell exteriors. The images consist of 39 z-stacked layers.

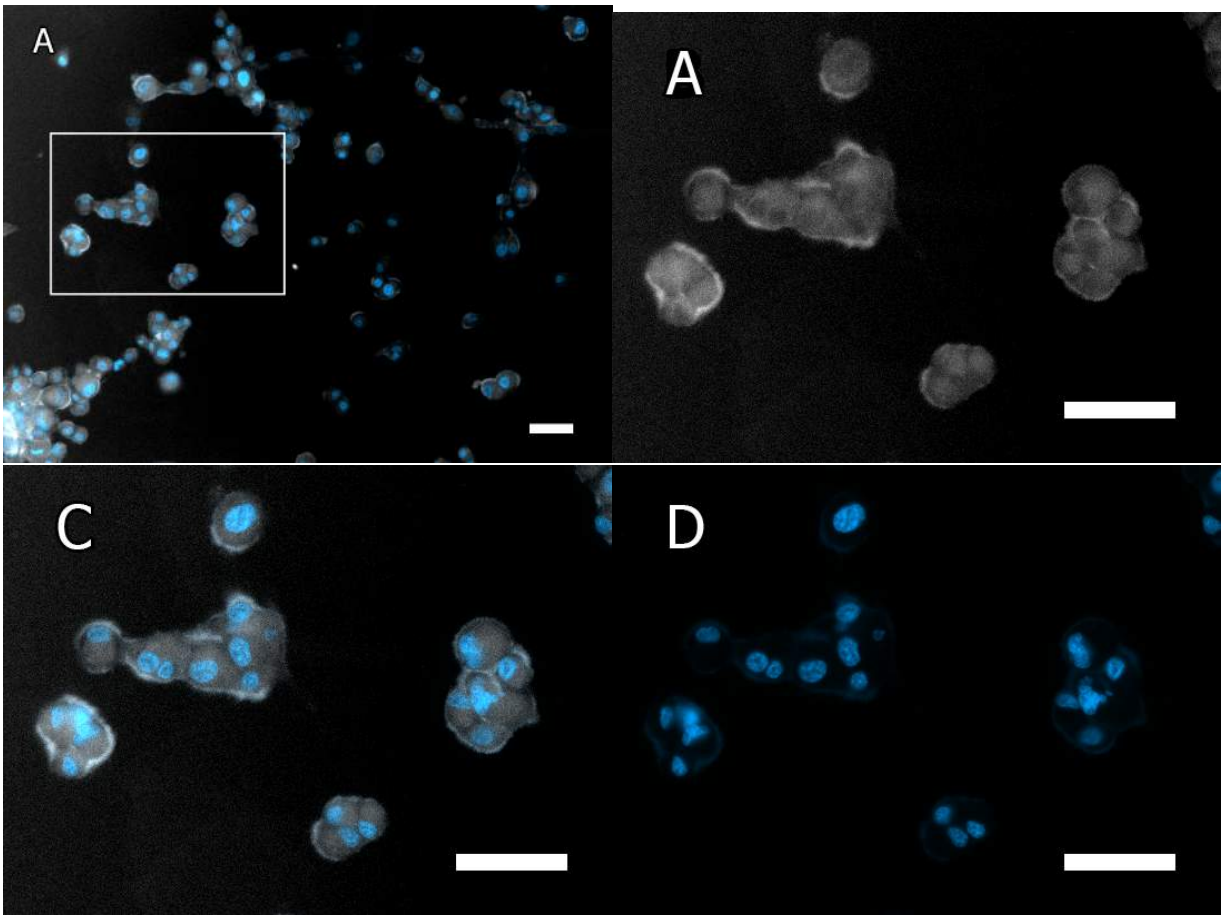

Figure 3.26: *Close-up image of glioblastoma cells in experiment II.* ***A*** *is an overview,* ***B*** *is through the curcumin filter,* ***C*** *is both filters, and* ***D*** *is hoechst only.*

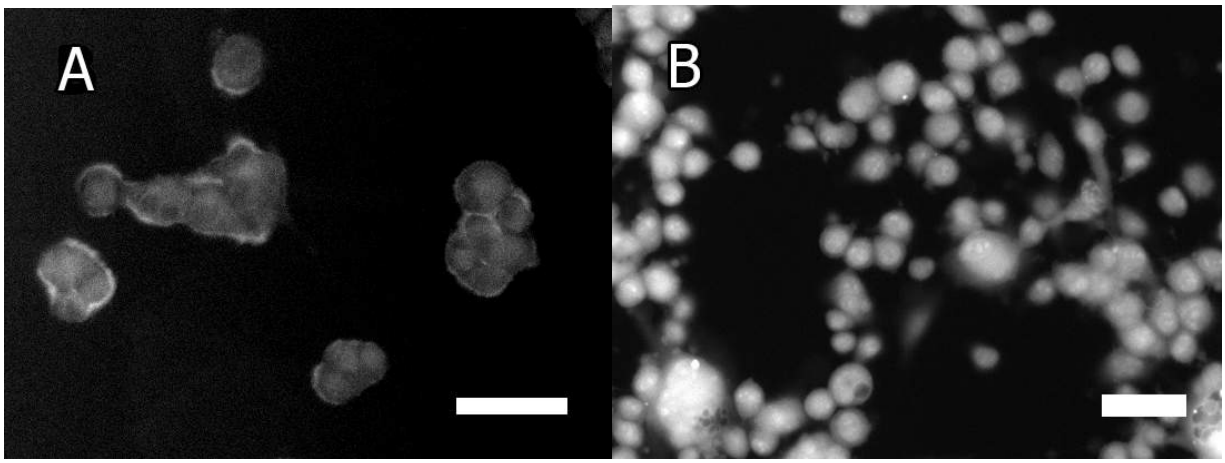

Figure 3.27: *Comparison of the increased intensity seen on the glioblastoma cell exterior through the curcumin filter in experiment II* ***(left)*** *versus the lack thereof in experiment III* ***(right)****.*

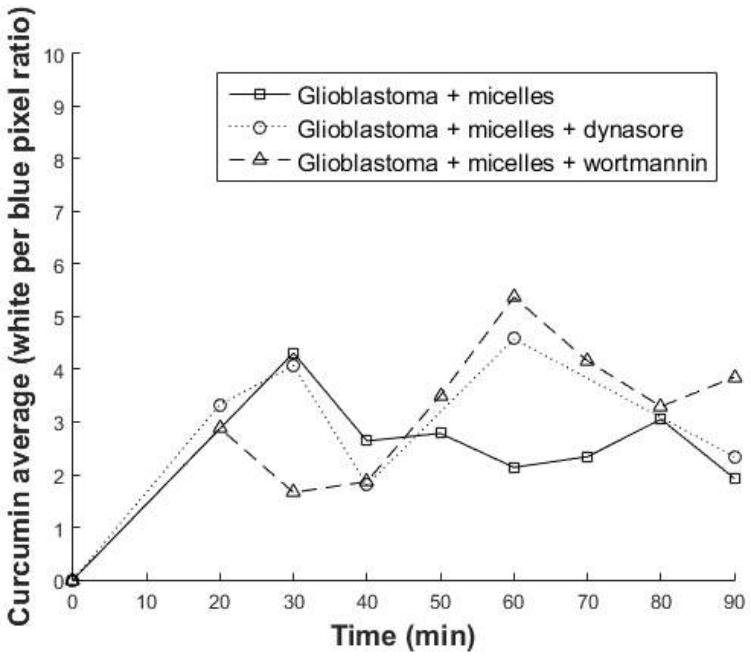

Figure 3.28: *Graph of pixel count ratio of white (curcumin filter) versus blue (hoechst filter) pixels. All three experimental lines are included in a time interval of 20 to 90 minutes. Generated using the MATLAB script of protocol 2.3.*

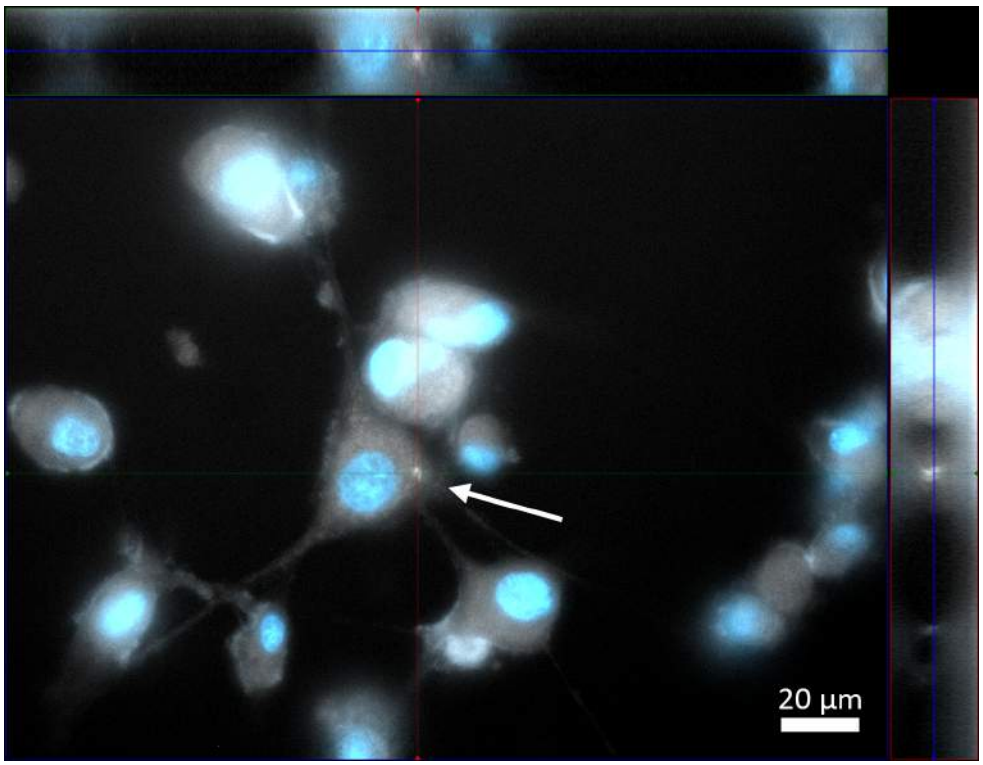

Figure 3.29: *3D image consisting of 39 z-stacked layers showing glioblastoma cells of microscopy experiment II. The arrows point to indications of a vesicle in the cell interior.*

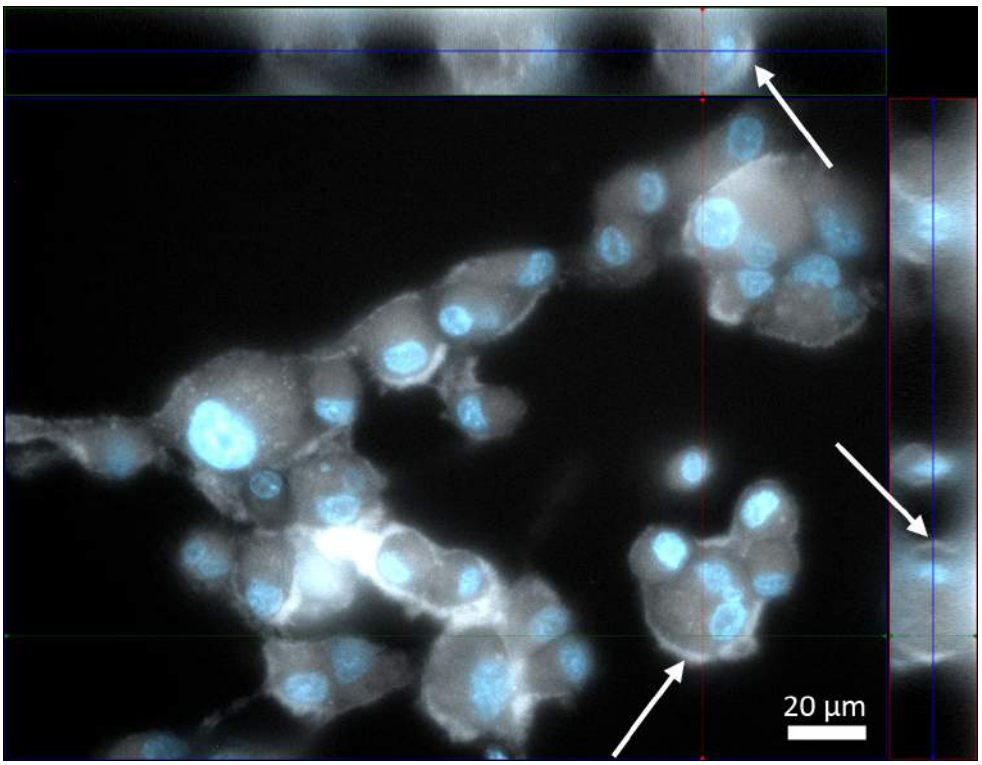

Figure 3.30: *3D image consisting of 39 z-stacked layers showing glioblastoma cells of microscopy experiment II. The arrows point to indications of aggregating curcumin on the cell exterior.*

3.5.3 Experiment III

Figure 3.31 shows a representative image of experiment III, with both filters on 3.31*A*, curcumin filter on 3.31*B*, and hoechst filter on 3.31*C*.

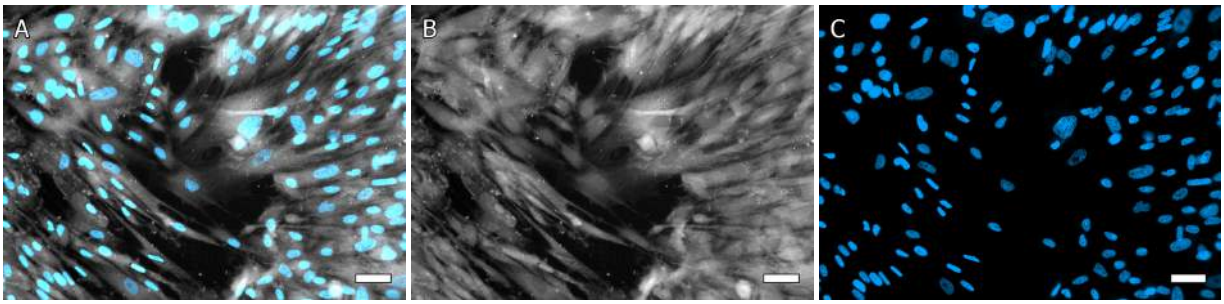

Figure 3.31: *A representative image of fibroblast cells of experiment III.* ***A****: both filters shown,* ***B****: curcumin filter shwown, and* ***C****: hoechst filter shown.*

Figure 3.32 shows a representative image of experiment III, with both filters on 3.32A, curcumin filter on 3.32B, and hoechst filter on 3.32C.

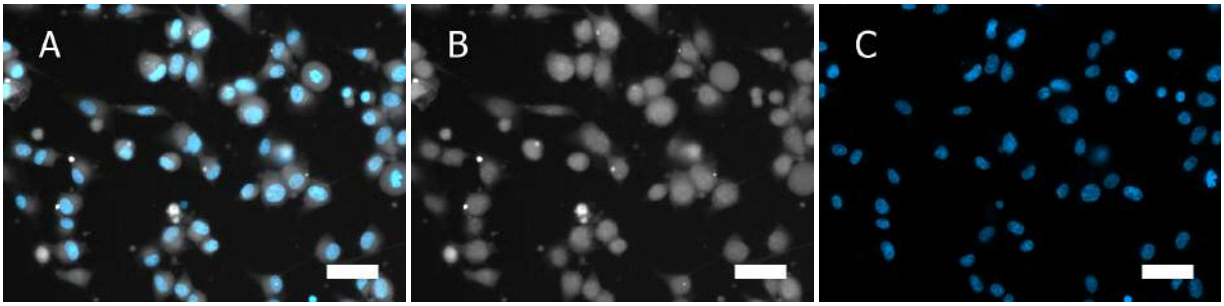

Figure 3.32: *A representative image of glioblastoma cells of experiment III.* ***A****: both filters shown,* ***B****: curcumin filter shwown, and* ***C****: hoechst filter shown.*

A graph is shown on figure 3.37 that quantitatively describes the curcumin uptake of the cells over the period of exposure for both glioblastoma cells (3.37*right*) and fibroblast cells (3.37*left*) from experiment III. The graph was produced by protocol 2.3, in a similar fashion to the one described in experiment II.

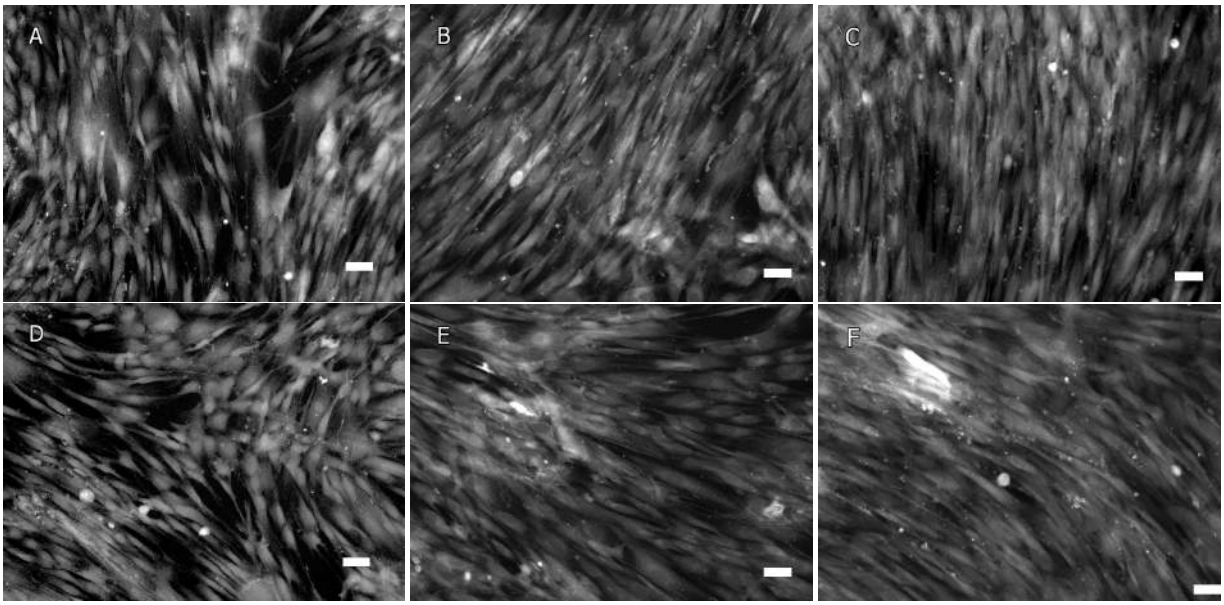

Figure 3.33: *Microscopy experiment III, fibroblast experimental lines* ***(blank, dynasore, wortmannin respectively)*** *at* ***t = 5 minutes (top row)*** *to* ***t = 30 minutes (bottom row)*** *shown through the curcumin filter.*

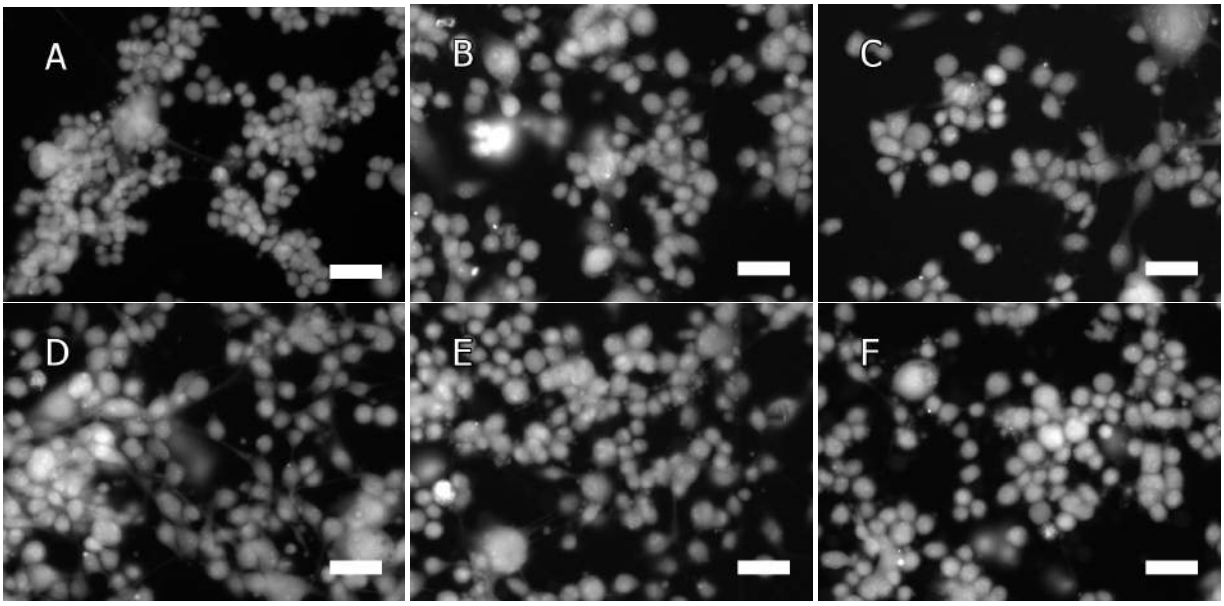

Figure 3.34: *Microscopy experiment III, glioblastoma experimental lines* ***(blank, dynasore, wortmannin respectively)*** *at* ***t = 5 minutes (top row)*** *to* ***t = 30 minutes (bottom row)*** *shown through the curcumin filter.*

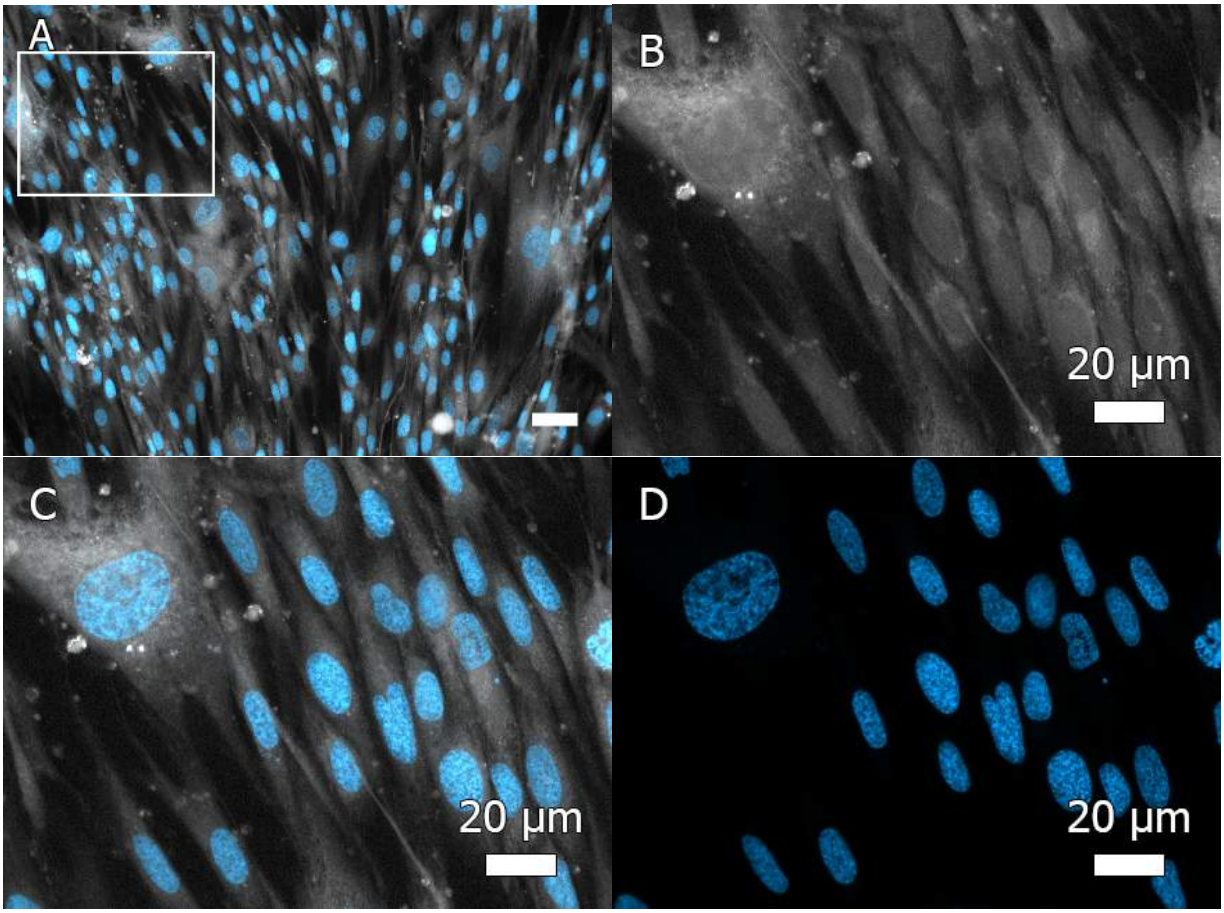

Figure 3.35: *Close-up image of fibroblast cells in experiment III.* ***A*** *is an overview,* ***B*** *is through the curcumin filter,* ***C*** *is both filters, and* ***D*** *is hoechst only.*

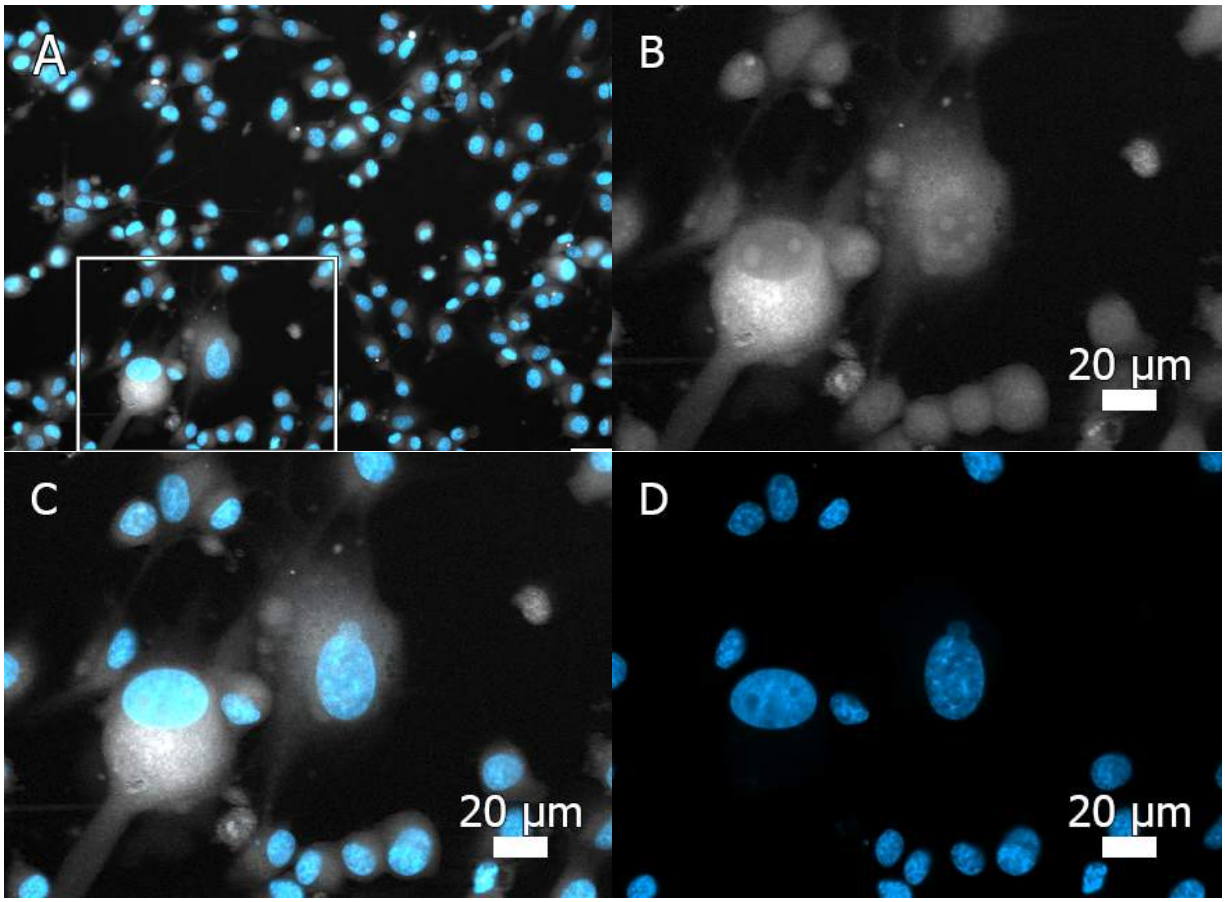

Figure 3.36: *Close-up image of glioblastoma cells in experiment III.* ***A*** *is an overview,* ***B*** *is through the curcumin filter,* ***C*** *is both filters, and* ***D*** *is hoechst only.*

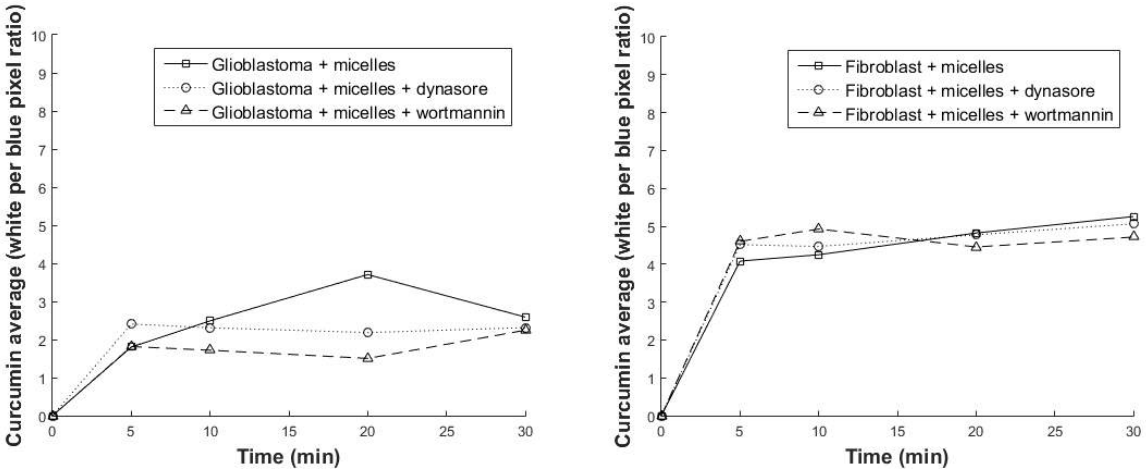

Figure 3.37: *Graph of pixel count ratio of white (curcumin filter) versus blue (hoechst filter) pixels. All three experimental lines are included in a time interval of 5 - 30 minutes.* ***Left:*** *Glioblastoma,* ***Right:*** *Fibroblast. Generated using protocol 2.3.*

Discussion 4

The discussion chapter is divided into three major sections; micelles, optical fluorescence microscopy and magnetic resonance imaging.

4.1 Micelles

Micelles were formed using both DiI and curcumin as hydrophobic model drug molecules. They would act as fluorescent dye for microscopy experiments as well as stabilising the micelles by forming a hydrophobic core along with octadecane. A schematic of the simple form of curcumin loaded PVP micelles (also applies to DiI loaded micelles) is shown on figure 4.1.

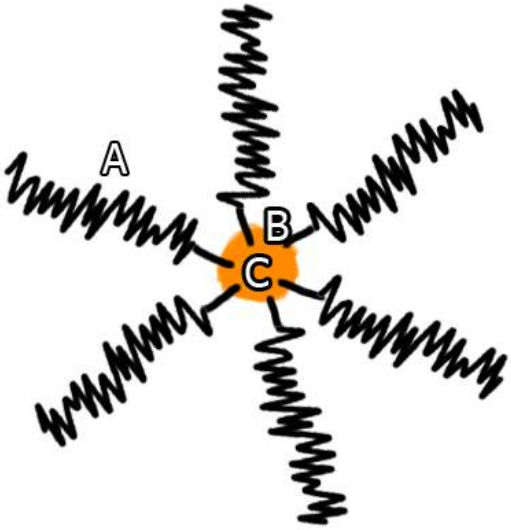

Figure 4.1: *Schematic drawing of a mixed PVP/PVP-COOH-Gd micelle.* ***A*** *is the non-carboxylated hydrophilic PVP block,* ***B*** *is the hydrophobic octadecane block, and* ***C*** *is curcumin or DiI comprising the core along with the strongly hydrophobic octadecane.*

DiI and curcumin are both strong in hydrophobicity, but curcumin is much smaller with a molecular weight of 368 g/mol against the 934 g/mol of DiI. This property may help stabilising smaller micelles, as

it does not push as much on the hydrophobic block of the polymer molecules by being internalised in the core.

PVP_{1000} micelles of the form shown on figure 4.1 were produced to a 30 nm size distribution. Change of organic solvent for the drug had no significant impact on the size, but using DiI as a model drug caused a high degree of polydispersity. The micelles produced with DiI exhibited size distributions in a range of 30-150 nm, also not influenced by surfactant molecular size to a significant degree.

Curcumin loaded PVP-COOH mixed micelles were on average larger than the micelles with only regular PVP as surfact molecule. Figure 3.5*left* shows this average, of all mixed micelles produced.

An overview of the size distributions can be seen on table 4.1, starting from smallest micelles to the largest ones.

It is seen from the table that the addition of various charged species and extra molecular weight in the corona has an impact on the size distribution.

On the one hand, micelles produced from PVP_{12000}-EN-DTPA-Gd polymer had a size distribution peak in a similar range to the simple PVP micelles, but also exhibited a broad tail region going up to 150 nm. On the other hand, mixed micelles containing peptide and gadolinium (row 4 on the table) had a higher minimum particle size, but exhibited a sharp distribution at 90 nm diameter. It is possible the preparation of samples with broad size distribution can be optimised.

Type of micelles	Size	Notes
PVP_{1000} (acetone)	30 nm	Narrow size distribution
PVP_{1000} (DCM)	30 nm	Narrow size distribution
PVP_{12000}-EN-DTPA-Gd	35 nm	Broad size distribution
PVP_{6000}-PVP_{12000}-COOH-Gd-AEGLAFK	90 nm	Narrow size distribution
PVP-PVP_{12000}-COOH-Gd	120 nm	Average of all mixed micelles containing PVP-COOH excluding peptide micelles
PVP_{1000} micelles (DiI)	30 - 150 nm	High polydispersity and broad size distribution peak
PVP_{12000} micelles (DiI)	40 - 150 nm	High polydispersity and broad size distribution peak

Table 4.1: *A table showing micelle types and their size distributions. All size analysis measurements are made using NTA protocol 2.2.3.2. The protocols used in order of appearence are: 2.2.2.2, 2.2.2.3, 2.2.6.2, 2.2.11, 2.2.9, 2.2.1.1, and 2.2.1.2.*

The loading efficiency was not investigated quantitatively. As a result, any uptake of curcumin observed by cells is assumed to be delivered by micelles.

4.1.1 Size distribution and preparation of micelles

The results section shows a number of comparisons of size distributions between micelles analysed by NTA with and without preparation. Being stored as lyophilisate after synthesis, excess curcumin and free polymer is still present in the sample. This can be seen by NTA as a much broader size distribution, due to microaggregates of various origin as well as poorly dissolved micelles. As a result, ultrasound is

necessary to dissolve these residuals of lyophilisate, and subsequent centrifugation to force precipitation of suspended material. Visible macroparticulates will also be removed by this step. The micelles are stable enough to stay in suspension at 10,000 rcf.

As the solution contains a percentage of organic solvent after sonication, it is not advisable to centrifugate the sample before lyophilisation, since this may force some of the curcumin and micelles out of the aqueous phase. It is possible to use rotary evaporation in vacuum to get rid of the solvent, and allow centrifugation, but resolvation can be difficult. After dried on the rotary flask bottom, the flakes are not easily soluble.

As a result of preparation and the assumption that free curcumin is precipiated during centrifugation, any uptake of curcumin observed by cells is assumed to be delivered by micelles.

4.1.2 Atomic force microscopy of micelles

Various phenomena were observed by AFM of the micelles. Simple micelles produced by 2.2.2.2 displayed polymer dispersed in no recognisable pattern across the mica surface. Curcumin cores were observed always accompanied by surrounding polymer. They appear as little bright dots on figure 3.6.

When looking at mixed micelles, a clearer image of the corona was formed around the cores, 3.7*D*. On this particular figure, larger aggregated structures are seen too (figure 3.7*A* and *B*). The sample, prepared by protocol 2.2.11, was subject to a large number of reactants which may explain the structures observed. They are not thought to be of micelle origin.

Mixed micelles prepared with a higher carboxylated polymer content than a 1:2 ratio featured much smaller core sizes when imaged by AFM. Figure 3.8*right* shows a cross-section profile of one of these cores. Its height of 2 nm is small compared to that of figure 3.7*E* at 15 nm. Nothing in the synthesis was changed with regards to curcumin.

4.1.3 Functionalisation of PVP

The functionalisation of surfactant molecule PVP-octadecane by DTPA and subsequent chelation of gadolinium proved to be a difficult task. The initial aim was a product like the one schematised on figure 4.2. Due to a string of unsuccessful attempts, each step of the process was investigated, starting with the epoxidation protocol.

4.1.4 Epoxidation of PVP groups

The initial attempt was to epoxidise the pyrrolidone of the PVP polymer using 2-chloroacetamide as a precursor to form poly(*N*-vinyl 2-glycidylamido pyrrolidone), PVGP. To check the degree of epoxidation, the titration protocol 2.2.4.1 was performed. [26]

Hydrochloric acid reacts 1:1 with the PVGP groups, and a titration of hydrochloric acid by sodium hydroxide provides a percentage of epoxidation by the molarity offset. However, to determine the exact relation between the practical versions of a 0.1 M hydrochloric acid solution and a 0.1 M sodium hydroxide solution, a pure titration was made first, shown on figure 3.12*left*. The point of equivalence is read at 15 ml, corresponding to a 0.06 M concentration. The same solutions were then used on the epoxy

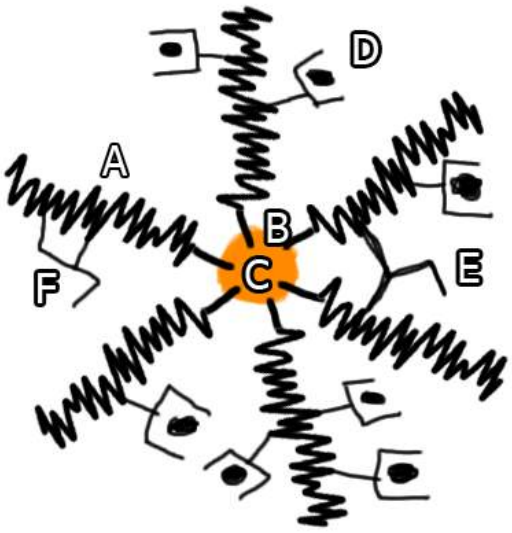

Figure 4.2: *Schematic drawing of a curcumin loaded PVP-DTPA-Gd micelle.* ***A*** *is the non-carboxylated hydrophilic PVP block,* ***B*** *is the hydrophobic octadecane block, and* ***C*** *is the curcumin comprising the core along with octadecane.* ***D****: Optimal situation of DTPA bound to a single PVGP unit, and chelating gadolinium.* ***E:*** *DTPA crosslinking between two or more PVGP units on adjacent PVP blocks.* ***F:*** *DTPA binding to multiple adjacent PVGP units on the same PVP block. Both situations E and F result in the loss of DTPA chelating ability.*

titration and equivalence occurs at the addition of 10 ml sodium hydroxide. The result is a rough estimate of the percentage of epoxidation at 4%, which is sufficient.

4.1.5 Functionalisation of PVGP by DTPA

The hypothesis was the reaction between PVGP and DTPA would be spontaneous and catalysed by imidazole. but this was not the observed result. The means of detecting the presence of DTPA, is by detecting the entire chelation complex of DTPA/Gd via either absorption spectroscopy (3.9*B*) or fluorescence spectroscopy (3.11*right*). Following the very first synthesis of PVP_{12000}-DTPA-Gd, the absorption peak seen on figure 3.9*A* was obtained following six rounds 0.5 ml ultrafiltration (a factor 10^6 upconcentration).

Referring to the spectra on figure 3.9*A* and figure 3.9*B*, it is evident that the peak observed corresponds to a complex of DTPA/Gd which lead to the initial assumption that the synthesis was a success. This was based on the fact that, in theory, the concentration of free DTPA/Gd was reduced by a factor 10^6. But, subsequent analysis by fluorescence spectroscopy and arsenazo assay revealed the presence of free Gd^{3+} ions in the sample, which in turn indicates improper ultrafiltration. The most probable cause is a lack of mixing when adding solvent (MilliQ in this case) to the ultrafiltration tube inbetween centrifugation, as this allows the concentrate to stay at the bottom of the tube below the filter outlets.

Following attempts at reacting DTPA with the PVGP were made by applying heat during the reaction and lowering the concentration of polymer compared to DTPA, to avoid multiple bindings of one DTPA molecule and crosslinking between polymers by keeping DTPA in excess. Neither approach yielded a success.

The last attempt using DTPA involved different chemistry. By binding ethylenediamine to the PVGP groups, it was instead possible to use amine coupling with EDC. The first protocol using this approach would dissolve the PVGP-PVP in MilliQ with ethylenediamine, under the hypothesis that the epoxy group would prefereably react with ethylenediamine instead of being hydrolised. Having ethylenediamine attached would ensure a free primary amine for the amine coupling by EDC to the carboxyl groups on DTPA. It was also important that the concentration of ethylenediamine was kept in excess to avoid the same problem as was speculated about DTPA, where one molecule would bind multiple epoxy groups and as such inhibit its function.

The reaction in aqueous environgment proved unsuccessful, and instead the reaction was changed to run in DMSO as it is inert to the epoxides. Furthermore, basic conditions were established to deprotonate the environment as protons also facilitate the ring opening reaction of the epoxy groups.

4.1.6 Functionalisation of PVP by DTPA dianhydride

However, the potential of the approach was never fully explored although the outlook was good. Instead the focus was turned towards using DTPA dianhydride reaction directly with primary amines. [27]

One experiment involved attaching ethylenediamine directly to PVGP, and afterwards DTPA dianhydride to ethylenediamine without the need for amine coupling. During preparation, the ethylenediamine attachment of protocol 2.2.6.2 was measured as a false positive by ninhydrin as the excess ethylenediamine had not been washed out to a sufficient degree. In addition, the DTPA dianhydride was added to the PVP-EN solution before buffering by carbonate buffer and adjusting pH with sodium hydroxide. As a result, three factors acted against the attachment of DTPA dianhydride to the PVP-EN molecules. One being the low amount of ethylenediamine binding to PVGP, second being the excess ethylenediamine still present in solution, and third the protonation of DTPA anhydride when exposed to the acidic reaction solution.

4.1.6.1 Amine coupling of ethylenediamine to carboxylated PVP

Attaching the ethylenediamine to the carboxyl groups on carboxylated PVP_{12000} (PVP_{12000}-COOH) with amine coupling facilitated by EDC was deemed a more fruitful approach, as with a 90% carboxylated, the amount of functional groups per PVP molecule of similar weight is roughly a factor 10 higher (assuming 5% epoxidation ratio).

In the first experiment coupling ethylenediamine to PVP-COOH, molar ratios were in the range of 1:1 using protocol 2.2.8. The resulting product was insoluble, and it is assumed that the amines and carboxyls formed a network of salt bridges. In theory, the PVP-COOH can form salt bridges with itself, but as it depends on distance it is not as likely to occur. However, with the added range of ethylenediamine as well as the introduction of a primary amine to facilitate interaction this property was enhanced.

4.1.6.2 Mixing surfactant solution to lower carboxylation ratio

To circumvent the formation of salt bridges, regular PVP_{1000} was introduced in a 2:1 weight ratio PVP:PVP-COOH in an attempt to increase the distance between the charged species. This was following protocol 2.2.9.1. The concentration of the amine coupling reaction solution was kept low due to the tendency of these electrostatic interactions. By fluorescence spectroscopy, the presence of primary amines was confirmed with fluorescamine, and the protocol continued. [28]

DTPA dianhydride is readily protonated when dissolved in water, and the result is DTPA, which does not react with primary amines as was the goal at this point of the experiment. This insight necessitated basic conditions in the PVP-COOH-EN solution, which further meant when running the micellisation protocol the conditions were still basic. Upon dissolving $GdCl_3$ in the reaction solution, the consistency became light cloudy, indicating a small degree of precipitation in the form of suspension. Micelles were formed nonetheless, exhibiting the size distribution seen on figure 3.5*right*, dotted line. An addition of a milimole NaOH was necessary after micellisation, as it had been observed to increase the solubility due to neutralising electrostatic interaction.

The resulting product was not quantified with respect to chelated gadolinium, until measured by MRI in vivo. The micelles were delivered intravenously, and the bolus signal measured to be a factor 5 off Dotarem, which is the regular gadolinium contrast agent. However no real signal was observed outside the vascular system. This would indicate the gadolinium observed by MRI is attached to the micelles and as a result not extravasating. Were that not the case, the signal would be distributed in all the tissue of the mouse.

4.1.6.3 Gadolinium polychelation by PVP-COOH

The composition of a monomer of PVP-COOH is reminiscent of DTPA, with tertiary amines in close vicinity of carboxyl groups. Gadolinium requires high denticity, such as 8 in the case of DTPA but sometimes higher. The high degree of freedom of the polymer allows wrapping around the gadolinium, to provide the needed amount of coordination numbers for chelation. When acting as a polychelating agent, the 90% PVP-COOH becomes hydrophobic, believed as a result of all the hydrophilic blocks coordinating around gadolinium, and leaving only the hydrophobic block intact. A schematic describing the situation can be seen on figure 4.3.

This means the percentage of pyrrolidone groups to carboxylic group needs to be increased to maintain some degree of structure and hydrophilicity, and this can be done much in the same manner as how the salt bridges were prevented. Introducing non-carboxylated PVP can, in effect, serve as a reduction of carboxylation ratio. A 2:1 ratio of regular:carboxylated PVP is assumed to act as a 30% PVP-COOH.

4.1.6.4 Mixed micelles to stabilise PVP-COOH during polychelative interaction

Forming micelles with PVP-COOH-Gd was not possible, as they form insoluble hydrophobic aggregates when not stabilised in the form of mixed micelles with PVP. Gadolinium needs to be chelated by the mixed micelles afterwards, at which point the micelles are already stabilised by curcumin in the core, as well as being held in place by adjacent PVP surfactant molecules. However, the absorption spectrum of curcumin overlaps the emission wavelength of chelated gadolinium which is in the 310-315 nm range, and therefore this method of synthesis does not allow quantification of gadolinium by either absorption spectroscopy or fluorescence spectroscopy. Changing the hydrophobic core component to stearic acid or a similar compound would be beneficial in this regard.

In terms of PVP:PVP-COOH ratios, anything less than a 2:1 ratio produced a large amount of precipitate post chelation, indicating a lack of stabilisation. Using a 2:1 ratio produced a neglible amount of precipitate and a size distribution peak at 80 nm. AFM images comparing various ratios constituting mixed micelles, displayed a significant difference in drug loading. Figure 3.7 shows cores, assumed to be curcumin, of 5 to 15 nm height with a flattened corona extending out 200 to 250 nm across the visible

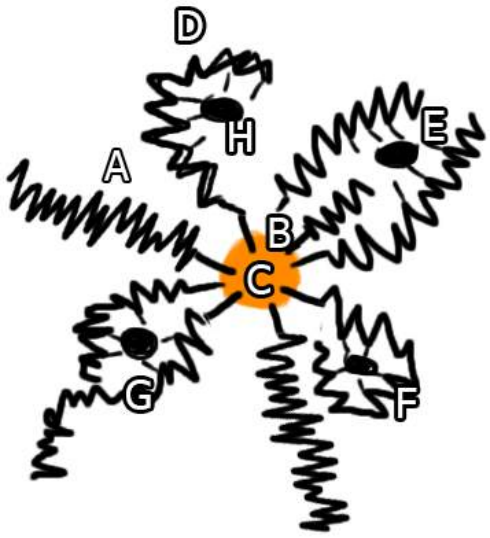

Figure 4.3: *Schematic drawing of a mixed PVP/PVP-COOH-Gd micelle.* ***A*** *is the non-carboxylated hydrophilic PVP block,* ***B*** *is the hydrophobic octadecane block, and* ***C*** *is the curcumin comprising the core along with octadecane.* ***D, E, F*** *and* ***G*** *represent various ways of PVP-COOH blocks chelating gadolinium (****H****). The optimal scenario is similar to that of E, in which the hydrophilicity of PVP-COOH is maintained by "dilution" via the addition of non-carboxylated PVP molecules. In this manner, the PVP-COOH is provided with steric stabilisation, and ideally shares chelation of gadolinium with neighbouring PVP-COOH.*

structures. This is significant in comparison to figure 3.8, having a core of no more than 2 nm height but coronas in the same order of magnitude at 50 - 200 nm.

4.2 Microscopy of glioblastoma and fibroblast cells exposed to PVP micelles

In terms of drug delivery, the smallest specimen of micelles was investigated. In vitro results display curcumin taken up by cells across both glioblastoma and fibroblast cell types, with 5 minutes of exposure to the micelles. Figures 3.37 shows the cells exhibit no difference in curcumin uptake when exposed to endocytic inhibitor dynasore, or receptor mediated endocytosis inhibitor wortmannin. The drug uptake covers the entirety of the cell. Removing the cell nucleus layer shows no difference in intensity, so it is assumed the inner membrane does not block the curcumin either.

Although it is not of optimal quality, the z-stacked (3D) image of figure 3.30 shows this effect, as the curcumin is distributed across the entire cell in an almost homogeneous fashion. It is observed mainly on images of experiment II of the optical fluorescence microscopy, although some images of experiment I are of sufficient quality to show the effect. It may be attributed to the lack of formalin preservation of the cell lines after micelle exposure. Inside the cell on figure 3.29, a spherical aggregate is observed that could be a vesicle containing curcumin. The effect was observed in lines with and without dynasore. A comparison between the fibroblast and glioblastoma experimental lines shows the spherical aggregates

have a higher tendency of forming in fibroblast cells.

4.2.1 Temporal resolution of drug uptake kinetics

It is relevant to adjust the protocol for exposing cell lines to curcumin loaded micelles. The time interval of interest at the given concentration of micelles is within the first 5 minutes. At least two approaches are possible: Lowering the concentration of micelles to slow down the reaction or the inclusion of exposure steps on a 10 second basis or similar.

For the first option, although of limited quality, microscopy experiment I shows the uptake in similar levels. The concentration of micelles are a factor 5 below that of experiment II and III, so reaching a point in concentration where the uptake is low enough to be quantitatively separated on a 5-10 minute basis may produce artefacts. Double or triple wells should be considered in that case.

The second option is subject to additional uncertainties. For each time interval in the current preparation protocol, there is an amount of seconds of exposure added due to several rinsing steps, pipetting wells one line at a time, preservation in formalin and residual micelles delivering curcumin post rinsing. They add up to 1-2 minutes total to clear a cell line (for instance the first well of the 5 minute line has ~2 minutes less exposure than the last, depending on the amount of wells). To eliminate this factor it would be necessary to handle each well individually. To provide an example, compare the protocol of cells of 6 wells needing 5 minutes and 10 seconds exposure (starting from the point of adding micelles, having added 200 μl DMEM to all wells in a preceding step):

5 minutes exposure to curcumin loaded micelles

1. Add 200 μl micelles to wells labelled 5 minutes
2. Wait 5 minutes
3. Wash wells two times with growth medium
4. Repeat for all time intervals
5. Add 400 μl formalin to all wells
6. Wash and store in PBS

10 seconds exposure to curcumin loaded micelles

1. Add 200 μl micelles to first well labelled 10 seconds
2. Wait 10 seconds
3. Wash well two times with growth medium
4. Add 400 μl formalin same well
5. Repeat for all wells

For 6 wells per step in time (counting three cell lines and duplicate) and 4 time steps a total of 4 repeats is necessary in the first example, whereas in the second example the same number is 6 times higher, 24. In practise it is possible, but time consuming due to the need to prepare each well in series instead of parallel and it adds experimental uncertainty between each well. In addition, the cells in the wells waiting to be exposed has longer wait in the sub-optimal conditions of room temperature and limited access to medium, but this is not a crucial factor.

A possible benefit from either of these two approaches is the increased temporal resolution around the linear area of what is to be assumed a sigmoid uptake curve (as per the graph on figure 1.1). This may help resolving the different kinetics of uptake between cells with and without dynasore and wortmannin, even if the final uptake is the same. The two approaches are of course not mutually exclusive, so a combination yields the best results.

Outside of optical fluorescence microscopy, it is also possible to get a quantitative measurement of drug uptake using a microplate fluorometer. Using a multipipette on, for instance, a 96-well plate reduces the amount of steps to one per time interval, eliminating the practical inconvenience in that respect, while also increasing the statistical confidence of the data.

These are the results of exposure to micelles in the 30 nm size range, and it is possible the mixed micelles of PVP_{6000}-PVP_{12000}-COOH-Gd and PVP_{6000}-PVP_{12000}-COOH-Gd-FALGEA do not exhibit the same drug delivery qualities, as their size distribution is closer to 80 nm. Referring to theory section 1.4.4, it was noted the optimal diamter of spherical nanoparticles to induce endocytosis was 60 nm (specifically mentioned 30 nm radius) [25]. Taking into consideration the protein corona adding several nanometres, it is not clear which type of micelle exhibits stronger endocytic activity.

4.2.2 Effects on microscopy resolution of borosilicate versus polystyrene wells

Microscopy experiment I was performed in polystyrene flat bottom wells. These wells feature a bottom thickness of 1.27 mm. This is close to a factor 10 thicker than the borosilicate coverslides at 0.15 mm used in experiment II and III.

As a result, also evident on the images in section 3.5, the background illumination in experiment I is substantial and in comparison almost gone in experiment II and III. Figure 3.22 provides a comparison, where it is seen that removing background (3.22*C* and 3.22*D*) from images of experiment I removes most of intensity through the curcumin filter. When comparing to the hoechst filter, it is seen some cells can be perceived as clear of curcumin. When comparing to the images with background 3.22*A* and 3.22*B*, it is seen that all the cells show curcumin uptake.

Figures 3.22*E* and 3.22*F* shown a sample of experiment II without having background removed, already providing clear images. Furthermore, figure 3.23 shows the resolution of the images is overall better with borosilicate bottoms, as even the hoechst filter is blurry in experiment I, 3.23*A*. It is improved on 3.23*B* from experiment II.

In addition to changing well type, the concentration of micelles is increased by a factor 5, although this does not seem to play a significant role. Considering the images 3.21, curcumin is present. No significant increase is seen across 60 minutes of exposure, so it can be assumed the cells are close to saturation within 10 minutes.

4.3 Magnetic Resonance imaging of polyvinyl pyrrolidone micelles as a contrast agent *in vivo*

A total of four different micelle preparations were injected intravenously in four different mice, and imaged by MRI. The first micelle sample yielded no observable results after injection in Mouse One, and the protocol was discussed in section 4.1.6

The second micelle sample, injected in Mouse Two, gave a measurable signal about a factor five less than Dotarem. An unfortunate combination of various experimental preparation factors, as well as a lack of dilution by heparin, resulted in the regrettable death of Mouse Two following the experiment. High pH, high viscosity and low osmolarity are possible factors.

Mouse Three and Four were subject to two injections each. The micelle sample was the same product as for Mouse Two but diluted 1:5 and 1:1 with heparin. Heparin helps lower the viscosity, as well as preventing clotting upon contact with the circulatory system. All in all, the fortuitous fact is that no more mice died as a result of micelle injections of this project. The sample, however, exhibited a weak signal when scanned in the mouse by MRI. In addition to dilution, the sample of the product used on Mouse Two was upconcentrated by ultrafiltration, which was not the for Mouse Three and Four.

4.3.1 Mixed micelle injections

Second round of MRI experiments on Mouse Three and Four were performed with micelles prepared in PBS buffer to further eliminate any toxicity of the sample. Mouse Three intravascular T1 signal is close to a factor 4 less than that of dotarem. It was diluted 1:1 with heparin, and by this standard exhibiting a stronger contrast than the previous samples. It was prepared following protocol 2.2.9.3, which uses a 1:1 ratio of PVP:PVP-COOH and relies on the polychelating effect of PVP-COOH. This effect means more charge in the corona due to the presence of COOH groups, but conversely contains less mass per chelated gadolinium, as it is bound to the surfactant molecules instead of the EN-DTPA link.

These two effects of charge and reduced mass (increased mass efficiency) counteract each other to some extent. As is seen the micelles formed by this protocol were about 100 nm in diameter. This explains the lack of rapid extravasation, as seen on figure 3.18. The signal is isolated to a large extent in the intravascular system.

With Mouse Four, the concentration was pushed even further. This product had the AEGLAFK peptide attached, and the micelles were formed using a 1:1:1 ratio of PVP:PVP-COOH:PVP-Peptide, following protocol 2.2.11. In effect, the ratio of carboxyl groups available for chelation was 30%, and the material exhibited the best results across all samples. The T1 MRI scan shows a concentration profile of about .4 mM at peak compared to 0.8 mM of Dotarem in the same experiment, shown on figure 3.17. The same conditions as Mouse Three apply with regards to extravasation. Figure 3.19 shows slices through the tumour area of Mouse Four and a low dispersion is observed outside the vascular system, even after 24 hours.

To a major extent, the success of this sample can be attributed to the high degree of solubility post micellisation, as this increases the concentration of gadolinium in solution, as well as reduces the need for heparin dilution.

4.3.1.1 Accumulation of micelles in tumour area

Slight accumulation is observed in the tumour area of Mouse Four. It is most pronounced in slice 6, t = 24, visible on figure 3.19. It is not present in Mouse Three at t = 24 hours and a number of considerations must be made with respect to this difference.

First, as it has been observed the micelles in general do not extravasate, it can be assumed that an extravascular accumulation is caused by enhanced permeability - a titular sympton of EPR. As the EPR effect is in play, it can also be assumed that the effect should be observed in Mouse Three after 24 hours, as it is a passive effect but this is not the case. Granted, the sample injected in Mouse Three does not serve as a blank due to different preparation parameters and higher degree of dilution by heparin. In essence, this means the injection in Mouse Four stands as an experiment with no blank and it is difficult to conclude much due to the nature of such.

Further consideration of the measured intravascular concentrations only adds to the uncertainty. The measured intravascular T1 signal in Mouse Four was 2.5 times greather than that of Mouse Three normalised by Dotarem (0.2 micelle-Gd/Dotarem versus 0.5 micelle-Gd-peptide/Dotarem), but the dilution factor was only 33% less. This indicates a higher percentage of reporter groups per unit volume, whether it be more micelles or a higher degree of gadolinium chelation by PVP-COOH units. In both cases it contributes to the increased signal after 24 hours, and only dims the case of whether the accumulation is caused exclusively by EPR, or if the targeting peptide contributes to the case.

According to literature [29], AEGLAFK exhibits higher binding affinity to EGFRvIII (epidermal growth factor receptor variant) and EGFR gene amplification is frequently observed in primary glioblastoma multiforme [30]. AEGLAFK was synthesised with good purity (only one peak showing up on the analytical HPLC run 3.14, but it is possible the result would be better with a purified product.

To determine the exact cause, it is advantageous to carry out in vitro experiments in a continuation of the optical fluorescence microscopy experiments. Lines of glioblastoma and fibroblast cells exposed to micelles with and without the peptide and with and without wortmannin blocking receptor mediated endocytosis would provide much needed insight. This experiment further necessitates the need to explore temporal drug uptake kinetics however, as not much information is gained past drug saturation of the cells. Proceeding, in vivo experiment with gadolinium chelated by DTPA and bound to the same targeting moiety, AEGLAFK, by amine coupling would contribute to the case. The latter molecule should be able to extravasate in a similar fashion to Dotarem, and also in the same concentration range if necessary. Observing increased signal in the tumour in such an experiment would be conclusive.

4.3.2 Theranostics and noninvasive cancer diagnostics

The EPR effect was observed to an extent in the MRI scans of this project. Combining the effect of diagnostics with therapeutic effects such the one intended to be loaded into the PVP micelles is part of a field called theranostics. However, investigating the potential of diagnostics with various nanoparticule carrier systems is also of great interest. A few approaches using mainly the EPR effect to enhance signal intensity are discussed. It is observed in general that the gadolinium or reporter molegroup experiences increased efficacy as a contrast agent when incorporated into larger systems.

One alternative approach to formulating Gd-loaded nanoparticulate systems could be the one presented in [31]. This system does not provide means of drug loading, but does display targeted enhanced MRI

potential.

Another attempt was made to incorporate the gadolinium contrast molecules into the hydrophobic core [32]. The relaxivity of Gd/DTPA was reported increased 13 fold inside the micelles. To adapt this protocol to this project, it would be necessary to convert the Gd-DTPA complex to a hydrophobic derivative, to force it into the core of the micelles. The sustained release of Gd/DTPA of [32] may be difficult to reproduce in a different system however.

The same type of core incorporation of Gd/DTPA has been explored by [33] and it mainly applies to cancer diagnostics. They report a 6 fold increase of relaxivity compared to free form Gd/DTPA and significantly enhanced retention time, utilising the EPR effect to increase accumulation of Gd/DTPA in the tumour.

Utilisation of the EPR effect is common practise in recent studies and gaining popularity [13]. Another study investigating the effect with highly sensitive MRI contrast agents is [34]. However, they use Superparamagnetic Ion Oxide (SPIO) nanoparticles relying on T2 relaxation instead. In addition, their carrier system, PICsome, is based on a tri-block polymer of crosslinked PEG by a polyion amino acid system as a linker. They apply the same reporter group incorporation to increase retention time by protecting them inside the particle.

On the one hand, the goal is often to increase retention time of a nano drug delivery system to utilise the EPR effect and diagnose tumours. On the other hand, long term retention is one of the biggest concerns about safety of the materials for *in vivo* application. A nanorod system of $Gd(OH)_3$ has been made to evaluate the excretion process of rare earth nanomaterials [35].

Conclusions 5

5.1 Micelle size distribution

Producing small polymeric micelles of PVP is possible. In this project, micelles of 30 to 120 nm were made using PVP, and derivatives PVP-COOH and PVGP. The micelles produced were stable in aqueous conditions from 4-10 pH for hours, but not days. This necessitates fresh preparation of lyophilisate before use. Proper preparation requires at least 30 minutes sonication in waterbath (60 minutes and periodic agitation, every 15-30 minutes, is optimal) and 10 minutes centrifugation at 10,000 rcf to remove large particles.

5.2 Micellar drug delivery

With the micelles produced by PVP, drug delivery is efficient in terms of time and concentration. 5 mg lyophilisate divided across 36 samples (0.14 mg in each well) of curcumin loaded PVP micelles was seen to almost saturate glioblastoma cells in less than 10 minutes. Fibroblast cells were investigated using 50 mg micelle lyophilisate across 48 wells, but showed the same degree of uptake after less than 5 minutes.

The observation was made on wells containing cells of both lines exposed to micelles, cells treated with the endocytic inhibitor dynasore and since exposed to micelles, and cells treated with receptor mediated endocytosis inhibitor wortmannin and since exposed to micelles. Both cell lines in all three environments exhibited no observable variation in curcumin uptake.

5.3 Optical fluorescence spectroscopy

Using chambered borosilicate slides for optical fluorescence microscopy increased the image quality significantly, compared to using polystyrene culture wells. Most relevant in this regard was the reduction of background illumination. Figure 3.22 provides a comparison of the effect.

5.4 PVP functionalisation

Modification of PVP show varied success. Epoxidising PVP with 2-chloroacetamide as a precursor was a success and yielded a 4% PVGP/PVP ratio.

Using DTPA to functionalise the epoxidised PVP derivative PVGP was not successful. Attempted methods include direct reaction of epoxide moiety with DTPA catalysed by imidazole and EDC facilitated amine coupling of ethylenediamine between epoxide moiety and DTPA. Neither approach resulted in the DTPA functionalisation of PVGP.

Functionalising PVP-COOH with ethylenediamine was successful and confirmed by fluorescence spectroscopy on figure 3.10, showing the presence of ethylenediamine in a PVP-COOH containing solution after rinsing. Subsequent non-catalysed reaction of DTPA dianhydride directly with the primary amines of PVP-COOH-EN, and further chelation of Gd^{3+} was confirmed by fluorescence spectroscopy of figure 3.11.

5.5 Gadolinium chelation

The polychelating property of PVP-COOH was used to form micelles containing high amounts of gadolinium. Formation of PVP-COOH-Gd micelles was possible only when "diluting" the percentage of carboxylated units by the addition of regular PVP. A 2:1 PVP:PVP-COOH mass ratio was found optimal.

Post modification micelle formation was possible in all instances of polymer modification, except when chelating gadolinium by 100% PVP-COOH. In that case the polymer insoluble in water and no longer retains amphiphilic properties.

5.6 Magnetic resonance imaging

MRI imaging showed varied degrees of T1 signal intensity depending on micelle product. Of decreasing intensity, the samples injected and scanned *in vivo* were (by protocol): 2.2.11, 2.2.9.3, 2.2.9.1, 2.2.6.2. This concludes that attaching an MRI contrast agent to drug loading PVP nano-micelles is possible. Note the last sample on the list provided no observable contrast. It was further observed that great care must be taken to minimize viscosity of the injected sample, and buffering it to physiological standards.

An accumulation of contrast bearing material was observed in the tumour area of Mouse Four after injection of micelles containing a targeting peptide. As no reference injection exists, it is not possible to conclude whether the accumulation is caused by the targeting moiety or the EPR effect. However, as the accumulation is extravascular, it is safe to assume the EPR effect applies to allow extravasation of the 100 nm sized micelles. Further experimentation is needed to determine the cause of accumulation.

Bibliography

[1] Cancer.net, *Side effects of chemotherapy*. URL: http://www.cancer.net/navigating-cancer-care/how-cancer-treated/chemotherapy/side-effects-chemotherapy, 2015. Retrieved: 10-09-2015.

[2] V. P. Torchillin, *Handbook of Experimental Pharmacology*. No. ISSN 0171-2004 in Methods in Molecular Biology, Springer, 2010.

[3] P. G. Corrie, "Cytotoxic chemotherapy: clinical aspects," *Systemic therapy*, vol. 36, 2007.

[4] S. R. Sirsi and M. A. Borden, "State-of-the-art materials for ultrasound-triggered drug delivery," *Advanced Drug Delivery Reviews*, vol. 72, pp. 3–14, 2014.

[5] A. W. El-Kareh and T. W. Secomb, "Two-mechanism peak concentration model for cellular pharmacodynamics of doxorubicin," *Peoplasia*, vol. 7, pp. 705–714, 2005.

[6] M. M. Gottesman, T. Fojo, and S. E. Bates, "Multidrug resistance in cancer: Role of atp-dependent transporters," *Nature*, vol. 2, pp. 48–58, 2002.

[7] L. J. Goldstein, H. GalsH, A. Fojo, M. Willingham, S.-U. Lai, A. Gaidar, R. Pirker, A. Green, W. Crist, G. M. Brodeur, M. Ueber, J. Cossman, M. M. Gottesman, and I. Pastan, "Expression of a multidrug resistance gene in human cancers," *Journal of the National Cancer Institute*, vol. 81, pp. 116–124, 1989.

[8] X. Cao, L. Tao, S. Wen, W. Hou, and X. Shi, "Hyaluronic acid-modified multiwalled carbon nanotubes for targeted delivery of doxorubicin into cancer cells," *Carbohydrate Research*, vol. 405, pp. 70–77, 2015.

[9] G. A. Husseini, L. Kherbeck, W. G. Pitt, J. A, Hubbell, D. A. Christensen, and D. Velluto, "Kinetics of ultrasonic drug delivery from targeted micelles," *Journal of Nanoscience and Nanotechnology*, vol. 14, pp. 1–6, 2014.

[10] T. M. Allen and P. R. Cullis, "Drug delivery systems: Entering the mainstream," *Science*, vol. 303, pp. 1818–1822, 2004.

[11] N. Frazier and H. Ghandehari, "Hyperthermia approaches for enhanced delivery of nanomedicines to solid tumors," *Biotechnology and Bioengineering*, vol. 112, pp. 1967–1983, 2015.

[12] C.-L. Fang, C. J. Wen, I. A. Aljuffali, C. T. Sung, C.-L. Huang, and J.-Y. Fang, "Passive targeting of phosphatiosomes increases rolipram delivery to the lungs for treatment of acute lung injury: An animal study," *Journal of Controlled Release*, vol. 213, pp. 69–78, 2015.

[13] J. Fang, H. Nakamura, and H. Maeda, "The epr effect: Unique features of tumor blood vessels for drug delivery, factors involved, and limitations and augmentation effects," *Advanced Drug Delivery Reviews*, vol. 63, pp. 136–151, 2011.

[14] J. He, X. Huang, Y.-C. Li, Y. Liu, T. Babu, M. A. Aronova, S. Wang, Z. Lu, X. Chen, and Z. Nie, "Self-assembly of amphiphilic plasmonic micelle-like nanoparticles in selective solvents," *Journal of the American Chemical Society*, vol. 135, pp. 7974–7984, 2013.

[15] K. K. Jain, *Drug Delivery System*. No. ISBN 978-1-4939-0362-7 in Handbook, Springer, 2014.

[16] M. Ferrari, "Cancer nanotechnology: Opportunities and challenges," *Nature*, vol. 5, pp. 161–171, 2005.

[17] V. P. Torchilin, "Structure and design of polymeric surfactant-based drug delivery systems," *Journal of Controlled Release*, vol. 73, pp. 137–172, 2001.

[18] F. Ciardiello and G. Tortora, "A novel approach in the treatment of cancer: Targeting the epidermal growth factor receptor," *Clinical Cancer Research*, vol. 7, pp. 2958–2970, 2001.

[19] L. Xing and W. L. Mattice, "Large internal structures of micelles of triblock copolymers with small insoluble molecules in their cores," *Langmuir*, vol. 14, pp. 4074–4080, 1998.

[20] Y. Teng, M. E. Morrison, P. Munk, S. E. Webber, and K. Prochazka, "Release kinetics studies of aromatic molecules into water from block polymer micelles," *Macromolecules*, vol. 31, pp. 3578–3587, 1998.

[21] V. Alakhov, P. Lemieux, E. Klinski, A. Kabanov, and G. Pietrzynski, "Block copolymeric biotransport carriers as versatile vehicles for drug delivery," *Expert Opinion on Biological Therapy*, vol. 1, pp. 583–602, 2001.

[22] H. Friebolin, *Basic One- and Two-Dimensional NMR Spectroscopy*. No. ISBN: 978-3-527-32782-9, Wiley-VCH, 2013.

[23] phys.org, *Lessening the Penalty for Creating Block Copolymer Nanostructures*. URL: `http://cdn.phys.org/newman/gfx/news/hires/lesseningthe.jpg`, 2010. Retrieved: 13-9-2015.

[24] K. Kataoka, A. Harada, and Y. Nagasaki, "Block copolymer micelles for drug delivery: Design, characterization and biological significance," *Advanced Drug Delivery Reviews*, vol. 47, pp. 113–131, 2001.

[25] A. E. Nel, L. Madler, D. Velegol, T. Xia, E. M. V. Hoek, P. Somasundaran, F. Klaessig, V. Castranova, and M. Thompson, "Understand biophysicochemical interactions at the nano-bio interface," *Nature Materials*, vol. 8, pp. 543–557, 2009.

[26] R. Devarajan, V. Arunachalam, M. D. K. Kumaraswamy, I. Tajuddin, and T. Joghee, "Darzens glycidic ester condensation reaction on poly-n-vinyl pyrrolidone," *Journal of Applied Polymer Science*, vol. 44, pp. 1473–1475, 1992.

[27] X. Wen, E. F. Jackson, R. E. Price, E. E. Kim, Q. Wu, S. Wallace, C. Charnsangavej, J. G. Gelovani, and C. Li, "Synthesis and characterization of poly l-glutamic acid gadolinium chelate: A new biodegradable mri contrast agent," *Bioconjugate Chemistry*, vol. 15, pp. 1408–1415, 2004.

[28] nanodrop.com, *Fluorescamine Protein Assay*. URL: `http://www.nanodrop.com/Library/Fluorescamine%20protocol.pdf`, 2013. Retrieved: 24-6-2015.

[29] C. L. Denholt, T. Binderup, M.-T. Stockhausen, H. S. Poulsen, M. S. Thomsen, P. R. Hansen, N. Gillings, and A. KjÃ¦r, "Evaluation of 4-[^{18}f]fluorobenzyl-falgea-nh$_2$ as a position emission tomography tracer for epidermal growth factor receptor mutation variant iii imaging in cancer," *Nuclear Medicine and Biology*, vol. 38, pp. 509–515, 2011.

[30] H. K. Gan, A. H. Kaye, and R. B. Luwor, "The egfrviii variant in glioblastoma multiforme," *Journal of Clinical Neuroscience*, vol. 16, pp. 748–754, 2009.

[31] A. Ahmed, C. Zhang, J. Guo, Y. Hu, and X. Jiang, "Fabrication and characterization of gd-dtpa-loaded chitosan-poly-acrylic acid nanoparticles for magnetic resonance imaging," *Macromolecular Bioscience*, vol. 15, pp. 1105–1114, 2015.

[32] P. Mi, H. Cabral, D. Kokuryo, M. Rafi, Y. Terada, I. Aoki, T. Saga, I. Tekohiko, N. Nishiyama, and K. Kataoka, "Gd-dtpa-loaded polymeremetal complex micelles with high relaxivity for mr cancer imaging," *Biomaterials*, vol. 34, pp. 492–500, 2013.

[33] P. Mi, D. Kokuryo, H. Cabral, M. Kumagai, T. Nomoto, I. Aoki, Y. Terada, A. Kishimura, N. Nishiyama, and K. Kataoka, "Hydrothermally synthesized pegylated calcium phosphate nanoparticles incorporating gd-dtpa for contrast enhanced mri diagnosis of solid tumors," *Journal of Controlled Release*, vol. 174, pp. 63–71, 2014.

[34] D. Kokuryo, Y. Anraku, A. Kishimura, S. Tanaka, M. R. Kano, J. Kershaw, N. Nishiyama, T. Saga, I. Aoki, and K. Kataoka, "Spio-picsome: Development of a highly sensitive and stealth-capable mri nano-agent for tumor detection using spio-loaded unilamellar polyion complex vesicles (picsomes)," *Journal of Controlled Release*, vol. 169, pp. 220–227, 2013.

[35] Y. Yang, Y. Sun, Y. Liu, J. Peng, Y. Wu, Y. Zhang, W. Feng, and F. Li, "Long term *in vivo* biodistribution and toxicity of gd(oh)$_3$ nanorods," *Biomaterials*, vol. 34, pp. 508–515, 2013.

Appendix A

A.1 Matlab script

The histogram function is modified to suit this use. All credit goes to the author mentioned below in the script.

A.1.1 Color histogram function

```
%============================================================
% createColorHistograms(im_str)
% im_str can be an image file location or a three-dimensional array
%============================================================

%============================================================
% Copyright (C) 2007-2008 Chaitanya Sai Gaddam (gsc at cns.bu dot edu)
% http://www.discerniblepreferences.com
% Redistribution and use in source and binary forms, with or without
% modification, are permitted provided that the following conditions
% are met:
% 1. Redistributions of source code must retain the above copyright
%    notice, this list of conditions and the following disclaimer.
% 2. Redistributions in binary form must reproduce the above copyright
%    notice, this list of conditions and the following disclaimer in the
%    documentation and/or other materials provided with the distribution.
% 3. Neither the name of the Chaitanya Sai Gaddam nor the names of its contributors
%    may be used to endorse or promote products derived from this software
%    without specific prior written permission.
%
% THIS SOFTWARE IS PROVIDED BY THE REGENTS AND CONTRIBUTORS ``AS IS'' AND
% ANY EXPRESS OR IMPLIED WARRANTIES, INCLUDING, BUT NOT LIMITED TO, THE
% IMPLIED WARRANTIES OF MERCHANTABILITY AND FITNESS FOR A PARTICULAR PURPOSE
% ARE DISCLAIMED.  IN NO EVENT SHALL THE REGENTS OR CONTRIBUTORS BE LIABLE
```

```
% FOR ANY DIRECT, INDIRECT, INCIDENTAL, SPECIAL, EXEMPLARY, OR CONSEQUENTIAL
% DAMAGES (INCLUDING, BUT NOT LIMITED TO, PROCUREMENT OF SUBSTITUTE GOODS
% OR SERVICES; LOSS OF USE, DATA, OR PROFITS; OR BUSINESS INTERRUPTION)
% HOWEVER CAUSED AND ON ANY THEORY OF LIABILITY, WHETHER IN CONTRACT, STRICT
% LIABILITY, OR TORT (INCLUDING NEGLIGENCE OR OTHERWISE) ARISING IN ANY WAY
% OUT OF THE USE OF THIS SOFTWARE, EVEN IF ADVISED OF THE POSSIBILITY OF
% SUCH DAMAGE.
%=============================================================

function createColorHistogramsDAPI(im_str)

if ~isstr(im_str)
    if ndims(im_str)==3
        try
            col_array_vals=double(im_str);
        catch
            disp('Input is not a valid three-dimensional array');
            return;
        end
    end
else
    try
        col_array_vals=double(imread(im_str));
        if ndims(col_array_vals)~=3
            disp('Input is not a valid three-dimensional array');
            return;
        end

    catch
        disp('Input string does not point to a valid image file');
        return;
    end
end



%===
%res_val: Binning resolution. Increasing the value gives coarsers bins
%===
res_val=4;



%===
%t_count: Color triplets are converted to a single value for purposes of
```

```
%binning
%===
t_count=res_val*floor(col_array_vals(:,:,1)/res_val)+256*(res_val*floor(col_array_vals(:,
t_count=sort(t_count(:));

%===
% Use unique to calculate the number of triplets (ind_last-ind_first) in each bin
%===
[col_val,ind_first]=unique(t_count,'first');
[col_val,ind_last]=unique(t_count,'last');

set(0,'DefaultFigureVisible','off');
%disp('Drawing color bars');
colorbars(col_val,ind_last-ind_first,1/3,1/4);
%disp('Drawing color cloud');
%colorcloud(col_val,ind_last-ind_first,1/3,1/4);
%disp('Drawing image');
figure(3);
set(gcf,'position',[5   61   274   236]);
imshow(col_array_vals/255);


%varargout{im_str}=createColorHistograms(im_str)



function colorbars(triplet_color,triplet_freq,varargin)

if nargin==2
    color_pow=1/3;
    freq_pow=1/4;
else
    color_pow=varargin{1};
    freq_pow=varargin{2};
end


%===
% Randomize bin ordering
%===
%N_rand=randperm(length(triplet_freq));
%triplet_freq=sqrt(triplet_freq(N_rand));
%triplet_color=triplet_color(N_rand);

%===
```

```
% Reconstruct color triplets from col_val
% Sphere triplets
%===
triplet_color=([rem(triplet_color,256) floor(rem(triplet_color,256*256)/256) floor(triplet_colo
triplet_color_norm=triplet_color./repmat(((sum(triplet_color.^(1),2))+.005),1,3);
max(triplet_color_norm);
triplet_diff=sum(abs(triplet_color_norm-repmat(triplet_color_norm(end,:),size(triplet_color_nor
%===
% colors are sorted with red [.9 0 0] as the anchor
%===
triplet_diff=sum(abs(triplet_color_norm-repmat([.9 0 0],size(triplet_color_norm,1),1)),2);

max(triplet_diff);
%===
% color_pow and freq_pow are used to obtain a suitable spacing of colors
% Ordering of a triplet in 2-d gives us an extra degree of freedom.
% How do we use this to align perceptual distance and euclidean distance?
%===
triplet_diff=(triplet_diff/max(triplet_diff).^(color_pow))+(triplet_freq*0).^(freq_pow);



[d,inds_sort]=sort(triplet_diff);
triplet_freq=(triplet_freq(inds_sort));
triplet_color=(triplet_color(inds_sort,:));

num_bars=length(triplet_color);
max_val=max(triplet_freq);

close all;
figure(1);
axis([0 num_bars 0 1]);


for i=1:num_bars
    tempColor=min(triplet_color(i,:),.9);
    %===
    % Use patch to draw individual bars
    %===

    patch([i-1 i-1 i i],...
        [0 triplet_freq(i)/(max_val+1) triplet_freq(i)/(max_val+1) 0],...
        tempColor,...
        'edgecolor',...
        tempColor);
```

```
end

set(gca,'xtick',[0.5:1:(num_bars-0.5)],'xticklabel',[1:1:num_bars]);
xlabel('Number of colour bins');
set(gca,'ytick',[0:0.2:1]);
ylabel('Ratio to bin with highest pixel count')
set(gcf,'position',[5 378 560 420]);
set(gca,'visible','on')

CutOff=num_bars*.10;
fG=CutOff;
%disp('Triplet frequency');
%global intensity
intensity=sum(triplet_freq([ceil(fG):1:num_bars]));

assignin('base', 'intensity', intensity);
%save('intensity.mat','intensity')
```

```
function colorcloud(triplet_color,triplet_freq,varargin)

if nargin==2;
    color_pow=1/3;
    freq_pow=1/4;
else
    color_pow=varargin{1};
    freq_pow=varargin{2};
end

%===
% Randomize bin ordering
%===

%N_rand=randperm(length(triplet_freq));
%triplet_freq=sqrt(triplet_freq(N_rand));
%triplet_color=triplet_color(N_rand);

%===
% Reconstruct color triplets from col_val
% Sphere triplets
```

```
%===

triplet_color=([rem(triplet_color,256) floor(rem(triplet_color,256*256)/256) floor(triplet_colo
triplet_color_norm=triplet_color./repmat(((sum(triplet_color.^(1),2))+.005),1,3);
max(triplet_color_norm);
triplet_diff=sum(abs(triplet_color_norm-repmat(triplet_color_norm(end,:),size(triplet_color_nor
triplet_diff=sum(abs(triplet_color_norm-repmat([.9 0 0],size(triplet_color_norm,1),1)),2);

max(triplet_diff);
triplet_diff=(triplet_diff/max(triplet_diff).^(color_pow))+(triplet_freq*0).^(freq_pow);

[d,inds_sort]=sort(triplet_diff);
triplet_freq=(triplet_freq(inds_sort));
triplet_color=(triplet_color(inds_sort,:));

num_bars=length(triplet_color);
max_val=max(triplet_freq);

figure(2);
axis([-.2 1.2 -.2 1.2]);
hold on;

num_total_freq=sum(triplet_freq);
disp(num_total_freq);

%===
% (Exp. A)
% The bins of triplet frequencies seem to follow a power law.
% Plotting a very large number for one triplet bin is unnecessary, so the
% number of points plotted for the maximally frequent triplet is set to 100
% and the median frequency is set to have about 45 points plotted
% (hence the number 45) in the equation below

%===
triplet_freq_normalizer=45/(median(unique(triplet_freq))*15);


for i=1:num_bars;
    tempColor=triplet_color(i,:);
    dist_scatter=min((triplet_freq(i)*100/num_total_freq),.1);

    %===
    % see (Exp. A) aboce
    %===
    for j=1:min(ceil(triplet_freq(i)*15*triplet_freq_normalizer),100);
```

```
        %===
        % A scatter cloud is produced for each bin by assigning a radius to
        % each cloud that is proportional to the number of triplets in that
        % bin. Therefore, a color appearing frequently in the image will
        % have a larger scatter radius.
        %===
        r_dist=rand*dist_scatter;
        r_angle=rand*pi*2;
        x_val=sigmoidVal((tempColor(2)-tempColor(1)+1)*.5,8);
        %x_exp=.8+round(1-x_val);
        x_val=(x_val)+r_dist*cos(r_angle);
        y_val=(tempColor(3)+.1)/(tempColor(2)+tempColor(1)+tempColor(3)+.3);
        y_val=y_val+r_dist*sin(r_angle);

        plot(x_val,...
            y_val,...
            '.',...
            'markerfacecolor',min(tempColor,.9),...
            'markeredgecolor',min(tempColor,.9));
    end

end

set(gca,'xticklabel','')
set(gca,'yticklabel','')
set(gcf,'position',[573 380 560 420]);
axis equal;
axis tight;
axis([-.03 1.03 -.03 1.03]);
set(gca,'visible','off');

%Live/Dead stain calculations
%lR=num_bars*0.15; %Last RED bar nr.
%fG=4; %First GREEN bar nr.

%disp('Triplet frequency')
%nRED=sum(triplet_freq([1:1:lR]))
%nGREEN=sum(triplet_freq([fG:1:num_bars])) % +/- misplaced bars
%GRratio=nGREEN/nRED
%Density=nRED+nGREEN
```

```
function y_val=sigmoidVal(x_val,varargin)

if nargin==1
    multip_val=15;
else
    multip_val=varargin{1};
end

y_val=1./(1+exp(-(x_val-.5)*multip_val));
```

A.1.2 Loop of histogram function

```
clear all

filedirectory = 'filename';

imgStruct=dir(strcat(filedirectory,'*.png'));
%imgStruct(~[imgStruct.isdir]) = [];  %remove non-directories
tf1 = ismember( {imgStruct.name}, {'.', '..'});
imgStruct(tf1) = [];  %remove current and parent directory.

c = struct2cell(imgStruct);

for i=1:4
c(2,:) = [];
end
clear('i');

num_subfolders = length(c);

for k=1:num_subfolders
cellpath1 = filedirectory;
cellpath2 = c{1,k};
cellpath3 = strcat(cellpath1,cellpath2);
%filename = strcat(cellpath3,k);
num_subfolders = length(c);
SubimgStruct = dir(cellpath3);
%SubimgStruct(~[SubimgStruct.isdir]) = [];  %remove non-directories
tf2 = ismember( {SubimgStruct.name}, {'.', '..'});
SubimgStruct(tf2) = [];  %remove current and parent directory.
s = struct2cell(SubimgStruct);
for z=1:4
s(2,:) = [];
end
clear('z');
```

```
directory(1,k)= s ;
clear('s');
end

%clear('i','c','SubimgStruct','tf1','tf2','imgStruct','num_subfolders','k','cellpath2','ce

for m = 1:num_subfolders

cellpath4 = filedirectory;
cellpath5 = c{1,m};
cellpath6 = strcat(cellpath4,cellpath5);
% %name = dir('C:\Users\Sven\Documents\MATLAB\CellImages\29-6-15\Processed\FibroblastMicel
name2 = strcat('\',directory(1,m));
sourcefilename = strcat(cellpath6,name2);
name3 = strcat('\',c(1,m));
destfilename = strcat(cellpath6,name3);
a =sourcefilename{1,1};
b =destfilename{1,1};
if a~=b
movefile(a,b)
end
end

num_img = length(directory);

for i=1:num_img

    path = strcat(filedirectory,c{1,i});

    createColorHistogramsDAPI(path);

    data(1,i)=intensity;

    clear('intensity');
end

clear('i');
```